Modelling microdomain-mediated protein sorting in immunological signalling

Edward Andrew Gilmore Long

July 2012

A thesis submitted to University College London for the Degree of Doctor of Philosophy

CoMPLEX
UCL
Physics Building
Gower Street
London, WC1E 6BT

I, Edward Andrew Gilmore Long, confirm that the work presented in this thesis is my own. Where information has been derived from other sources, I confirm that this has been indicated in the thesis.

For David, Georgina and William

Acknowledgements

I would like to thank my supervisors, Professor Alexey Zaikin and Professor Brian Henderson, for their guidance, encouragement, helpful criticism and assistance with planning, without which this work would not have been possible.

For their patient and understanding support, sympathy, generosity and tolerance I owe an enormous amount to my parents and family and thank them deeply.

I am hugely grateful to my examiners: Professor Benny Chain and Professor Carmen Molina París for giving up their time and expertise to examine this thesis.

Dr Denis Goldobin provided invaluable guidance and commentary on the mathematical techniques employed.

For fruitful academic discussions and advice I would like to thank Dr Sylvia Nagl, Dr Stephen Barrett, Professor Shamshad Cockroft, Dr Nick Ovenden, Dr Dean Willis, Professor Alan Johnson and Professor Rob Seymour.

For years of peer support, friendship, proof-reading, feedback and geeky banter I'm very grateful to all the students of CoMPLEX, especially Matt Caldwell, Lisa Willis, Sam Tazzyman, Lorette Noiret, Dorothy Kuipers, Mae Woods, Zena Hadjivasiliou, Raphaela Heussen, Nuno Nene, Mike Cohen, Tom Sumner and Alex Stewart; also to Chih-Chun Chen and Rubi Bilal.

I'd also like to thank Richard Makin, Hugo Carr and David Sturgeon for their continual reassurance and support.

This thesis was funded by CoMPLEX, which receives funding from the EPSRC as well as the MRC, BBSRC, CRUK, NERC, SAHFOS and UCL.

Abstract

Compartmentalisation is a fundamental feature of biological systems. The organism as a whole can be seen as a single compartment of the wider ecosystem. At lower scales, we observe biological processes compartmentalised into organs, cells, cell subtypes and organelles. In the highly complex discipline of immunology, compartmentalisation is key in order to respond efficiently to foreign antigens and to maintain the balance between immunity and tolerance. Recent studies have raised questions about the role of compartmentalisation in lipid membranes, from the relatively well described immunological synapse, to the smaller, more transient lipid raft or microdomain. This thesis asks whether, and how, microdomains could influence the formation of small receptor complexes.

Specifically, we approach what appears to be a simple surface reaction-diffusion problem from multiple viewpoints: explicitly simulating particle diffusion using a probabilistic pixel-based model, and deriving a deterministic relation between spatial parameters and the timecourse of chemical concentrations throughout the model space. We also show the equivalence between the predictions of these two models, further supporting the validity of our approach.

We also embed the results of our model output in an existing model of the immunological response in order to determine the downstream consequences of enhanced receptor organisation. The study gives a broader understanding of the mechanisms involved in microdomain-mediated protein sorting, highlights the degree of interdependence on multiple spatial and chemical parameters and suggests numerous avenues for future research.

Contents

List of Figures

List of Tables

Chapter 1

Introduction

The mammalian immune system is in a constant battle to maintain a balance between tolerance and response. Many microorganisms have a neutral or beneficial relationship with the host and, as such, to mount a response would be counterproductive. But the host immune system cannot learn through evolution every single peptide sequence that indicates the presence of a harmful microorganism: microorganisms evolve at a much faster rate than the host and are so diverse that host organisms lack the genetic resources to code for receptors to recognise any potential threat that they encounter. As such, an appropriate immune response relies on a decentralised network of specialised cells which share information and constantly readjust their behaviour based on previous experience [76, 55].

As well as generating a response to the huge range of potential pathogens, the immune system must also actively maintain tolerance to host tissues, which it comes into contact with much more frequently, raising the likelihood of autoimmune reactions.

The key player controlling the progress from pattern recognition to immune response in the adaptive immune system is the T cell and the primary signalling molecule driving T cell proliferation in the immune response is the cytokine interleukin 2 (IL-2). Appropriate responses to immune challenge require a high degree of sensitivity and specificity to the extracellular ligand. In the antigen recognition phase, this involves specialised spatial organisation of T cell surface components into a structure termed the *immunolog-*

ical synapse[46]. Other immune signalling mechanisms, however, may also be facilitated by the organisation of specialised signalling platforms in the form of *lipid rafts* or *microdomains*[104, 48, 49].

The involvement of spatial organisation as a fundamental component to biological signalling pathways represents an additional layer of complexity on many of the popular models of immunological function. As Kholodenko et al. note:

> Signal transduction was once viewed as a collection of linear information transporting pipelines that related extracellular cues to specific genes [58].

However, our increasing understanding of the spatial and temporal dynamics of signalling reinforce the importance of immunological signals being *in the right place at the right time*. These developments mitigate the preeminence of gene regulatory networks as determiners of cell fate and assign instead significance to cell geometries and subcellular structures in organising proteins into signalling complexes.

The small and transient nature of membrane microdomains [62] make them a slippery object of study, which has led to a diverse range of hypotheses about their properties and function in cell biology [16, 57]. In such a situation, computational modelling approaches allow us to systematically test existing hypotheses across a wide range of parameters, and mathematical modelling allows us to determine causal relationships in the fundamental mechanisms of the system under study.

In this thesis, we develop computational, mathematical and hybrid models of microdomain-mediated protein complex formation in order to investigate the potential for regions of low diffusion rate to act as 'entropic traps' which facilitate protein complex formation.

The primary hypothesis of the thesis is: 'The presence of multiple finite regions of low diffusion in a space enhance the formation of modelled heterotrimeric protein complexes in a reaction-diffusion system'.

The secondary hypothesis of the thesis is: 'There exist optimal geometric properties of microdomains which maximise modelled protein formation in the above system'.

1.1 Objectives

The objectives of this thesis are:

1. To investigate the influence of spatial heterogeneity in diffusion rates on the organisation of modelled membrane protein complexes using simple numerical simulations
2. To create and analyse simulations to determine the interplay of a range of diffusion schemes, combining the effects of spatially varying diffusion rates and affinity for defined regions
3. To rigorously determine the underlying diffusion dynamics by finding novel analytical solutions to reaction-diffusion problems on a heterogeneous space
4. To test the hypothesis using the above two approaches that microdomains have 'optimal' spatial characteristics
5. To explore and characterise the space of solutions to the analytical model
6. To combine the novel solutions with existing immunological signalling models and determine the overall impact of heterogeneity on signalling
7. To quantify the interdependence of any heterogeneity-mediated effects on trimer organisation and other determining physical and chemical parameters

1.2 Thesis overview

Chapter 2 contains a review of the experimental research which provides a background and a motivation to this thesis. We will describe the development, diversity and function of the T cell and the role in which IL-2 plays in the immune response. We also provide a history of the relatively recent experimental literature on membrane microdomains (or 'rafts'), explain why it is a field that still has many unanswered questions and synthesise the current understanding of membrane heterogeneity. Finally we describe how modelling plays an important role in many fields in biology, including immunology. We review key

papers in immunological modelling and modelling of membrane diffusion processes and describe our stance in this thesis in relation to the existing literature.

In Chapter 3 we construct a new probabilistic model of a cell membrane reaction-diffusion system in order to readily test several key hypotheses on the role of membrane compartmentalisation on the organisation of immune signalling receptors. The models explore physical mechanisms (the retardation of diffusion proteins within fixed membrane regions) as well as chemical mechanisms (selectivity within fixed membrane regions for particular membrane proteins) for sequestering diffusing proteins in order to facilitate the organisation of a trimeric receptor, which models the heterotrimeric receptor for the cytokine IL-2. This chapter addresses objectives 1, 2 and 4 of the thesis.

The results of the model in Chapter 3 give an interesting insight into the role of membrane heterogeneity in protein complex formation. The probabilistic nature of the model, however, makes it difficult to draw clear causal relationships between modelled membrane structure and the diffusional behaviour of the embedded proteins over time. In Chapter 4, we re-approach the problem from a deterministic angle and derive novel solutions to the diffusion equation in heterogeneous spaces representative of membrane microdomains. We also validate this analytical model against a simplified version of the probabilistic model developed in Chapter 3 and find good agreement. The analytical solution provides a better understanding of the evolution of the system in long timescales (running the probabilistic model on very long timescales is computationally intensive) and the greater ease of computation also allows us to investigate a wide range of chemical parameters more readily. Objectives 1, 3, 4 and 5 are addressed in this chapter.

In order to better understand the fundamental properties of the theoretical system under study, Chapters 3 and 4 deliberately simplified parameters and ignored the place of receptor formation in the wider context of T cell signalling. For that reason, Chapter 5 combines the new models derived in this study with an existing T cell proliferation model to elucidate the significance of greater receptor expression on downstream signalling and T cell population growth. This chapter addresses objectives 1, 4, 5, 6 and 7, exploring the parameter space of the model with greater emphasis on biologically relevant values for the

parameters used.

1.3 Publications

Part of the work in this thesis has been published in:

- E. Long, B. Henderson, and A. Zaikin. In silico analysis of microdomain-mediated trimer formation in the T cell membrane. *The European Physical Journal - Special Topics*, 187(1):21–30, 2010

Chapter 2

Literature review

The immune systems of animals are incredibly complex systems, having evolved over time to recognise harmful elements and, within the lifetime of an organism, developing further via ongoing selective mechanisms. This system faces a number of challenges in terms of balance: it must respond to as wide a variety of pathogens as possible while minimising the risk of attacking the self and it must generate a sufficiently intensive response to remove harmful material without causing excessive damage to surrounding tissues. This balance requires constraining the action of effector cells in both magnitude and duration.

One of the challenges faced by the immune system is to be able to respond appropriately to a huge variety of stimuli with only limited resources in terms of cell phenotypes and signalling molecules. In order to increase the logical complexity of the system processing the stimulus, the immune system leverages heterogeneity between cell types so that the response depends on a synergistic or antagonistic combination of signals from different cells. Over the last decade or so, there is also increasing evidence that heterogeneity *within* cell structures allows combinatorial expansion of the possible responses to an external stimulus [58].

There are a number of barriers which must be passed sequentially in order for a pathogen to become established within the host. The first of these is the skin and mucosa which provide a physical barrier to invasion by foreign agents. Once inside, physiological conditions may also prevent survival of the pathogen, for example unfavourable tempera-

ture or pH. The final two barriers are the *innate* and *adaptive* components of the immune system – where the adaptive immune system shows a much higher degree of specificity but takes longer to react to novel stimuli. Importantly, the organism is only aware of invasion once the pathogen engages either the innate or adaptive immune system and it is at the cell membrane of the immune system's detector cells where first contact takes place. It is here that the intelligence operation begins and the immune system begins a programme of computation and communication which identifies the attacker and triggers an appropriate response.

2.1 T cell immunology

The T cell is a central actor in the adaptive immune response, although it plays diverse and sometimes contradictory roles; both initiating, amplifying and carrying out the host immune response to potential threats as well as suppressing autoimmune responses and preventing an overaggressive mobilisation of effector cells to less acute challenges or to host cells.

T cells derive their name from their place of maturation – the thymus – and act in concert with B cells, another lymphocyte, that is formed in the bone marrow in mammals. The B cell name, however, is derived from the organ where they are formed in birds – the *bursa of Fabricius*[93].

Naive conventional T cells are activated via the T cell receptor (TCR). The TCR itself is a membrane-bound heterodimer consisting of α and β subunits, whose ligand is a complex formed of the major histocompatibility complex (MHC) molecule, bound to an antigen peptide. Soon after ligation, however, the T cell rapidly organises a more complex molecular assembly in the immediate region of the receptor, forming a structure termed the *immunological synapse*[46, 33]. A second, much smaller, population of T cells expresses a different form of the TCR – the $\gamma\delta$ TCR which appears to bind a wider range of ligands, not restricted to MHC-bound peptides. These may include heat shock proteins or bacterial lipid antigens[55]. T cells expressing this form of receptor belong to a class of 'innate-like' lymphocytes, which behave more like the innate components of the immune

system in recognising predetermined antigen patterns, rather than learned patterns[76].

MHC molecules occur in two main classes: class I and class II. Broadly speaking, MHC class II is involved in the identification of potential immune challenges and MHC class I is involved in the effector stage of an immune response. MHC class II molecules are primarily expressed on a family of cells which specialise in processing and presenting foreign antigen peptides. These are termed antigen presenting cells (APCs) and include dendritic cells, macrophages and B cells, though dendritic cells are the most effective for stimulating IL-2 production[35].

When an organism is challenged by a pathogen, antigen presenting cells process foreign peptides in the infected region and migrate to lymph nodes[77]; a space where interaction with T cells is greatly enhanced by the tightly packed reticular network. The T cell receptor is highly specific, generally recognising an exact peptide sequence, which is around 8–10 amino acids in length when bound to the MHC class I molecule, or 13–17 amino acids in length when bound to an MHC class II molecule[23]. Because of this specificity, efficient recognition of novel pathogen epitopes must be effected by creating a highly diverse set of T cell cells and ensuring that the interaction between T cells and APCs is optimised.

On successful binding between a TCR and MHC complex, the cell begins to organise the immunological synapse. During this process, other TCRs on the cell's surface migrate towards the synapse area, which covers 10–20% of the cell's surface area[46]. The binding between the TCR and MHC itself is fairly low affinity [99], so the connection to the APC surface must be stabilised by accessory proteins CD4 or CD8. These are both transmembrane glycoproteins. CD4 binds to the MHC class II molecule and CD8 binds to the MHC class I molecule. The expression of one or the other of these accessory proteins determines the role that T cells will play in the adaptive immune system as either helper or regulatory lymphocytes ($CD4^+$ T cells) or cytotoxic effector lymphocytes ($CD8^+$ T cells).

Transmembrane signalling is effected with the aid of a collection of signalling proteins: four proteins collectively referred to as CD3 and a mostly intracellular homodimer consisting of two ζ chains. These signalling molecules contain amino acid sequences called

immunoreceptor tyrosine-based activation motifs (ITAMs) which are phosphorylated by the tyrosine kinases Fyn and Lck, allowing the cytoplasmic protein ZAP-70 to bind to the ζ chains, initiating downstream signalling that leads to T cell activation. After activation

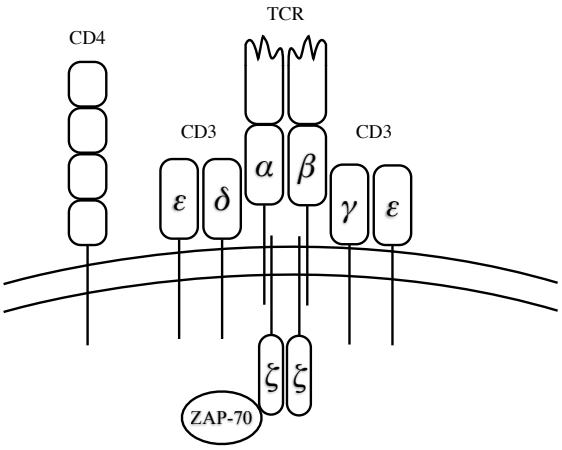

Figure 2.1: A cartoon of several of the membrane-bound elements comprising the TCR complex.

of an individual TCR, the TCR complex is internalised [1] and other TCRs within the immunological synapse may then be activated by the same peptide-MHC ligand on the antigen presenting cell.

T cell activation also depends on the amplitude of the stimulation, that is, the number of peptide-MHC complexes successfully binding to TCRs on its surface. A 2002 paper by Irvine et al. suggested that the threshold number needed for activation is in the range of 20–30 for activation of a $CD8^+$ T cell, and up to 500 for activation of a $CD4^+$ T cell[53]. Later work by Manz et al. also examined threshold signalling behaviour of clustered T cell receptors in the immunological synapse in $CD4^+$ murine T cell blasts. They argue that, rather than thresholds determined at a whole-cell level, T cell clusters control calcium signalling, with downstream effects being triggered when around four pMHC molecules bind within a single TCR cluster[72].

In addition to transient clustering, TCR complexes also form more stable oligomeric structures. Kumar et al. [61] study the prevalence of TCR oligomer formation in multiple T cell subtypes and showed that memory T cells and other T cells which have been previously stimulated form larger oligomers. They also show that these cells have a larger

proportion of TCR complexes organised into oligomers than naïve cells. They also show that oligomer size correlates with antigen sensitivity, and suggest that the formation of these structures is the mechanism by which T cells acquire increased sensitivity to subsequent stimulation.

Although all T cells express the TCR complex and elements of the signalling behaviour of the lymphocytes is uniform across all T cell subtypes, other surface molecules expressed by T cells determine the exact role that they play in the immune response. This is determined by their development and differentiation, summarised in the next section.

2.1.1 T cell differentiation

Like B cells, mammalian T cells also originate in the bone marrow as haematopoietic stem cells, which are precursors to all blood cells, including red blood cells. These differentiate to lymphoid progenitor cells, some of which migrate to the thymus where the commit to the T cell lineage in response to the Notch signal[131].

In the thymus, immature thymocytes proliferate rapidly. Few leave the thymus, however: around 98% undergo death by neglect (apoptosis) as they fail to receive the positive selection signals necessary to fully develop and leave the thymus. Selection is dependent on a pseudorandom process in which frequent gene rearrangements produce a wide number of varieties of the two proteins making up the TCR. The cell is then subjected to a three-stage test in which, depending on the protein structure of the TCR and pre-TCR, it receives either the necessary signals to survive and differentiate or is removed from the pool in response to apoptotic signalling or neglect.[55]

The first test stage is the ability of the cell to form a functional β component of the pre-TCR. Only these cells generate the signal to differentiate from cells expressing neither CD4 or CD8 on their surfaces (double negative – DN – thymocytes) to expressing both CD4 and CD8 on their surfaces (double positive – DP – thymocytes)[54]. Once cells express a functioning β component of the receptor, they begin to generate the diverse varieties of α protein needed to bind the repertoire of peptide-MHC ligands that it might possibly encounter in the periphery. Since the potential repertoire of TCR structures is

so large, it is not pre-encoded in the genome, but rather generated by a mechanism which rearranges a vocabulary of genes to produce the necessary diversity of combinations.

The second two tests within the thymus are a *positive selection* stage – in which those cells which interact at low avidity with MHC complexes on stromal cells and dendritic cells in the thymus receive a survival signal – and a *negative selection* stage, in which high avidity interactions with host-specific antigen peptides trigger an apoptotic signal. Those cells which are positively selected differentiate to become *single positive* (SP) thymocytes, expressing only $CD4$ or $CD8$. Negative selection ensures that cells leaving the thymus do not trigger immunological responses to host tissues; thereby establishing *central tolerance*[112].

After a period of around 12 days [112], SP thymocytes mature, beginning to express CD62 ligand (L-selectin) and CD69 - an important cell surface glycoprotein involved in later proliferative responses. These mature, but naive, T cells then exit the thymus and enter the circulation.

In circulation, T cells play a number of roles and are classified into subsets based, in part, on the expression profiles of their surface molecules. The subset of $CD4^+$ cells includes T helper cells (T_H cells) and regulatory T cells (T_{reg} cells), where T_{reg} cells express the α chain of the IL-2 receptor (IL-2Rα) and forkhead box p3 protein (FoxP3), and T_H cells express neither.

T_{reg} cells are a relatively recently taxonomised subset of $CD4^+$ T lymphocytes and are responsible for maintaing tolerance and controlling immune responses by inhibiting the magnitude of the T_H cell response. Signalling via the IL-2 receptor is fundamental to maintaining this balance [70, 130], as described below.

2.1.2 T cell proliferation and interleukin 2

Although T cells proliferate in response to a number of growth factors, the first to be identified was interleukin 2 (IL-2). Smith *et al.* demonstrated its role in promoting both proliferation and survival in T cells *in vitro*[107].

Notably, however, T cells are not dependent on IL-2 for proliferation: IL-$2^{-/-}$ mice

display a lower degree of T cell proliferation, but it it is not prevented entirely, suggesting some degree of redundancy in the signalling mechanism responsible for mounting immune responses. *In vitro* studies of IL-$2^{-/-}$ T cells also show a similar behaviour [100]. In addition to a slight impairment of T cell proliferation, mice lacking IL-2 also developed autoimmune disorders which led to death between 12 and 25 weeks [18].

This evidence led to the conclusion that IL-2 is a vital signalling molecule in the development of T_{reg} cell subsets and so mice that lack IL-2 are destabilised towards an elevated immune response state rather than a tolerance. This interpretation was supported by evidence that transferring T_{reg} cells into mice lacking IL-2 prevented the development of autoimmune disease[98]. This evidence has contributed to the view that, although IL-2 is a potent cell proliferation signal for all cell types, it is tolerance, rather than immunity that depends on the IL-2 signalling process [70, 130, 71].

Other interleukin molecules implicated in T cell proliferation and homeostasis include IL-7 and IL-15. IL-15, in particular, shares components of the IL-2 receptor: the transmembrane β and γ chains also form part of the IL-15 receptor complex when combined with the IL-15Rα subunit [68]. Knockout mouse models examining the role of IL-15 revealed that IL-$15^{-/-}$ mice are deficient in $CD8^+$ memory T cells, natural killer cells and intra-epithelial lymphocytes [56]. IL-$7^{-/-}$ mice have severe deficiencies in both B and T cell populations, implying that the cytokine is functionally significant in development and homeostasis in these cell types[121].

Despite their reliance on IL-2 for proliferation and homeostasis, regulatory T cells do not produce IL-2 themselves [88]. Instead they consume IL-2 produced by nearby T_H cells. This relationship establishes a negative feedback loop between two subpopulations of $CD4^+$ T cells: the helper cells producing IL-2, which stimulates proliferation in both cell subtypes; and the regulatory cells consuming the IL-2, thereby limiting further T_H cell expansion. Some experiments also suggest that regulatory cells even directly inhibit the production of IL-2 by T_H cells [115].

We have reviewed signalling via the IL-2 receptor as a single unit. In the next section, we examine the structure of the IL-2 receptor and its downstream signalling pathways.

2.1.3 The IL-2 Receptor

The IL-2 receptor is a heterotrimeric receptor, made up of three transmembrane protein subunits: IL-2Rα (CD25), IL-2Rβ (CD122) and IL-2Rγ (CD132). The combination of all three subunits is commonly termed the *high-affinity* IL-2 receptor, and binds its ligand with a K_d around 10pM. IL-2 can also signal via the dimer composed only of the β and γ subunits, though binding is at an intermediate affinity of around 1nM. Thus, the α subunit stabilises binding of the IL-2 ligand and facilitates transmembrane signalling [123].

There was, for some time, a lack of clarity on the extent to which the trimeric receptor is pre-formed before the binding of ligand. Fluorescence resonance energy transfer studies by Damjanovich et al. [26] showed that there was strong colocalisation between the three subunits. The authors argued that the intermediate-affinity receptor (the $\beta\gamma$ dimer) was most likely a pre-formed dimer, whereas the $\alpha\beta\gamma$ dimer was in a 'dynamic equilibrium' that was strengthened by the binding of IL-2 ligand.

The crystal structure of the full quaternary (ligand/trimeric receptor) signalling complex was described by Wang et al. in 2005 at a 2.3Å resolution[126]. They showed that the transmembrane tails of the β and γ subunits are closely positioned, while the IL-2 ligand binds in the 'fork' between the globular heads. IL2-Rα, on the other hand is positioned apart from the $\beta\gamma$ dimer at the membrane, and the head of the protein binds, via a long, connecting peptide, to a dorsally located site on the IL-2 ligand (see Fig. 2.2).

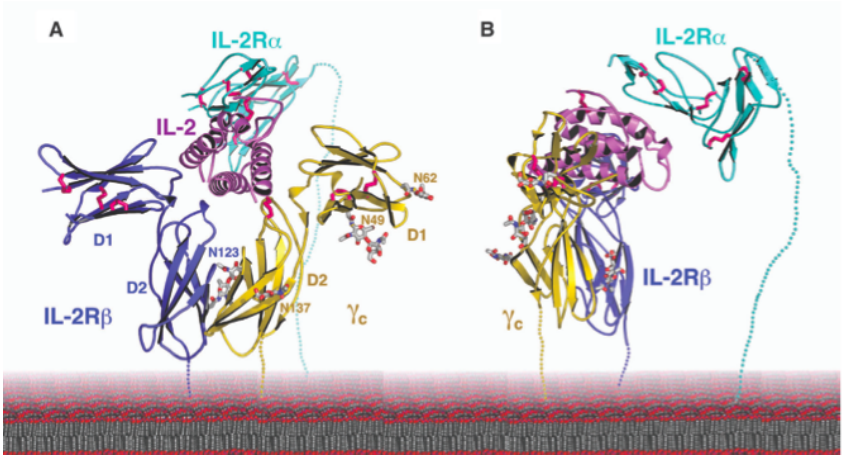

Figure 2.2: A model of the structure of the IL-2/IL-2R signalling complex. Reproduced from [126], with permission from Prof. K Christopher Garcia.

The authors state that the complex is held together via four binding sites: the ligand binds to the α, β and γ subunits independently; and the β and γ subunits bind to each other.

Later studies by Stauber et al. [109] provide further detail on the particular subunit interactions of the receptor. Of the interactions with the ligand and the various subunits, the largest buried surface area is between IL-2 and the α subunit, with around 1640Å^2 of total buried surface area. The contact between IL-2 and the β subunit is the second largest surface interaction at around 1155Å^2, and the smallest area of surface interaction is with the γ subunit at around 975Å^2. There are no covalent interactions between any of the constituent proteins. Instead, subunits are bound by van dar Waals contacts and hydrogen bonds, with the ligand forming 6 hydrogen bonds with the α subunit, 10 with the β subunit and 2 with the γ subunit.

The interaction between the β and γ receptor subunits, although again not covalently linked, is strong. The authors found around 1625Å^2 of total buried surface area; 14 hydrogen bonds and 90-97 van der Waals contacts binding the two components[109].

On the formation of the signalling complex, downstream signalling is initiated via tyrosine kinases Jak1 and Jak3[80, 71, 70]. Jak1 is associated with the cytoplasmic domain of the β subunit and Jak3 is associated with the γ chain. The transmembrane domain of the α subunit is very short and is not involved in transmembrane signalling [18]; the subunit serves only to localise diffusing IL-2 ligand at the cell surface and to increase the affinity of the ligand-receptor binding.

When ligand binds the high-affinity receptor, the Jak kinases phosphorylate tyrosine residues in three distinct regions of the intracellular tail of the β subunit, inducing the recruitment of the SHC adaptor protein (SRC-homology-2-domain-containing transforming protein C)[113, 18]. Phosphorylation of sites in the carboxy-terminal region of the β chain recruits STAT5 (signal transducer and activator of transcription 5). STAT5 is subsequently phosophorylated, leading to formation of homodimers, in which form it migrates to the cell nucleus, where it regulates genes involved in T_{reg} development[18, 70].

The SHC adaptor protein binds Grb2 and Gab2 (growth-factor receptor-related adap-

tor proteins), initiating the mitogen-activated protein kinase (MAPK) signalling cascade and the AKT (protein kinase B) signalling cascade, see Fig. 2.3. The signalling mecha-

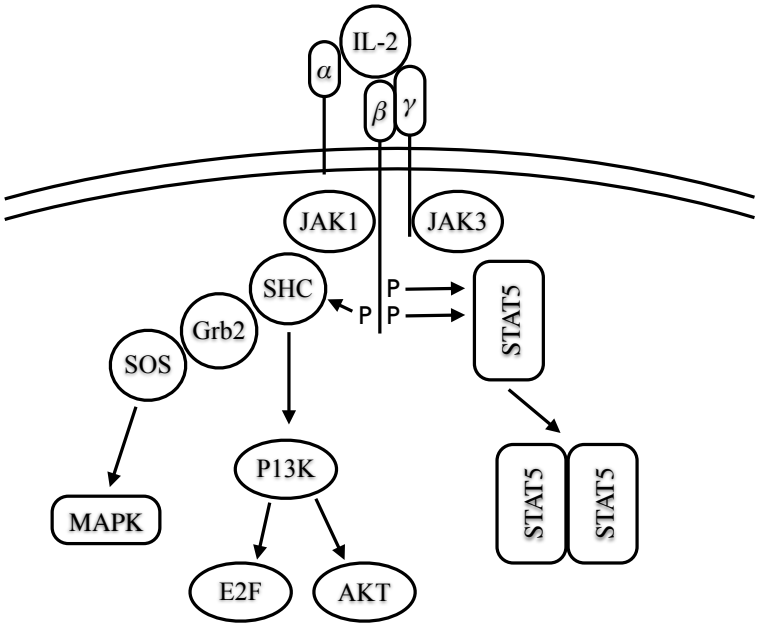

Figure 2.3: A diagram of the high-affinity IL-2 receptor with the associated recruited downstream molecules involved in signalling following ligation. Based on a figure from [70] by Malek et al.

nism described above contributes to growth, differentiation and survival of regulatory T cells.

IL-2 usually binds receptors on the T cell surface as a soluble factor. Recent studies by Wuest et al. [128], however, have identified alternative mechanisms for signalling by the IL-2 receptor, in which mature dendritic cells (mDCs) 'present' IL-2 to T cells tethered to IL-2Rα proteins on the mDC surface. They posit that this trans presentation of IL-2 mDCs to stimulate high-affinity-like signalling via the intermediate-affinity IL-2 receptor.

We have seen that specialised structures organised in the cell membrane (the immunological synapse) are necessary for effective T cell responses to foreign antigen signalling via the TCR. We now review studies examining the structure of the cell membrane and evaluate whether similar, smaller structures could be a more general feature of membrane-based signalling events.

2.2 The cell membrane

Cell membranes are made up chiefly of phospholipids, sphingolipids and cholesterol as well as a multitude of embedded proteins. They form an outer covering around the entire cell as well as compartments separating intracellular organelles. Phospholipids and sphingolipids have a hydrophilic head (usually positively charged or zwitterionic) and a hydrophobic tail and, when in solution, self-organise in order to form structures which minimise interaction between the hydrophobic tail segments and the water. These structures include *micelles*: small spheres with the phospholipid heads outermost and the tails innermost; *vesicles*: spheres with a bilayer surface with water both inside and outside; and *bilayer sheets*. The two halves of the bilayer are termed *leaflets*.

Phospholipid membrane bilayers are impermeable to water, allowing the cell to control molecular and ionic concentrations within the cytoplasm independently of the extracellular conditions and also to maintain diverse compartments within the cell with different functions. At the same time, they are flexible enough for the cell to deform its shape, either for migration, uptake of particles or other cells or mitosis. Parts of the membrane can bud off to form vesicles for trafficking molecules between organelles or delivering them to the extracellular membrane. The membrane also forms a support for proteins which may be embedded in a single leaflet, often via a lipid anchor covalently attached to the protein, or spanning the whole bilayer (*transmembrane proteins*).

This structural model in which protein species are embedded in the membrane but distributed essentially randomly has been termed the *fluid mosaic model* after a 1972 paper by Singer and Nicholson[106]. Recent evidence, however, points to a degree of lateral heterogeneity in the distribution of both proteins and lipids whereby patches of the membrane are enriched in particular molecular species. A term to describe this phenomenon which has become popular is the *lipid raft*: describing small, mobile patches of membrane with particular lipid compositions and associated protein content. While the lipid raft concept is useful in illustrating the spatial segregation believed to exist in membrane systems, the term has been used in the literature to describe a number of distinct phenomena in both cells and model membranes which has led to a degree of confusion in the field since its

inception.

2.2.1 Lipid rafts

The term *lipid raft* was coined in a 1997 paper in *Nature* by Kai Simons and Elina Ikonen[104]. Prior to this paper it had been noted that cells contained glycolipid-rich membrane complexes which were resistant to solubilisation by detergents (often termed DRMs or DIGs). DRMs are complexes which float to a low density during sucrose gradient centrifugation, typically after treatment with the detergent Triton X-100 at 4°C. Early studies observed that DRMs were enriched particularly in the lipids sphingomyelin (SM) and cholesterol and contained above-average proportions of certain proteins. Proteins found to be associated with these membranes included glycosylphosphatidylinositol (GPI)-anchored proteins and a number of palmitoylated and myristoylated proteins such as Src-family kinases[75]. At the outset, however, it is important to note that the particular location of DRMs within the cell – whether in the external plasma membrane or part of the intracellular organelles – was not clear and, furthermore, the presence of two proteins within the detergent-insoluble fraction is not necessarily indicative that they would interact, since they could have originated from two different locations within the cell. It was also known that sorting mechanisms for lipids existed within cells since studies of polarised Madin Darby Canine Kidney (MDCK) epithelial cells showed that a glycosphingolipid – glucosylceramide – was preferentially trafficked to the apical membrane of the cell rather than the basolateral membrane. Simons and Ikonen suggested that these lipid sorting mechanisms were used in cells of all types to facilitate lateral organisation within the cell membrane and that – in non-polarised cells – this lateral organisation would take the form of small, mobile patches, or *rafts*, of sphingolipids and cholesterol along with associated, embedded membrane proteins.

Additional evidence for the existence of specialised domains characterised by their particular lipid and protein content subsequently grew. Bagnat & Simon showed that rafts played a role in yeast polarisation during mating [7, 8]. Researchers investigated whether membrane rafts concentrated all diffusing species or whether particular membrane

proteins showed an affinity for raft regions. Glycosyl phosphatidylinositol (GPI)-anchored proteins were identified early as being preferentially associated with lipid rafts [17] as well as palmitoylated or myristoylated proteins [16].

2.2.2 Experimental methods

The use of cold Triton X-100 extraction as an investigation of membrane composition has been subject to criticism. An obvious argument is that the extraction is at 4°C: this is much colder than physiological temperatures and could artificially induce the formation of domains which would not be present in *in vivo* conditions. One study[50] has also used a combination of NMR and calorimetry to show that, in certain cases, the Triton X-100 treatment itself induced domain formation rather than simply separating existing domains from the remaining membrane.

Since the publication the paper by Simons and Ikonen, a degree of controversy has surrounded the raft hypothesis. This is mainly due to the blurring of distinctions between entities commonly associated with the raft hypothesis. In model bilayers formed from a mixture of phosphatidylserine (PS), SM and cholesterol (a somewhat simplified model of the lipid composition of mammalian cell membranes), the lipids naturally self-organise into distinct phases, especially at low temperatures. The SM – with relatively straight chain tails – and cholesterol forms *liquid ordered* regions where the lipid molecules are tightly packed and the phase is liquid crystalline in nature. This phase is often denoted l_o. The PS, on the other hand, has unsaturated lipid chain tails which contain kinks preventing tight packing of the molecules. This leads to a *liquid disordered* phase, denoted l_d, where lipid molecules have more freedom of diffusional, rotational and conformational motion. A third phase seen in lipid membranes is the gel phase, in which the degree of lateral order is even higher than in the l_o phase. Increasing the temperature of the system leads to phase transitions from gel to liquid phase, passing through l_o only in certain molar combinations of lipid components. When there is heterogeneity in the lipid composition of the membrane then certain ranges of temperature allow a coexistence of both gel and liquid phases or of l_o and l_d phases and equimolar amounts of SM and cholesterol seem to

favour this coexistence[39].

Liquid ordered domains also show resistance to detergent solubilisation which has led to the identification of DRMs with l_o membrane patches and with lipid rafts. A number of papers strongly advise against this automatic association: Lichtenberg et al.[66] stress that we must keep three separate categories distinct:

1. *DRMs*: the product of incomplete solubilisation of membranes, either *in vivo* or in model membranes

2. *Liquid-ordered domains*: a local discontinuity of phase formed by sterol-rich patches which facilitate an ordered conformation of lipid chain tails

3. *Rafts*: functional microdomains in an *in vivo* system which are enriched in sphingolipids and cholesterol

Specifically, the authors note that there is no evidence that rafts are necessarily *all* resistant to detergent extraction – even though this seems to be a property of complexes of that composition – and that detergent resistant fractions obtained from cells do not necessarily relate to rafts.

It should be noted that extraction of raft lipids by detergents other than Triton X-100, or by detergent-free methods yields different typical compositions. These differences are reviewed by Pike[89] who notes that the product of extraction by detergents Tween 20, Brij 58 or Lubrol WX does not show elevated levels of cholesterol or sphingolipid and that the use of Brij 96 and Brij 98 showed slight elevation of these components, but still much lower than the Triton extraction. Explanations for the discrepancy in composition could be that certain detergents have a higher selectivity for rafts (i.e. some also remove elements of the surrounding membrane) or that, in some extraction processes, only a fraction of the raft is obtained. A useful comparison is with detergent-free extraction methods. These methods include lysis by sonication or shearing through a syringe prior to gradient centrifugation. A version of the latter method outlined by Macdonald and Pike [69], is claimed to produce more consistent results across different cell lines than previous detergent or detergent-free extraction methods and also remove only plasma membrane rafts without contamination

from membranes in intracellular organelles such as the Golgi or ER.

Mukherjee and Maxfield[79] review research on intracellular lipid sorting mechanisms and how they may be involved in determining membrane composition. They challenge the assumption that the liquid ordered regions of a cell membrane (if these are taken to be synonymous with the detergent-insoluble fraction) form the minority of the membrane surface as detergent extraction with Triton X-100 at physiological temperature yields less than half of the plasma membrane. This would indicate that the 'raft' part of the membrane in fact formed the majority, leaving only small areas of higher fluidity.

The authors review evidence of lipid sorting mechanisms at a number of sites in the cell. Aside from sorting within the plasma membrane, they reviewed results detailing the trafficking of different lipid species within the sorting endosome. Whereas lipids with short, unsaturated tails and cholesterol were rapidly processed and recycled to the plasma membrane, other lipids with longer, saturated tails were transferred to the late endosomal/lysosomal pathway.

They hypothesise that it is preference for regions of different fluidity and curvature which facilitates the sorting of lipids at different locations. The sorting endosome itself has a structure with a central vesicle, sometimes with invaginations, and a number of long, branching tubules which detach to deliver lipids elsewhere. The authors propose three possible scenarios by which this sorting may take place:

1. That the tubules have a higher degree of fluidity than the central vesicle and hence shorter chain, unsaturated lipids migrate preferentially to those regions

2. That only the neck where the tubules attach to the vesicle has higher fluidity, creating a bottleneck allowing only the short-chain lipids to pass

3. That the invaginations on the central vesicle become enriched in the longer-chain lipids because of curvature properties

Many studies suggest that there are multiple types of membrane microdomain in living cells. A study on murine sperm membrane composition used a non-detergent method to separate membrane fractions and identified three subtypes of raft, each of which had a

reproducible signature of lipid and protein content [5].

2.2.3 Imaging of rafts

Pralle et al.[91] conducted one of the first studies investigating size and dynamics of lipid raft patches in cell membranes. They used a laser trap to measure the rate of diffusion of a fluorescent bead attached via antibodies to a single membrane GPI-anchored protein (placental alkaline phophatase – PLAP) in both Baby Hamster Kidney (BHK)-21 fibroblasts and male rat kangaroo kidney epithelial cells (PtK_2). GPI-anchored proteins are known to be associated with DRMs and hence are potential markers for lipid rafts. Using a model of lateral Brownian diffusion in a bilayer due to Saffman and Delbruck [97], the authors estimated the size of lipid rafts within the membrane as between 13 and 39 nm. It was observed that the lateral viscous drag of the fluorescent bead, denoted γ in the study, increased at two points in time, which the authors took to represent the bead first coming into contact with the plasma membrane and secondly binding to a membrane protein. The viscous drag was measured for a series of bead-attachment experiments both both before and after cholesterol depletion of the membrane using methyl-β-cyclodextrin. It was observed that viscous drag was decreased roughly threefold after the cholesterol depletion, indicating that the protein was bound in a cholesterol-dependent complex, increasing its effective area and hence viscous drag. Using the Saffman-Delbruck model of viscous drag for a cylindrical particle in a membrane:

$$\gamma = \frac{4\pi\eta_m h}{\ln\left(\frac{\eta_m h}{\eta_w r}\right) - \epsilon} \tag{2.1}$$

where the subscripts m and w denote, respectively, the viscosity of the lipid bilayer and the surrounding fluid; ϵ is Euler's constant (0.5772) and h and r are the thickness of the bilayer and the radius of the cylindrical particle. Using this model gives an estimate of the raft radius as 26±13nm. The authors also investigated attachment of a bead to a non raft-associated protein: YFP-GT46, finding that it had a low viscous drag which was unaffected by cholesterol depletion. This indicates that the increase in drag is linked

to raft-association rather than an overall change in membrane viscosity determined by cholesterol content.

Various fluorescence microscopy techniques have also been employed to study membrane heterogeneity. Although microdomains are typically on the lower limit of optical resolution, using two-photon microscopy on giant unilamellar vesicles (GUVs), researchers were able to successfully label coexisting l_o and l_d domains, and to examine the dependence of membrane curvature on domain composition [9]. An example of the fluorescence microscopy study from this paper is shown in Figure 2.4. Hao et al.[47] examined the effect of cholesterol depletion on the size and dynamics of domains formed in Chinese hamster ovary (CHO) cells. They used fluorescent lipid analogs with a known preference for either lipid ordered or disordered phase to discern the existence of membrane microdomains. While clustering was not observed in untreated cells, cells that had been depleted of cholesterol showed micrometer-scale patches of increased concentration of markers associated with lipid ordered phases, indicating that cholesterol plays a role in preventing domains from reaching this size *in vivo*. Replenishment of the system with cholesterol led to the disappearance of these domains over a time scale of around 10 minutes. The authors also used fluorescence recovery after photobleaching (FRAP) to investigate the dynamics of lipids involved in these micron-sized domains. While fluorescence recovery using the l_o-associated markers was slower in the patched areas of the cholesterol depleted cells than in the untreated cell, the difference was not great (mean half-life increase from 28 seconds to 68 seconds), indicating that the raft marker lipid was present in both the ordered and non-ordered region of the cholesterol-depleted cell membrane and that there was fairly unrestricted diffusion of molecules between the two regions.

Electron microscopy gives a much higher resolution image of a cell membrane. Because the process of preparing a sample for electron microscopy involves fixing the membrane in formaldehyde, this can interfere with sensitive systems such as microdomain formation and early studies were inconclusive. A paper by Hullin-Matsuda and Kobayashi[52], however, successfully observed spatial heterogeneity of SM domains in Jurkat T cells using gold particles attached via antibodies to a novel raft marker: lysenin. The domains were of the

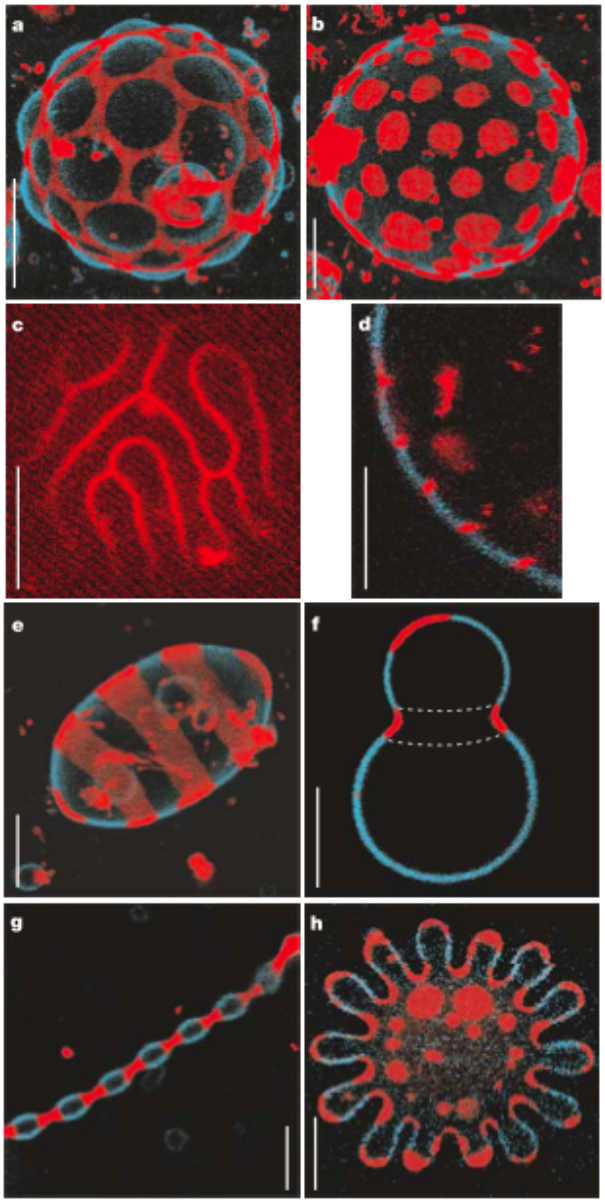

Figure 2.4: Two-photon microscopy images of l_o/l_d phase separation in giant unilamellar vesicles (GUVs). Reproduced with permission of Prof. Watt W Webb[9].

order of 60–80nm in radius.

2.2.4 Alternative models and terms in membrane heterogeneity

The increased focus on membrane compartmentalisation has led to other models in addition to the raft hypothesis on the exact structures which could compartmentalise cellular processes.

Many single particle tracking studies focus on the anomalous 'hop' diffusion which is observed in many membrane-bound proteins. This phenomenon describes an apparent paradox in which proteins are observed to diffuse at a relatively fast rate on short length scales, but at a slower rate on long length scales. Kusumi, Suzuki et al. showed that protein diffusion appeared to be slowed over longer length scales because proteins were temporarily confined to cellular compartments and took on the order of a millisecond to a second to hop to an adjacent zone [62, 111].

The authors propose that protein diffusion is mediated by a two-level system of compartmentalisation, with regular cytoskeleton-based 'fences' or cytoskeleton-bound protein 'pickets' creating a regular lattice driving hop diffusion of membrane-bound components by steric hindrance. They also propose a second, lipid-mediated system of *transient confinement zones* (TCZs), which slow short length scale diffusion and are embedded within the larger cytoskeleton-based compartments.

The TCZs of Kusumi et al. and the lipid raft model of Simons et al. are essentially two terms describing the same hypothesised structure. The difference in terminology stems from the experimental methods used to study them: TCZs are defined by retardation of protein diffusion in single-particle tracking studies and lipid rafts are defined by resistance to detergent solubilisation. Several studies combine the two approaches: Sheets et al. [102] showed that molecules with higher raft affinity displayed transient confinement diffusional behaviour more than molecules with low raft affinity. In addition, Dietrich et al. [32] showed that transient confinement behaviour was markedly reduced by cholesterol extraction.

Figure 2.5: An illustration of the actin cytoskeleton 'fence' model and the cytoskeleton-bound protein 'picket' model of membrane compartmentalisation. Original appears in [62].

2.2.5 Membrane organisation in signalling and disease

Membranes play diverse roles in cell function: as barriers maintaining different concentrations of ions and signalling molecules in different cell compartments; as structures in which proteins are embedded and trafficked and as a medium for the formation of tubules and vesicles which detach and deliver cellular components to other areas. Certain lipid components of cell membranes such as phosphatidylinositol (PI) also participate in signalling pathways: various phosphorylated species of PI are involved in the regulation of actin polymerisation in chemotaxis and phagocytosis.

The influence of membrane organisation and cholesterol metabolism on health and disease is reviewed by Simons and Ehehalt[103]; and Maxfield and Tabas[75]. One signalling system mentioned in the review that has been studied in some detail is the triggering of allergic reactions via IgE receptor interactions in mast cells. After crosslinking, the IgE receptor is found to be increased in detergent-resistant fractions along with the Src-family kinase Lyn. Lyn is ordinarily inactivated by a transmembrane phosphatase. Since transmembrane proteins ordinarily show preference for liquid-disordered domains, researchers hypothesise that lateral lipid organisation prevents Lyn inactivation, resulting in an increase of IgE phosphorylation. Depletion of cholesterol has been shown to inhibit signalling via this pathway[51].

As altering cholesterol content has a marked effect on plasma membrane structural properties and function, levels within the cell must be kept within an acceptable range. Maxfield and Tabas state that cholesterol levels are relatively high in the plasma membrane, endocytic recycling compartment (ECR) and trans-Golgi and that these areas show higher degrees of lipid order. On the other hand, a lower cholesterol level is maintained in the endoplasmic reticulum (ER).

The source of cholesterol is primarily from dietary intake and a number of mechanisms exist to buffer cellular levels including esterification by acyl CoA:cholesterol acyltransferase (ACAT), leading to storage of cholesterol within the cytoplasm in droplet form. At the systemic level, excess cholesterol is delivered via high-density lipoprotein (HDL) metabolism into the circulation, then to the liver where it is excreted into the bile.

The main disease linked to defects in cholesterol metabolism is atherosclerosis. This is an inflammatory process involving large-scale recruitment of macrophages and T-cells (although not neutrophils) in response to the formation of lipoprotein aggregates within the arteries. Uptake of the lipoproteins – oxidised low-density lipoprotein (LDL) is believed to be chiefly responsible – leads to phenotypic changes in the macrophages: increased rates of cholesterol uptake due to upregulated actin-dependent membrane protrusions and deposition of large quantities of cholesterol ester droplets within the cells. In this state, the macrophages are termed *foam cells* and, although in some cases they pass through the circulation and contribute to excretion of cholesterol, they also risk adhering within the arterial lumen, eventually occluding blood flow and increasing the risk of stroke, angina or myocardial infarction.

Simons and Ehehalt also describe the involvement of raft lipids in viral infection, prion diseases and Alzheimer disease (AD). A number of viruses, including influenza virus and HIV, interact with the apical membrane of polarised epithelial cells, either during the budding phase of the virus's life cycle or during transcytosis in order to cross through the host's mucosa.

In the case of AD, senile plaques are formed by aggregates of amyloid-β-peptide (Aβ). This peptide is formed by a process termed β-cleavage of amyloid precursor protein (APP)

– a transmembrane protein. There is a competing process (α-cleavage) which produces a different fragment, which does not lead to the formation of plaques. There is evidence that these processes are spatially segregated, with β-cleavage hypothesised to take place within lipid rafts and α-cleavage outside of them. Cholesterol depletion has further been shown to inhibit the β-cleavage process and formation of Aβ fragments in neurons [25].

Prion diseases also involve the formation of abnormal protein forms (PrPsc) of a host protein (PrPc). Both of these proteins are associated with DRMs unless the cell is cholesterol depleted. Depletion also downregulates the formation of the abnormal PrPsc protein.

The epithelial growth factor receptor (EGFR) is a molecule that has been found to be associated with lipid rafts and it has been demonstrated that manipulating membrane cholesterol content alters cell signalling behaviour via this pathway. Orr et al.[84] investigated the diffusional dynamics of EGFR and its dimerisation partner, HER2, using single-molecule fluorescence imaging. They found that, in the wild type cell, both molecules demonstrated periods of transient confinement during otherwise free diffusion. They also noted that cholesterol depletion almost completely prevented free diffusion of both types of receptor, whereas cholesterol enrichment increased the radius of the confinement zones.

It has been proposed that lipid rafts play a role in the recognition of bacterial LPS since a number of the membrane proteins involved in the LPS-stimulated MAPK activation pathway are found, either constitutively or following stimulation, in the 'raft fraction' obtained from lysed cells having undergone sucrose gradient centrifugation.

Triantafilou et al.[117] investigated the presence of a number of membrane proteins in the raft fraction both before and after stimulation by LPS in a human monocyte cell line (Monomac-6) as well as Chinese hamster ovary cells. They found that CD14 is constitutively present in the raft fraction and is excluded from the non-raft fraction. The centrifugation assay also showed that small quantities of the heat shock proteins Hsp70 and Hsp90 were found in the raft fraction with no stimulation, but that the majority were found in non-raft phases. After LPS stimulation, the distribution of CD14 was unchanged, whereas there was an increase in the levels of Hsp70 and Hsp90 within the raft fraction and TLR4, CXCR4 and GDF5 were also detected in the raft fraction where they had pre-

viously been excluded. This result was verified by recording FRET measurements between the membrane proteins in question and GM1 ganglioside – a protein which had previously been found in rafts and which was also constitutively present in the raft fraction in this study. The FRET measurements agreed with the centrifugation assay in that the distribution of CD14 was unchanged; levels of raft-associated heat shock proteins were increased after stimulation and TLR4, CXCR4 and GDF5 were not found before stimulation but migrated to the raft phase after stimulation.

The researchers also investigated the effect of disrupting raft formation by treating cells with nystatin or methyl-β-cyclodextrin (MβCD). They found that this treatment inhibited the association of all of the above proteins with lipid rafts and also that production of TNF-α was reduced after treatment with either substance.

Microdomain association is also implicated in the clustering of the ζ chain as a prelude to TCR complex organisation. Gosse et al. [45] modified transmembrane sequences in order to influence crosslink-dependent partitioning into microdomains and found that subsequent cellular signalling responses were highly dependent on such transmembrane sequences.

More recent studies by Cho et al. [24] suggest a central role for lipid microdomains in maintaining $CD8^+$ T cell sensitivity to interleukin signalling. In response to low-level self signalling via the TCR, naive $CD8^+$ cells upregulated the expression of GM1, which is associated with lipid rafts and became hypersensitive to IL-2, IL-7 and IL-15. In order to establish the dependence on microdomain organisation, the researchers pre-treated cells with MβCD and found that cells did not become hypersensitive.

De Mello Coelho et al. [30] also found that microdomains appeared to be linked to T cell differentiation as microdomain-associated GM1 expression differed between murine $CD4^+$ and $CD8^+$ thymocyte and T cell subsets. They also noted that GM1 expression was relatively constant on thymic thymocytes and peripheral $CD4^+$ T cells as the mice aged, but that it was increased on $CD8^+$ T cells in the periphery.

As can be seen, hypotheses relating to the exact physical and chemical function of membrane microdomains or rafts are highly diverse and experimentally complex to answer

comprehensively. For this reason, modelling approaches help to clarify the exact physical nature of the mechanism under discussion and test predictions which are hard to explore experimentally. We review several such approaches below.

2.3 Modelling membrane diffusion and immunological signalling

Mathematical and computational modelling is a tool that is increasingly being employed to clarify the complex dynamics underlying biological signalling processes. Callard & Yates [20] review the arguments for further integration between mathematical and biological research groups arguing that the non-intuitive behaviour which arises from systems composed of multiple components require a modelling approach to adequately and systematically probe mechanistic hypotheses. They assert that the general shift from a taxonomic to a systems understanding of biology necessitates a more comprehensively quantitative statement of biological hypotheses and that the 'interdisciplinary approach combining experimental immunology with mathematics is rapidly becoming the norm rather than the exception.'

Below, we summarise the basic mathematical and computational approaches used in this thesis. We also review several studies which use mathematical and computational methods to investigate possible mechanisms and ramifications of domain formation in the plasma membrane, as well as some general models of immune function. Some of these approach the problem from the perspective of the raft formation mechanisms and some model the interactions between pre-formed rafts and embedded proteins.

2.3.1 Microdomain formation

Almeida et al. [3] review thermodynamic principles governing the self-organisation of lipid membranes based on a parameter called the *unlike nearest-neighbour interaction Gibbs free energy*, usually denoted ω_{AB}. This parameter is sufficient to design a lattice-based simulation with two lipid types, which segregates according to the value or ω_{AB}. High values of ω_{AB} leads to complete separation into domains of lipid A and lipid B; a value

of zero allows random mixing whereas a negative value penalises self-association and the two species tend to alternate in position, forming a checkerboard arrangement.

Yethiraj and Weisshaar [132] use a similar modelling approach to propose reasons for the lack of micron-scale domains in living cells. They include immobile structures representing membrane proteins in the Monte Carlo simulation that have no energetic interaction with the surrounding lipid. They show that including obstacles significantly disrupts the tendency of the mixture to phase separate, with the boundary of the two phases tending to coincide with the obstacles. Of course it is unrealistic to assume that the energetic interaction of membrane proteins with the membrane is a neutral one, but the simulation demonstrates that these interactions should be taken into account, and goes some way to explain why different behaviour is seen in model membranes and live cells.

Turner et al.[118] take a different approach to explaining limited domain sizes in live cells. They consider a system where domains are formed by constant fusion and scission processes and where there is membrane recycling, i.e. removal and replenishment of rafts in the system. This analytical approach shows that, under biologically plausible parameter values, removal of rafts from the membrane prevents domains from coalescing to micrometer sized patches and that average domain radius would be in the range 10–70nm: a result which agrees well with the estimate of Pralle et al.

Richardson et al.[94] also consider an analytical model of domains undergoing fusion and scission processes, deriving a two-parameter distribution of domain sizes at equilibrium. They then show that this distribution can be fitted well with experimental measurements of microdomain sizes, which the authors measure in artificial membranes composed of various compositions of phosphatidylcholine (PC) and cholesterol. Domains were measured using fluorescence microscopy and atomic force microscopy was also used to probe the membrane topography.

A reaction-diffusion simulation modelling particle trajectories in the cell membrane reproduced diffusional behaviour similar to raft-associated proteins simply as a result of protein clustering effects. The cross-linking of other proteins in the membrane corralled

proteins in small domains of around 0.2 μm in diameter. This study was not dependent on lipid heterogeneity, rather on the spontaneous formation of protein clusters which trapped other membrane components for short periods of time[6].

Various research groups have also created computationally intensive molecular dynamics (MD) simulations to study spontaneous microdomain formation in membranes composed of multiple lipid types. Pandit et al. managed to demonstrate spontaneous phase separation in a MD model of binary and ternary mixtures [87]. Berkowitz et al. [11] created a molecular dynamics model of both binary mixtures (phospholipids with cholesterol) and ternary mixtures (two phospholipid species with cholesterol), but failed to find a 'clear molecular picture' explaining microdomain formation. Risselada & Marrink were more successful [95], creating an MD model that featured spontaneous separation of a ternary saturated phosphatidylcholine/unsaturated phosphatidylcholine/cholesterol mixture into both l_o and l_d domains with similar properties to experimental data.

2.3.2 Immunological signalling

Given the complexity of the many cellular and molecular interactions in the immune system, the field has long been explored using mathematical and computational models to test, generate and clarify hypotheses.

Kleinstein [60] illustrates the contributions made to immunology through computational models examining affinity maturation in B cells and notes the tendency for modelling papers to be published more and more in leading immunology journals, rather than more specialist computation biology publications.

Andersen et al. [4] took a mass action approach to fit T cell response to determine a mathematical relationship between T cell activation and ligand affinity, calibrated using immobilised ligand attached to fixed plastic surfaces.

Given the complex networks on which biological processes depend, many modelling approaches analyse the structural and logical properties of the networks themselves. Beyer et al. [12] merged logical models of the TCR signalling network and the IL-2 signalling network, leading to a better understanding of crosstalk between the two systems and the

dependence of ERK and STAT activation on the various upstream enzymes.

An ordinary differential equation (ODE) model of T cell proliferation in response to extracellular IL-2 stimulation was developed by Fallon & Lauffenburger [36]. This model was motivated by the desire to elucidate the mechanism by which an IL-2 variant (2D1) resulted in increased proliferation in KIT-225 T cells. The model suggests that, although the variant ligand has similar binding affinities to the IL-2 receptor, the difference in behaviour can be explained by an enhanced rate of receptor recycling from the endosome[37].

This model was later adapted by Bidot et al. [13] in order to increase the scope and incorporate upstream signalling events: the link between ligation of the TCR and subsequent expression of IL-2 and IL-2 receptor.

Several models also approach T cell proliferation at the cellular, rather than protein, scale. Deenick et al. [31] model the temporal regulation of cell proliferation and death rates over successive cell divisions in response to varying levels of IL-2 stimulation. This stochastic model assigned a Gaussian distribution to cells determining the time they take to enter the first division and the proportion that die with each division. Fitting the model to experimental data, the authors found that IL-2 contributed strongly to the proportion of cells entering the first division stage, but not the time to the first division. This model was later reformulated by de Boer et al. [29], in order to explore data on cell proliferation studies using the dye carboxyfluorescin diacetate succinimidyl ester (CFSE). By making the death rate of cells dependent on the number of divisions through which they have passed, they improve on the descriptive power of Deenick's model.

Another model examining the T cell proliferation response at the cellular level is the *crossregulation* model developed by Carneiro et al. [22, 41]. This model describes the balance between regulatory and helper T cells in competition for extracellular ligand, as described above in Section 2.1.2.

Busse et al. [19] also examine the competition between T_{reg} and T_H cells for IL-2 in the extracellular space. Their model supports the role of a feedback loop between IL-2 secretion by T cells, and the expression of high-affinity ($\alpha\beta\gamma$) IL-2 receptors to produce switch-like behaviour in the proliferation of helper T cells, but also to increase the rate

at which regulatory cells consume the ligand. They note that T_{reg} cells must be within a range of a few tens of micrometers to T_H cells in order to regulate effector expansion.

This model is further developed by Feinerman et al. [38] who challenge some of the results of Busse et al. In particular, they argue that paracrine, rather than autocrine signalling loops are important in regulating T_H cell activation. They also argued with the model's prediction of a 'digital' secretion of IL-2α components, noting that this behaviour was observed at relatively long timescales, but that more varied levels of expression could be observed in the early phases of the model.

2.3.3 Microdomains in immunological signalling

Models have also been developed to investigate the interplay of raft dynamics and protein interactions. Rather than model raft formation from the bottom up, Nicolau et al.[81] took a 'designed dynamics' approach in order to investigate what the effect of changing raft size would be on protein-protein collision rates. The parameter space was explored based on three key system properties: the total area covered by rafts; the size of individual rafts (all rafts in the system are taken to be the same size) and a quantitity ρ which represented the ratio of the step size per timestep within a raft area to that in a nonraft area. Rafts were mobile and diffused according to the Saffman-Delbruck equation and proteins could move in and out of rafts freely. An interesting result was that, for all degrees of raft coverage, the rate of protein-protein collisions was maximised at around $\rho = 0.5$, but for different raft sizes. With 10% coverage, collisions were maximised in the case of 6nm rafts, whereas with 50% coverage the collision rate was greatest when rafts were 14nm in diameter. This result suggests that, for rafts to play a role in signalling via mediating protein-protein interaction, the effect is fairly sensitive to both size and total membrane coverage, and that the domain size which yields the greatest effect is extremely small: far smaller than can typically be observed experimentally.

Several authors also address the importance of spatiotemporal effects in binding kinetics. For example, Aleksic et al. [2] model the influence of spatial confinement to improve the predictive power of models of TCR interactions with major histocompatibil-

ity complex (pMHC). They find that considering the immobilisation of the receptor and ligand increases the effective half life of the interaction, and results in greater agreement with *in-vivo* behaviour than models based on kinetic measurements in solution. These results motivate further study of spatiotemporal factors in understanding and modelling cell surface signalling mechanisms.

2.4 Thesis stance

Given the complex debate around the exact structure, role and significance of lipid microdomain in cellular function, and the dependence of many of the central tenets on the hypothesis on the experimental techniques involved, we aim to take an agnostic position on the question of whether or not specialised microdomains exist in living cell membranes or their exact size or prevalence. Instead we concentrate on two physical properties associated with microdomains:

- The reduction in diffusion rate within microdomains
- The affinity of particular protein species for microdomains

Using a purely mathematical and computational approach, we investigate whether or not the simple presence of microdomains enhances protein complex formation in a simplified model membrane. We use IL-2 receptor formation as an example mechanism integrated into the diffusion model on a heterogenous space. Because of the many simplifications made, however, this work does not seek to create a realistic simulation of the IL-2 receptor organisation; rather to use this mechanism as a model in order to understand the fundamental properties of systems of monomers diffusing and interacting in a space with heterogeneous diffusion rates.

In addition to seeking evidence for the positive role of microdomains in facilitating receptor complex organisation, we will also investigate the interdependence of several physical and chemical parameters in order to determine which molecular mechanisms would be enhanced by the presence of microdomains of a particular scale, and which would not.

We will employ both purely computational and purely mathematical modelling techniques and show, where possible, the agreement between the two approaches.

Chapter 3

Trimeric receptor formation in a heterogeneous medium: a probabilistic modelling approach

3.1 Introduction

Compartmentalisation is central to biology. Multicellular organisms delegate key processes to specialised organs, themselves composed of various distinct tissues. These are, in turn, composed of cells, each adapted to fulfil its own function. At the subcellular level, lipid membranes partition the cell into distinct organelles, controlling the passage of functional molecules from organelle to organelle, and from the inside of the cell to the outside.

Since 1997, compartmentalisation in the lipid membranes themselves has also come under scrutiny. This was in response to a review paper in *Nature* by Simons & Ikonen [104] suggesting that small areas in the cell membrane enriched in cholesterol and saturated lipids (membrane *microdomains* or *rafts*) might act as protein sorting platforms regulating cell signalling and trafficking.

Membrane protein organisation is critical in signalling by cells involved in the immune response. In the formation of the T cell receptor (TCR), for example, lipid and protein species are coordinated to a single area where the T cell comes into contact with

an antigen-presenting cell (APC)[129, 46, 133]. The TCR is an example of membrane compartmentalisation on a fairly large scale, but smaller microdomain-mediated sorting of component proteins in order to form larger receptor complexes could be important in optimising the sensitivity of cells to low-concentration immunostimulatory signals in order to effect a timely and proportionate response.

We are interested here in the organisation of the trimeric membrane receptor for the short-range cell signalling molecule (cytokine) interleukin 2 (IL-2). IL-2 is an autocrine signalling molecule expressed by T cells in response to TCR binding and is involved in the activation and proliferation of cytotoxic T cells as well as the maintenance of populations of regulatory T cells (T_{reg} cells)[18]. This system is of interest because there exists relatively little modelling of multi-component membrane receptor organisation involving microdomains and because controlling sensitivity of T cells to IL-2 ligand is of interest in therapies for immune deficiency and leukaemia.

3.1.1 Compartmentalisation in lipid membranes

The model in which protein species are distributed essentially randomly in the membrane was termed the *fluid mosaic model* after a 1972 paper by Singer and Nicholson[105]. Recent evidence, however, points to a degree of lateral heterogeneity in the distribution of both proteins and lipids whereby patches of the membrane are enriched in certain species and, rather than migrating freely throughout the membrane, protein diffusion may be constrained by interaction with the lipid environment, other membrane proteins or cytoskeletal components.

Studies in cholesterol-enriched model membranes show phase separation into liquid-ordered and liquid-disordered domains on the scale of several micrometers[44]. *In vivo*, domains of this scale are not ordinarily observed, but evidence for lateral segregation of lipid and protein species on a smaller scale (around 10–100nm) exists based on methods such as fluorescence resonance energy transfer (FRET), fluorescence recovery after photobleaching (FRAP), atomic force microscopy (AFM) and single-particle tracking (SPT)[63].

Computational approaches have shed light on the role of lateral segregation in protein

sorting. Pandit[87] and, more recently, Risselada & Marrink [95] have shown spontaneous phase separation into distinct domains in near-atomic scale simulations of ternary lipid mixtures; the latter are working on models of diffusion of the membrane-integrated syntaxin proteins. Nudelman *et al.* created a Monte Carlo simulation to probe the influence of lipid microdomains on B cell receptor interactions with multivalent ligands [83].

Nicolau *et al.* [81] constructed a stochastic model to determine 'optimal' characteristics of membrane microdomains in terms of their individual size and total membrane coverage. The authors measured the number of collisions within a population of diffusing 'protein' particles and the proportion of proteins which were sorted into microdomains. They found the proportion of proteins sorted into microdomains was highest when the ratio of the diffusion rate inside microdomains relative to the rate outside the microdomains was low and when the total microdomain coverage was high. Furthermore, the protein-protein collision rate was almost unaffected by the presence of microdomains unless the microdomains were mobile but, when mobile microdomains were present, there existed an 'optimal' microdomain radius which maximised the collision rate.

In this study, we examine a system where three distinct diffusing proteins species interact to form a trimeric complex. We determine the influence of microdomain characteristics and affinities between microdomains and diffusing proteins on the equilibrium state of the system.

3.1.2 Formation of the IL-2 receptor

The IL-2 receptor (IL-2R) is a complex made up of three subunits termed α, β, and γ. The subunits of the receptor are involved in diverse signalling pathways: the γ subunit is also involved in transducing signals initiated by the binding of at least six other cytokines: IL-4, IL-7, IL-9, IL-15 and IL-21[14]. In the case of IL-15, the β subunit is also part of the receptor complex and there is a distinct IL-15Rα component which makes up the trimer. Molecular models of the individual components of the IL-2 receptor are shown in Figure 3.1 and a representative diagram of the receptor embedded in a microdomain region of the membrane is depicted in Figure 3.2. Although both IL-2 and IL-15 can signal through

(a) The α subunit (b) The β subunit (c) The γ subunit

Figure 3.1: The three subunits of the IL-2 receptor. (PyMOL renderings of protein database structures, courtesy of Wikimedia user Emw).

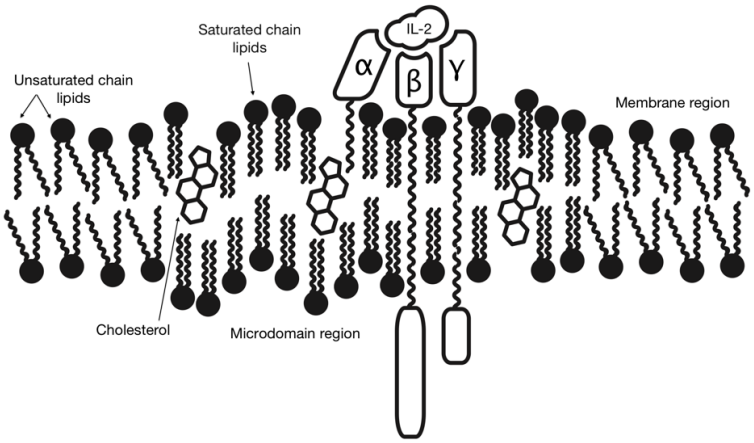

Figure 3.2: A cross section of the membrane, showing a microdomain region containing mainly saturated chain lipid molecules and cholesterol with a bound trimeric IL-2 receptor. The α subunit is inserted only into the outer leaflet of the membrane, whereas the β and γ subunits contain long, transmembrane domains.

the partially formed $\beta\gamma$ complex, the addition of the α subunit increases the affinity of the ligand binding[113]. Thus there is competition between the two cytokines at two levels: both compete to bind to the $\beta\gamma$ receptor and the IL-2Rα and IL1-5Rα subunits compete to form a complete heterotrimer in order to bind their ligand with high affinity. In this type of system, the sorting of component proteins in the membrane could be crucial in determining whether the cell responds to an IL-2 or IL-15 signal as each cytokine has the potential to act as an antagonist for the other.

There is evidence that sorting of membrane proteins is involved in receptor formation: subunits have been found associated with membrane microdomains both by detergent extraction methods and FRET co-localisation measurements. Exactly which subunits are microdomain-associated, however, varies in different investigations.

Matkó *et al.* found all three subunits of the IL-2 receptor in the detergent-resistant (microdomain) fraction, both in the presence and absence of IL-2 ligand. FRET efficiency measurements also indicated co-localisation between all subunits and microdomain-associated proteins including CD48[74, 120]. An independent study by Goebel *et al.*, however, examined the distribution of the subunits of the IL-2R and IL-15R and found only the β subunit expressed in the detergent-resistant fraction[43]. On ligation, there was partial translocation of the β subunit into the membrane fraction. A third investigation by Marmor & Julius found only the IL-2Rα subunit enriched in the microdomain fraction[73].

Vámosi et al. combined fluorescence cross-correlation microscopy with FRET measurements to determine that all the subunits of the IL-2 receptor form clusters in lipid microdomains, along with the IL-15Rα subunit, which shares the β and γ chains in forming the trimeric IL-15 receptor, and the MHC class I and II glycoproteins. The domains were also rich in the lipid raft marker protein GM1[119].

Studies by Bene et al. [10] examined the clustering behaviour of the IL-2Rα chain in the cell surface by measuring homotransfer of fluorescence between membrane-bound proteins, including IL-2Rα and MHC molecules. They found evidence for clustering of IL-2Rα subunits in the membrane, and also for colocalisation of the α subunit with MHC molecules, supporting the earlier evidence by Vereb et al. [120] for microdomains to

influence the clustering of IL-2 receptor components.

De Bakker et al. [28] also examined clustering of α chains in the surface of FT7.10 cells, using near-field scanning optical microscopy (NSOM), finding that both IL-2Rα and the related IL-15Rα formed clusters on the spatial order of 350-450nm in diameter.

More recent work combining FRET analysis with centrifugation of cell membrane components by Pillet et al. [90] confirms the localisation of bound IL-2 receptor complexes to membrane domains in which diffusion is slowed, and also finds them present in the lipid raft fraction following centrifugation. The authors find a similar mechanism for the IL-7 receptor, where bound, preformed receptors are localised to membrane microdomains enriched in cholesterol and reduced diffusion speeds, which promote downstream signalling[96].

The balance between the two downstream pathways initiated by binding IL-2 or IL-15 ligand is a system of some complexity and the involvement of protein sorting would add further detail. As such, predicting the behaviour of a cell in response to competing IL-2 and IL-15 stimuli is not at all straightforward. Constructing models of the dynamics of the component proteins provides a tool quantitatively to assess how a cell responds to its environment in this situation.

Based on *in vitro* assays, IL-2 was assumed to be essential to T cell proliferation in response to TCR binding. Later studies with both IL-2 and IL-2Rα double knockouts, however, did not result in the expected impairment of the proliferative response in a murine model. This result led to the hypothesis that there were redundant growth factors active *in vivo* which could replace the IL-2 signalling pathway. IL-2 does play a role in managing the function of immune cells, however: mice unable to express IL-2 later develop autoimmune problems and an accumulation of activated $CD4^+$ cells[68]. Thus, the function of IL-2 is twofold: as well as inducing proliferation in activated T cells, it also sensitises them for activation-induced cell death in order to self-limit the scale of the immune response.

Regulatory T cells (T_{reg} cells) are a particular subset of the T cell population that are influenced by IL-2 and related cytokines. In mice which do not make IL-2 or the IL-2Rα subunit, T_{reg} cells disappear after 8 weeks of age. Those which lack IL-2Rβ also have severely reduced T_{reg} counts and those lacking the γ-chain produce no T_{reg} cells at

all[18].

IL-2 receptors are being considered as a possible therapeutic target to stimulate T cell populations in patients who are immunodeficient due to HIV/AIDS[59], or to block overproliferation of T cells in leukaemia[124]. An important consideration is that IL-2 has a high rate of systemic depletion and affects a large number of cell types. For that reason, high doses are currently required in therapy which can be toxic or lethal. Fallon & Lauffenburger used a computational model to identify parameters which increased T cell sensitivity to IL-2 ligand and thus design a mutant which could be used at a lower dose[36]. The model, however, assumed that the receptors for IL-2 were pre-formed. Optimising the formation of the receptor could lead to higher sensitivity to ligand and enable lower therapeutic doses.

3.2 Method

We construct a computational framework to examine the effect of varying quantitative and qualitative characteristics of the membrane environment on a ternary protein-protein interaction system. The reaction-diffusion system models the formation of IL-2 receptors in two stages. First, the β and γ subunits form a dimer (the medium-affinity receptor), subsequently the dimer binds to the α subunit to form the high-affinity $\alpha\beta\gamma$ receptor. The membrane is represented by a rectangular grid and the proteins and complexes follow a random walk trajectory.

In the following subsections we define four qualitatively distinct diffusion schemes, each of which is based on hypotheses raised in the experimental literature (see Figure 3.3).

3.2.1 Reduction in rate of diffusion within microdomains

In Scheme 1, a discretised membrane is uniformly seeded with subunit monomers and they are allowed to diffuse based on the values of the diffusion rate, D at their location (see Figure 3.3a). The value of D is lower within microdomains than in the remaining membrane. This is represented by the smaller size of the arrows in Figure 3.3a. If two subunits which can bind together to form a complex are positioned on the same grid point

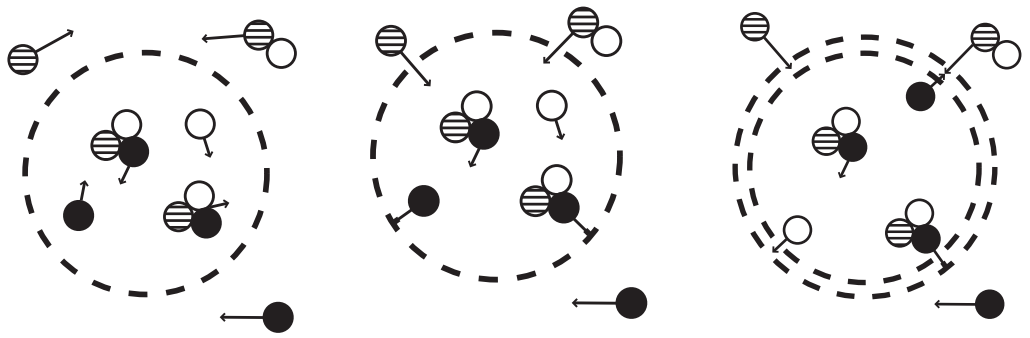

(a) Scheme 1: diffusion rate of all species is reduced inside the microdomain.

(b) Scheme 2 & 3: exiting the microdomain is limited either for certain species (Scheme 2) or all species (Scheme 3).

(c) Scheme 4: a boundary zone defines a region in which microdomain-associated and membrane-associated species can interact.

Figure 3.3: The four diffusion schemes investigated in this paper: solid black discs denote α subunits and striped and clear discs denote, respectively, β and γ subunits. The dashed line represents the boundary of the microdomain.

(voxel) then they may react together at a fixed rate. We vary the microdomain radii and total microdomain coverage and measure the number of monomers and complexes over time. We ran simulations until the number of protein complexes reached an approximate equilibrium and tested total microdomain coverage of 0%, 10%, 25% and 50% of the membrane and microdomain radii of 1, 2, 3, 4, 5 and 6 voxels.

3.2.2 Protein species with affinity to microdomain

Experimental studies indicate that membrane-bound proteins may have different affinities to microdomains, in that some species cluster together with saturated-chain lipids while others do not. We model this by defining probability values which dictate whether, on an attempt to move from a microdomain region to a membrane region, the move is permitted. Thus, a value of 0 means that the protein cannot cross the boundary, whereas a value of 1 means that there is no constraint on diffusion.

Ellery and Nicholls [34] hypothesise a mechanism whereby the α subunit segregates preferentially to the microdomain region. They propose that when subunits are segregated into microdomains, the microdomain radius is key in allowing or preventing formation of

	α	β	γ	$\beta\gamma$	$\alpha\beta\gamma$
Scheme 2: in	1	1	1	1	1
Scheme 2: out	p	1	1	1	p
Scheme 3: in	1	1	1	1	1
Scheme 3: out	p	p	p	p	p
Scheme 4: in	1	p	p	p	p
Scheme 4: out	p	1	1	1	p

Table 3.1: The probability, under diffusion schemes 2, 3 and 4, that a diffusing protein or protein complex will be allowed into or out of a microdomain. A value of 1 shows that the protein may diffuse freely across the boundary. The probability $p, 0 \leq p \leq 1$ denotes the strength of affinity for a microdomain or for the membrane. For the case $p = 0$, a protein or complex is irreversibly trapped in its current compartment (membrane or microdomain).

the trimeric receptor complex: small microdomains mean that α subunits can more easily interact with β and γ subunits at the boundary, but trimer formation would be inhibited by large microdomains. The sorting of α subunits to microdomains is also supported by the experimental results of Marmor *et al.*[73]

We investigated two diffusion schemes (see Figure 3.3b): in Scheme 2 we define an affinity of the α subunit (and any complexes which include it) for the microdomain, but no affinity for the remaining subunits (see Table 3.1). In Scheme 3 we apply an affinity for microdomain regions to all diffusing species. In these two schemes all diffusing species are free to enter the microdomains but, on an attempt to move out of the microdomain region, the move is only allowed with a probability p. Hence, a lower value of p describes a higher affinity for a particular species for the microdomain. We maintained microdomain coverage at 50%, and instead tested affinity values of $p = 0, 0.2, 0.5, 0.8$ and 1, and varied microdomain radii as in the previous case.

3.2.3 Proteins interact in boundary zone

To simulate the case where protein species are segregated into microdomain and membrane regions we modified the simulation to include a boundary zone of 1 voxel beyond the edge of the microdomain (Scheme 4). Both microdomain-associated and membrane-associated proteins can diffuse freely into this zone, but if proteins attempt to diffuse further into or further out of the microdomain area they can only do so with a fixed probability as

before. The probabilities for each protein species are shown in Table 3.1. This scheme more closely matches the hypothesis of Ellery and Nicholls[34], in which constituent components of the signalling receptor are segregated by the microdomains and can only interact in a boundary region.

In these simulations, we again maintained a constant microdomain fraction of 50% and varied the microdomain or radii, and the conditions on the boundary.

3.2.4 Simulation method

The simulation uses an implementation of the Gillespie algorithm to select which event will occur next and the waiting time between each event. Protein and complex locations are encoded by a rectangular matrix $X_n; X_n(\mathbf{i}) \in \mathbb{N}$, where the value of n encodes the particular species of protein or protein complex and the vector $\mathbf{i}$ gives the position. The value of each element $X_n(\mathbf{i})$ is the number of proteins or complexes at that position. A second matrix $D; D(\mathbf{i}) \in \mathbb{R}$ determines the relative diffusion rates at different spatial locations $\mathbf{i}$, representing the location of microdomains. The rate of diffusion of all species is reduced inside microdomains.

The membrane grid is initially seeded with proteins of different species distributed randomly. More than one protein of any species may occupy the same voxel. The radius, r of the microdomain is specified for each simulation. In placing the microdomains, a centre point (x_0, y_0) is chosen uniformly at random in two dimensions and then the surrounding voxels (x_i, y_i) are marked as within a microdomain if $(x_i - x_0)^2 + (y_i - y_0)^2 \leq r^2$.

The model uses the Gillespie algorithm direct method to calculate the order and time at which events take place, following the methodology in Gibson & Bruck[42]. All events have an associated rate and at each 'Gillespie step' one event is chosen at random according to the relative value of its rate. The time increment is dependent on the sum of all event rates.

The model is composed of five diffusing entities: three monomers representing the α, β and γ subunits of the IL-2 receptor, as well as the $\beta\gamma$ dimer and the $\alpha\beta\gamma$ trimer. In the model formation of the trimer is always in two stages, first by forming the dimer and

then by the α subunit binding to the dimer.

Events in the model can either be a movement event, a complexation event (either dimer or trimer formation) or a degradation event (the dissociation of a dimer or trimer).

For each diffusing entity, the movement rate is equal to the diffusion coefficient at its location. Hence the total sum of of movement rates is the sum of the occupancy of all grid points by each species multiplied by the diffusion coefficient at that point. We express this as:

$$S_{mov} = \sum_{p_D} \sum_{\mathbf{i}} X_{p_D}(\mathbf{i}) \cdot D(\mathbf{i}) \tag{3.1}$$

Here p_D represents the different diffusing species.

At each time step, dimers and trimers may form if subunits occupy the same grid point. Hence the rate of complexation at a single grid point is equal to the product of the number of subunits at that point that could potentially combine to form a larger complex, multiplied by the on-rate for the reaction. Hence the total rate is equal to the sum of these products over the whole grid. We express this as:

$$S_c = \sum_{p_{m_1,m_2}} \sum_{\mathbf{i}} k_c X_{p_{m_1}}(\mathbf{i}) \cdot X_{p_{m_2}}(\mathbf{i}) \tag{3.2}$$

where p_{m_1} and p_{m_2} are two species that have the potential to form a complex.

Finally, degradation occurs at a rate equal to the off rate multiplied by the total number of protein complexes in the whole system. This is:

$$S_d = \sum_{p_C} \sum_{\mathbf{i}} k_d X_{p_C}(\mathbf{i}) \tag{3.3}$$

The elapsed time between calculated steps in the system is calculated depending on the total sum of all event rates in the model. We first calculate a real value R_1 in the interval [0,1]. Then let the sum S of all event rates be:

$$S = \sum_{p_D} \sum_{\mathbf{i}} X_{p_D}(\mathbf{i}) \cdot D(\mathbf{i}) + \sum_{p_{m_1,m_2}} \sum_{\mathbf{i}} k_c X_{p_{m_1}}(\mathbf{i}) \cdot X_{p_{m_2}}(\mathbf{i}) + \sum_{p_C} \sum_{\mathbf{i}} k_d X_{p_C}(\mathbf{i}) \tag{3.4}$$

Where p_D are the protein species diffusing in the membrane, k_c is the rate of complex

formation for each pair of complex components p_{m_1} and p_{m_2} occupying the same grid point, p_C are the protein complexes and k_d is the rate of complex decay. From this we calculate the timestep $\Delta t = -\frac{\log(R_1)}{S}$.

After incrementing the timestep, the we choose an event to occur by choosing a second uniform random number, R_2 in the interval [0,1]. Then, if $s(i)$ is the rate at which event i occurs such that $\sum_i s(i) = S$, we choose event n to occur if:

$$\begin{aligned} \sum_{i=1}^{n-1} s(i) < R_2 S \leq \sum_{i=1}^{n} s(i), n \geq 2 \\ 0 < R_2 S \leq s(1), n = 1 \end{aligned} \tag{3.5}$$

Events in the simulations include: movement of proteins and complexes to adjacent grid points; formation of a complex from subunits situated on the same voxel; and decay of a complex to its constituent subunits. Movement to an adjacent voxel is chosen uniformly at random from the four neighbouring voxels and the space has periodic boundary conditions. In Schemes 2–4 a move is proposed but only accepted with probability p determined by the affinity of the protein species. If the move is rejected then the time is incremented but the protein remains on the same voxel.

For the results shown, simulations were run on a square grid with 2500 voxels, with 600 of each of the monomeric subunits α, β, and γ. The rate of diffusion of all species (proteins and complexes) was set to 4 diffusion steps per time-unit in the membrane and 1 diffusion step per time-unit in the microdomains. The values for k_c and k_d were 1 and 0.5 respectively. Simulations were run until the timepoint $t = 20$ and repeated 100 times for each parameter set.

3.3 Results

We constructed stochastic simulations of a ternary protein reaction-diffusion system and evaluated the influence of small microdomains in which diffusion was slowed. We also tested the effect of defining degrees of affinity between diffusing species and microdomains; either having affinity for a single protein species, all protein species or segregating protein

species so that protein-protein interactions are confined to a boundary zone.

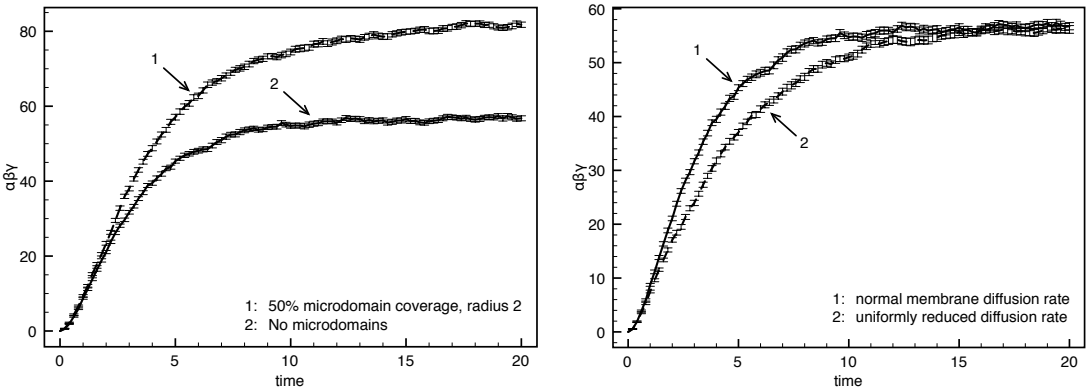

(a) The number of trimeric receptors formed plotted against time, averaged over 100 runs with protein diffusion slowed inside the microdomains.

(b) The number of receptors formed over time for the case where either there are no microdomains or the entire membrane has a reduced diffusion rate.

Figure 3.4: Plots of simulation ouput for Scheme 1 comparing reduced diffusion rate in microdomains with uniformly reduced diffusion rate. Error bars show standard error of the mean.

3.3.1 Presence of microdomains increases equilibrium number of trimers

Figure 3.4a shows the average time evolution of the Scheme 1 simulation for microdomains of radius 2. The presence of microdomains in which diffusion is slowed increases both the rate of $\alpha\beta\gamma$ trimer formation and the equilibrium number of trimers. For comparison, Figure 3.4b shows the time evolution where the diffusion rate is reduced to the microdomain diffusion rate across the entire membrane. In this case, the equilibrium outcome is unaffected but the rate of trimer formation is slowed.

We ran the same scheme for a range of microdomain radii and microdomain fraction values. The effect of varying these parameters on the equilibrium number of trimeric complexes is shown in Figure 3.5a. For all values that we tested, the presence of microdomains increased the number of trimers formed at $t = 20$. For microdomain coverage of 10% or 25%, the increase in trimer formation was highest for the smallest microdomain radii. At 50% microdomain coverage, smaller microdomains were also favoured, but the results indicate an 'optimum' microdomain radius of 2 voxels.

Although in most of the simulations we incremented the microdomain radius in whole voxels, we re-ran this simulation with fractional radii to check the value for the radius of 1 voxel and 50% microdomain fraction was not an anomaly. Although the radius is a non-integer, the microdomains are still discrete since voxels are included based on satisfaction of the inequality $(x_i - x_0)^2 + (y_i - y_0)^2 \leq r^2$ as in Section 3.2.4. The greatest number of trimers formed at equilibrium was obtained when the membrane microdomain fraction was at 25% and the microdomain radius was 1.5 voxels.

3.3.2 Microdomain affinity amplifies increase in equilibrium state

For 50% microdomain coverage, we tested five values of microdomain affinity by imposing a probability that a diffusion step will be accepted or rejected when a diffusing species attempts to move out of a microdomain region into the membrane. Figure 3.5b shows the equilibrium number of trimers formed in Scheme 2, where only the α component and the $\alpha\beta\gamma$ trimer have affinity for the microdomains. As in the results for Scheme 1, it implies an optimal microdomain radius of 2 voxels for all affinity values. As microdomain affinity is increased, the equilibrium number of trimeric complexes also increases dramatically. In Figure 3.5c the results for Scheme 3 – where all component proteins and protein complexes have a microdomain affinity – are similar to those for Scheme 2, but the increase in the number of trimers is amplified to an even greater extent. See appendix 3.6.1 for further results.

3.3.3 Confinement of protein-protein interaction to microdomain boundary inhibits receptor formation

Figure 3.5d shows the results for Scheme 4, where proteins and complexes can diffuse uninhibited into a boundary zone 1 voxel thick around the microdomains but diffusion from the boundary zone either into microdomains or out of microdomains is subject to affinity constraints. In the results shown, α proteins and $\alpha\beta\gamma$ trimers have affinity for microdomains given by the value of p, whereas the remaining species have affinity for the membrane and are prevented from entering the microdomains.

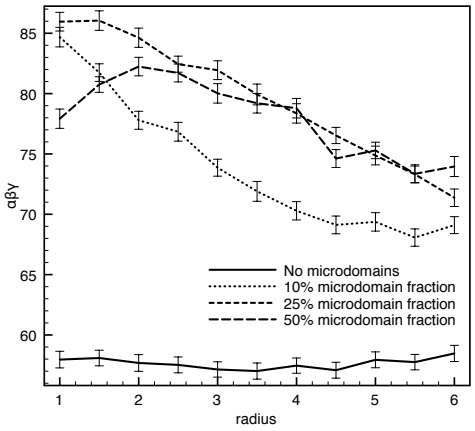

(a) Average number of trimers in the simulation at $t = 20$ plotted against microdomain radius, for four different values of microdomain coverage (Scheme 1).

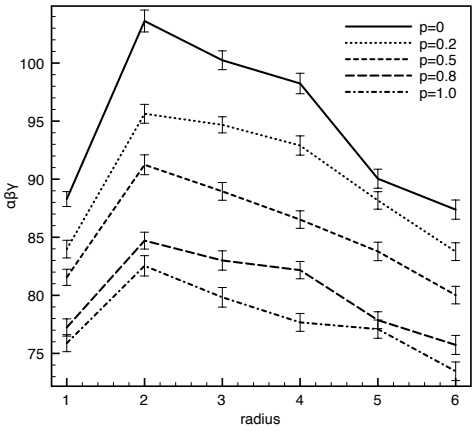

(b) Average number of trimers in the simulation at $t = 20$ plotted against microdomain radius where α subunits had affinity for microdomains (Scheme 2).

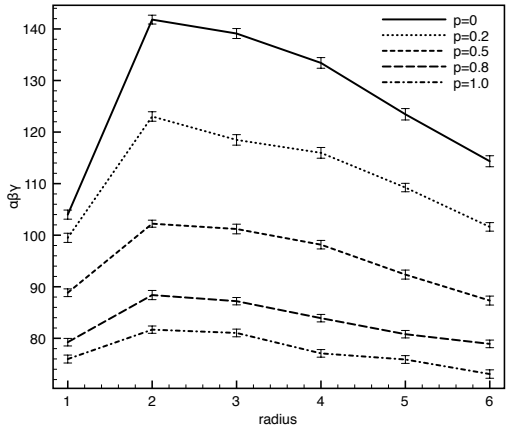

(c) Average number of trimers in the simulation at $t = 20$ plotted against microdomain radius where all subunits had affinity for microdomains (Scheme 3).

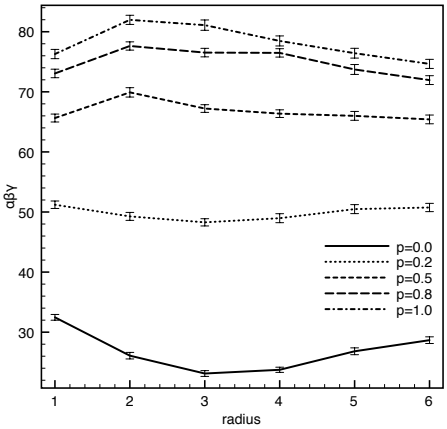

(d) Average number of trimers in the simulation at $t = 20$ plotted against microdomain radius where protein interactions were localised to microdomain boundaries (Scheme 4).

Figure 3.5: Plots showing the average number of trimers formed in equilibrium for all four diffusion schemes. Values are averaged over 100 simulations runs and error bars show the standard error of the mean.

In this case, as would be expected, stronger affinity values segregate the components of the receptor more severely and lead to lower numbers of trimers formed in equilibrium. For the strongest affinity values $p = 0$ and $p = 0.2$, the number of receptors formed is lower than the system with no microdomains. The effect of varying the microdomain radius depends on the strength of microdomain affinity. For strong affinity ($p = 0$), the results suggest that microdomain radii of 3 voxels lead to the strongest segregating effect and the lowest number of trimeric complexes in equilibrium. For weak affinity ($p \geq 0.5$), however, microdomain radii of 2 or 3 voxels results in a comparatively high number of trimers formed in equilibrium. See appendix 3.6.1 for further results.

Figure 3.6 shows the spatial distribution of trimers, averaged over 100 runs of the simulation for Scheme 4 with the microdomain coverage at 25%, strong microdomain affinity ($p = 0$) and the microdomain radius set at 4 voxels. The evolution from a low concentration and broad spatial distribution, to concentrated clustering of trimers on the boundaries of the microdomain can be clearly seen. Figure 3.7 shows the distribution of three of the diffusing species from the simulations: the γ subunit, the $\beta\gamma$ dimer and the trimer at time point $t = 20$. The varied spatial distribution of the different components is clear: γ subunits and dimers are sequestered to the non-microdomain regions of the membrane in the simulation, whereas trimers form only on the boundaries of the microdomains, where dimers are able to come into contact with the α subunit, which has strong affinity for the microdomain region.

3.4 Discussion

In this study, we have created an *in-silico* model of a cell membrane, incorporating compartmentalised diffusion processes, protein-protein interactions and membrane-protein affinity terms. Using this model, we investigated four qualitatively distinct hypotheses for the role of microdomain-mediated protein sorting on the formation of trimeric protein receptor complexes.

The simulation results show that the presence of microdomains with a reduced diffusion rate can increase the equilibrium number of trimeric receptor complexes in the cell

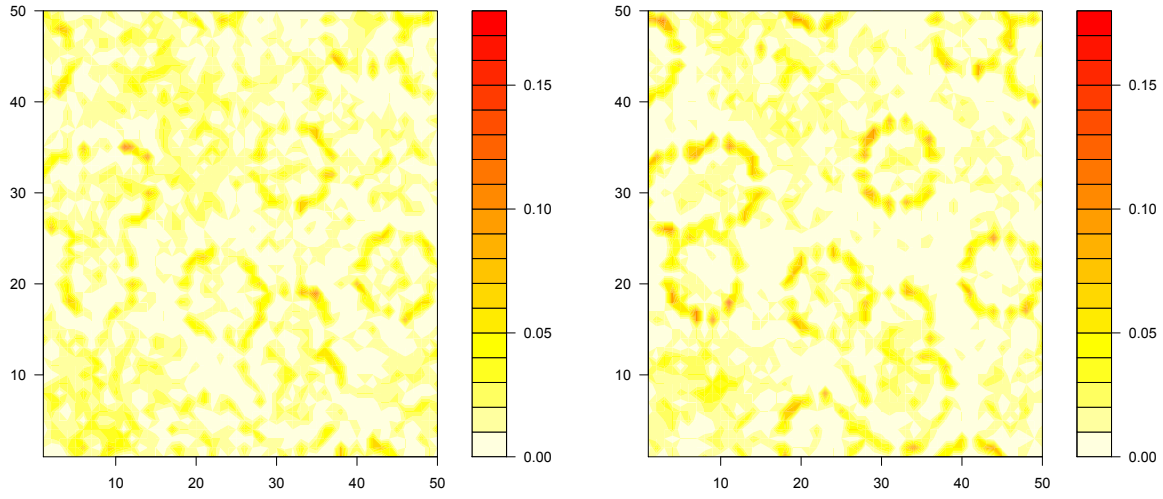

(a) $t = 5.0$

(b) $t = 10.0$

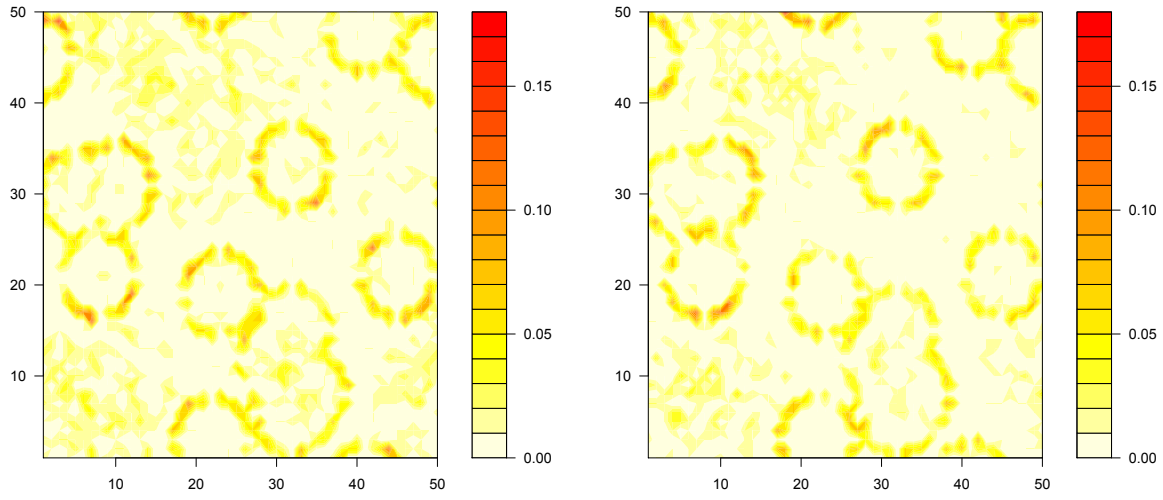

(c) $t = 15.0$

(d) $t = 20.0$

Figure 3.6: Heatmap plots showing the average number of trimers formed at subsequent time points in Scheme 4 with $p = 0$ and microdomain radius 4 voxels. Total microdomain coverage is 25%.

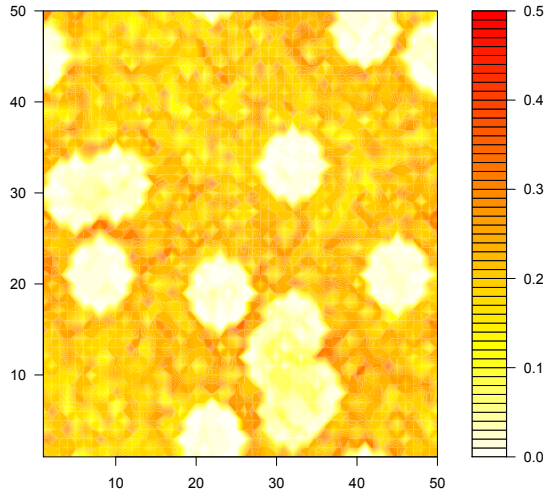

(a) γ subunits

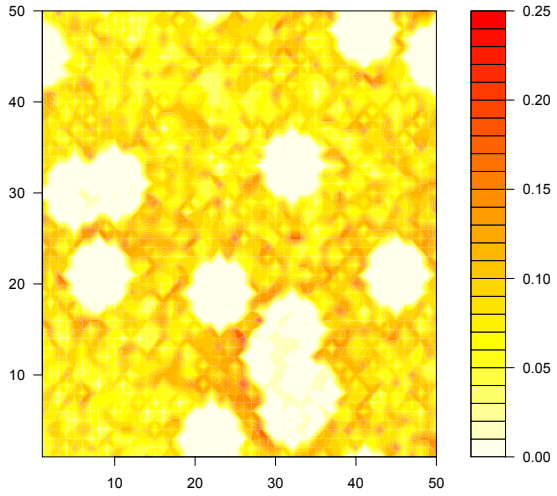

(b) $\beta\gamma$ dimers

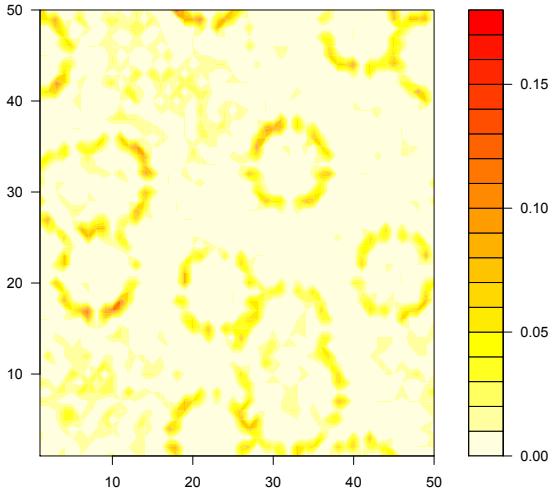

(c) $\alpha\beta\gamma$ trimers

Figure 3.7: Heatmap plots showing the average spatial distribution of various species in the simulation, with $p = 0$ at time $t = 20$. The microdomain radius is 4 voxels.

membrane. In the model, small microdomains maximise receptor formation. For relatively high (50%) membrane microdomain coverage, the results indicate the existence of an 'optimal' microdomain radius of around 2 voxels. As observed microdomains are indeed small (10–100nm), it could be explored whether there is an evolutionary mechanism selecting for microdomain size. The existence of optimal microdomain radii to facilitate protein-protein interactions is in agreement with the results of Nicolau *et al.*[81], but we saw this property for static rather than mobile microdomains. The reason for a difference in outcomes for a model based on binding and dissociation rather than protein-protein collision could be the number of distinct components needed to form the complex, meaning concentrating the subunits in a small area is more important.

An increase in the number of receptors when there was a high affinity for all protein species was unsurprising, but receptor numbers also increased when only the α subunit had increased affinity for the microdomains. This result could suggest that modifying protein subunits, by creating analogs or posttranslational modification, could be used to augment receptor complex formation. Also, since IL-2 and IL-15 share the $\beta\gamma$ complex, modifying one of the α subunits to increase its affinity for microdomains could be a potential tool to alter T cell fate by promoting the IL-2 signalling pathway over the IL-15 pathway or vice versa.

Finally the results from the Scheme 4 simulations show a role for the segregating effect of microdomains. Ellery & Nicholls[34] suggest that larger microdomains would inhibit receptor formation and small microdomains would promote it. Our results indicate that the strength of the segregating effect (microdomain affinity) is key in determining the number of receptors formed and that microdomain sizes that promote the greatest number of receptors when proteins have a low microdomain affinity can result in the lowest number of receptors when they have a high microdomain affinity.

Several limitations of the model should be addressed. First, the size of the simulated membrane is relatively small in order to generate a sufficient range of results in a short amount of time. The results of larger simulations (with 4×10^4 voxels) of Scheme 1 were similar to results shown here. Secondly, parameters were chosen for simplicity rather than

biological accuracy so results should be interpreted as a proof of principle rather than predictive of *in vivo* behaviour of the IL-2 receptor. The diffusion rate, particularly, was set equal for all proteins and protein complexes. In future work, we plan to make more biologically relevant predictions by using experimentally determined diffusion rates for all species. The model also did not limit the occupancy of each voxel; in later models we intend to investigate the limitations imposed by crowding inside microdomains. Finally, we have considered the formation of the IL-2 receptor in this model, but no ligand-receptor binding dynamics. We hope to address this mechanism and its influence on the proliferative response in future work.

In conclusion, we have discussed a model of IL-2 receptor formation in the T cell membrane in relation to the presence of microdomains in which diffusion is slowed and for which the diffusing species may have a particular affinity. While remaining agnostic to the mechanisms contributing to the formation of microdomains and indeed their prevalence *in vivo*, we have demonstrated that the presence of small membrane compartments with these characteristics can promote the formation of receptors relevant to signalling and suggested ways in which this could be therapeutically exploited. In light of these results, we think that spatial heterogeneity in the membrane is an important factor to consider in constructing larger models which incorporate transmembrane signalling components.

3.5 Further work

In future work, we plan to further explore the outcome of the above simulation using different parameter sets, and to address some of the limitations mentioned in the discussion section.

In particular, the model previously assumed that all species diffuse at the same rate. As mentioned in the introduction, there exists a predictive model from Saffman & Delbrück [97] for the diffusion rates of a cylinder diffusing in a lipid bilayer. In a more recent paper by Gambin et al., however, comparison with measured diffusion rates of a range of transmembrane peptides showed that diffusion rates are described better by a $1/R$ law than by Saffman & Delbrück's logarithmic relation. This was true both for single proteins

Symbol	Description	Proposed range of values
r	Microdomain radius	1–6
ϕ	Total microdomain coverage	0.0–1.0
p	Rejection probability at boundary	0.0–1.0
L	Size of simulation space	50px–500px
$k_{\beta\gamma}, \chi_{\beta\gamma}$	Formation/decay rate of dimer	
$k_{\alpha\beta\gamma}, \chi_{\alpha\beta\gamma}$	Formation/decay rate of trimer	
$D_{Z,1}$	Diffusion rate of species Z within microdomains	
$D_{Z,2}$	Diffusion rate of species Z in membrane	

Table 3.2: Summary of all parameters in the simulation described in this chapter.

of various sizes and multimeric complexes of increasing size [40, 65].

In order to test the effect of this result, we re-ran the simulation with an adjustment to the diffusion rate for the dimeric and trimeric complexes, where the diffusion rate was reduced by a factor of $\sqrt{2}$ for the dimer and a factor of $\sqrt{3}$ for the trimer. The results of this simulation are shown in Figure 3.8. Comparing them with Figure 3.5a shows no dramatic change in outcome. This is not unexpected, since one would expect the diffusional behaviour of the constituent subunits to affect the simulation outcome more than the diffusion of the formed complexes.

Further scenarios we aim to explore are: varying the ratio of the diffusion rate inside microdomains to the diffusion rate outside the domains; increasing the size of the space; imposing a restriction on microdomains to prevent them from overlapping and including more biologically realistic on and off rates for the formation of the protein complexes. An overview of all the parameters which can be varied in this model is displayed in Table 3.2.

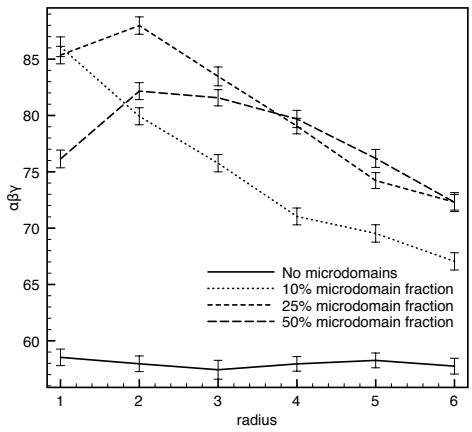

Figure 3.8: Average number of trimers in the simulation at $t = 20$ plotted against microdomain radius for Scheme 1, but with larger complexes diffusing more slowly according to a $1/R$ law.

3.6 Appendix A

3.6.1 Supplementary results

Simulations of Schemes 3 and 4 were also run with intermediate microdomain coverage values. The output of these simulations is shown in Figure 3.9.

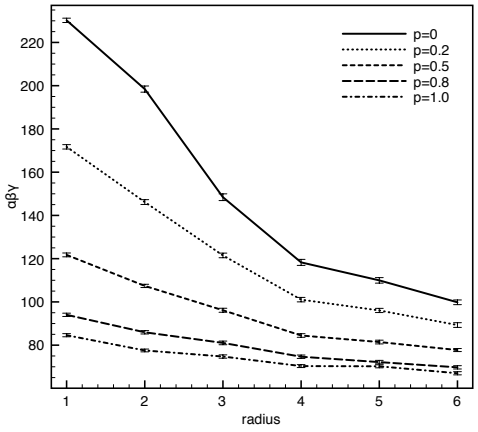

(a) Average number of trimers in the simulation at $t = 20$ plotted against microdomain radius, for Scheme 3 with 10% microdomain coverage.

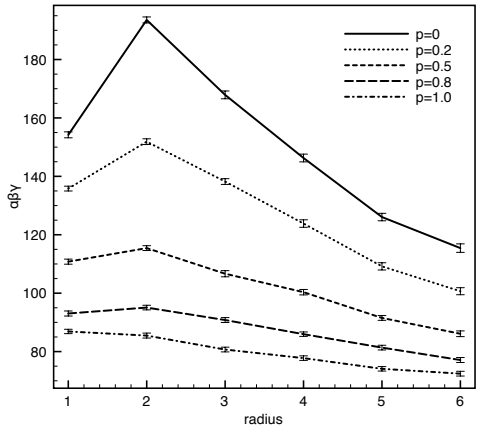

(b) Average number of trimers in the simulation at $t = 20$ plotted against microdomain radius, for Scheme 3 with 25% microdomain coverage.

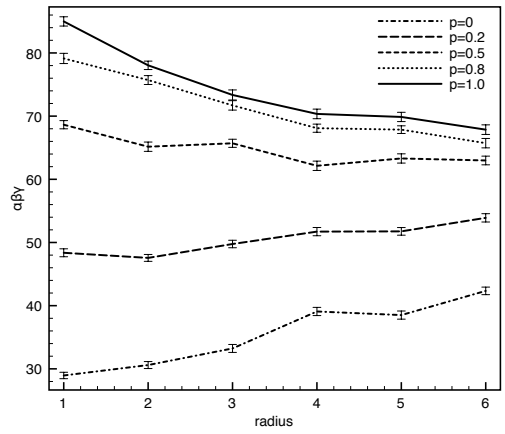

(c) Average number of trimers in the simulation at $t = 20$ plotted against microdomain radius, for Scheme 4 with 10% microdomain coverage.

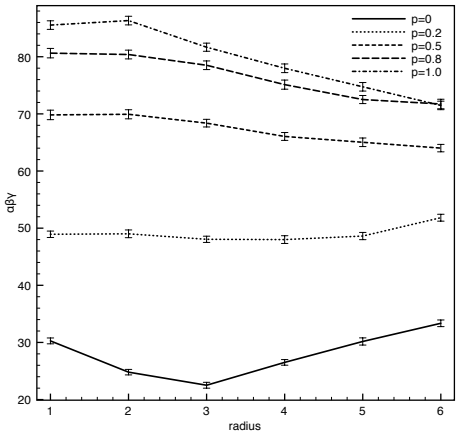

(d) Average number of trimers in the simulation at $t = 20$ plotted against microdomain radius, for Scheme 4 with 25% microdomain coverage.

Figure 3.9: Plots showing the average number of trimers formed in equilibrium for diffusion schemes 3 and 4 with microdomain coverage at 10% and 25%. Values are averaged over 100 simulations runs and error bars show the standard error of the mean.

Chapter 4

Reaction-diffusion processes with locally varying diffusion coefficients

4.1 Introduction

The simulation results in Chapter 2 suggest a mechanism by which small microdomains promote the formation of trimeric species from diffusing subunits in the membrane. Furthermore, smaller domain sizes have a greater effect in promoting trimer formation for the same degree of microdomain coverage. To gain greater insight into the diffusion behaviour promoting this effect, and its dependence on the key parameters of microdomain size and total area coverage, we re-implemented the model as a stochastic particle diffusion system in a one-dimensional space.

4.2 Numerical simulation in one dimension

4.2.1 Method

We simplified the numerical model in the previous chapter in order to examine the behaviour in a one-dimensional system and examine more closely the concentration profile of

monomers and complexes inside and outside the defined microdomain regions. Although we saw that microdomains were enriched with monomers in the previous chapter, we did not examine the local concentration profiles in order to determine the local distribution of particle.

Here we consider systems in which only monomers diffuse on a heterogeneous space and later examine dimerisation and trimerisation reactions.

We consider three numerical schemes in this section, which are illustrated in Figure 4.1. They are the following:

1. Monomers diffuse on a fixed one-dimensional space with no flux at the boundaries and one discontinuity (a step function) in the diffusion coefficient

2. As above but with two discontinuities (a square function) in the diffusion coefficient

3. Monomers diffuse on a periodic space with a square function discontinuity in the diffusion coefficient

We also consider the formation of dimers and trimers in the above three schemes. The

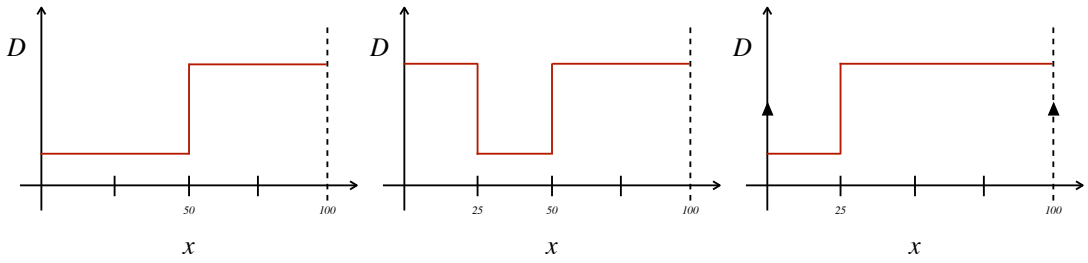

(a) Scheme 1 (b) Scheme 2 (c) Scheme 3

Figure 4.1: The three numerical schemes investigated in this section. The parallel arrows in Scheme 3 denote periodic boundary conditions, the other schemes have no-flux boundary conditions

simulation method is analagous to that used in the previous chapter, using an implementation of the Gillespie algorithm [42] to select events (either diffusion, complex formation or complex decay) at random; incrementing the timestep and then recalculating rates of all possible events. In this section, however, species instead diffuse independently on a 1×100 voxel grid.

In Scheme 1, we set the diffusion rate $D(i)$ to 1 diffusion step per time unit in the range $[0-50)$ and 4 diffusion steps per time unit otherwise. We implement the no-flux boundary condition by reflecting any diffusion steps beyond the edge of the space so that attempts to diffuse to the position $X(n+1)$ are reset to the position $X(n)$, where n is the grid size.

In Scheme 2 we use the same no-flux boundary conditions but instead define our microdomain region of lower diffusion speed in the range $[25-50)$.

In Scheme 3 we define the microdomain region in the range $[0-25)$ and define periodic boundary conditions such that diffusion to the position $X(n+1)$ is reset to position $X(1)$.

As there is a degree of stochasticity in the model and the grid size is not particularly large, the results plotted in the next subsection are the mean curves over 100 individual simulations.

4.2.2 Results

Examining the simulation profiles here gives us a better spatial understanding of the dynamics underlying the results of the previous chapter. Although we saw previously that areas of low diffusivity were relatively enriched in monomers, the exact spatial patterning was not evident.

We see the spatial pattern formed by diffusing monomers under scheme 1 in Figure 4.2. This shows that there is a sharp discontinuity in monomer numbers either side of the discontinuity in diffusion rate (at $x = 50$). Monomers are enriched immediately inside the low-diffusion region and depleted immediately outside it. With increasing time, the area which is enriched spreads further into the low-diffusion region and the depleted area spreads further into the high-diffusion region. The maxima and minima of the monomer profile appear to be relatively steady, increasing only slightly with time.

Including reaction-diffusion processes in the system, we see (Figure 4.3) that a similar profile is formed by the dimers in the system (under scheme 2) and the trimers (in scheme 3). For the purposes of this simulation, the forward and backward rates of the dimerisation and trimerisation steps were held at $k_c = 1$ and $k_d = 10$ respectively.

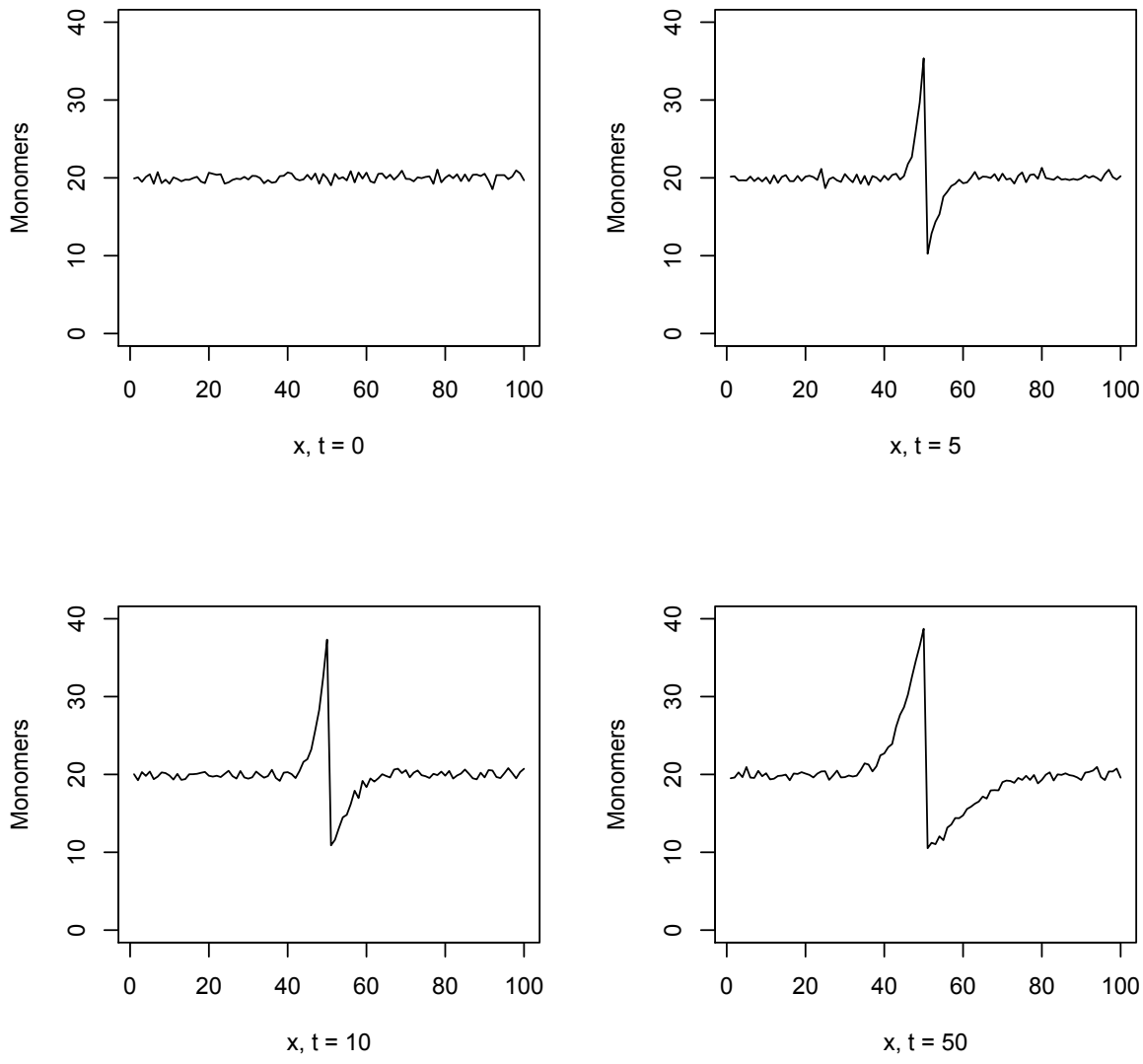

Figure 4.2: Evolution of the diffusion scheme 1 at subsequent time points. The space is initially seeded randomly with 2000 monomers over 100 grid points.

Figures 4.4 and 4.6 show the time evolution of the monomer profile under diffusion

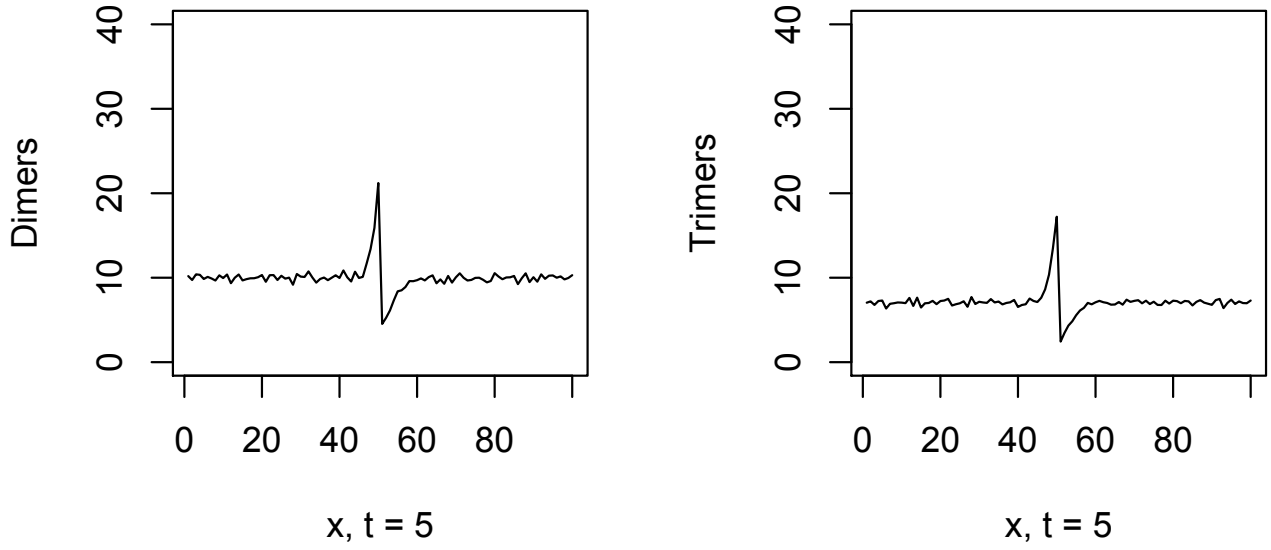

Figure 4.3: A profile of the dimer and trimer numers under diffusion schemes 2 and 3 at time $t = 5$. The space is seeded randomly with 2000 of each species involved: the left hand system contains only β and γ components and the right hand system contains α, β and γ components.

schemes 2 and 3. Scheme 2 illustrates diffusion in and out of a single microdomain of finite size. As might be expected, we see similar discontinuities in monomer number with enrichment inside the microdomain area and depletion outside it. Scheme 3 has periodic boundary conditions and so more accurately models a larger space with a series of square function discontinuities in diffusion rate. In Figures 4.5 and 4.7 we also see that this profile develops in the distribution of dimer and trimer complexes.

4.3 Analytical approach to heterogeneous diffusion

The numerical simulations detailed in the previous section show a slightly surprising form, with a sharp step in concentration at the microdomain boundary rather than a smooth variation as is usually found in diffusion problems.

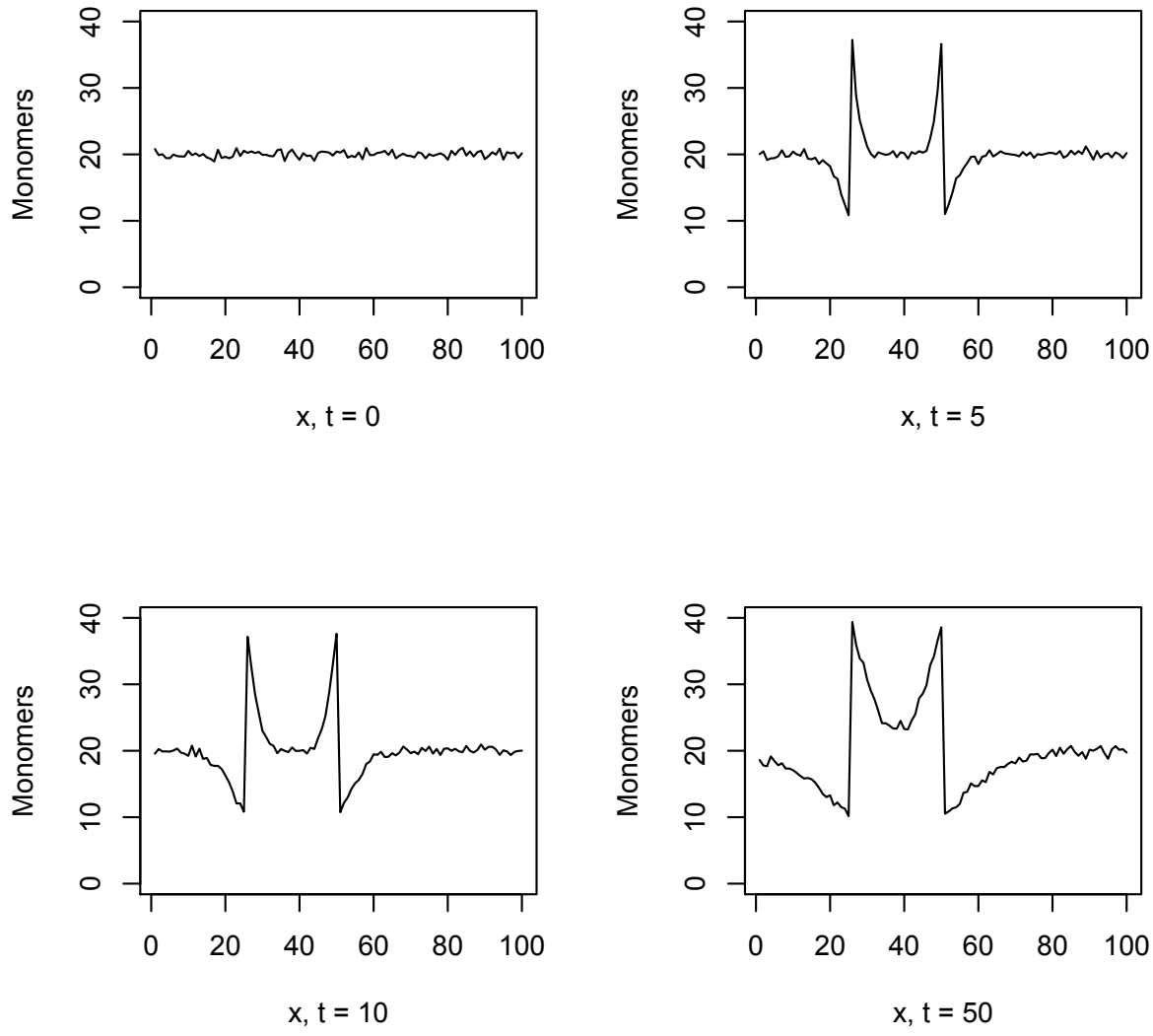

Figure 4.4: Evolution of the diffusion scheme 2 at subsequent time points. The space is initially seeded randomly with 2000 monomers over 100 grid points.

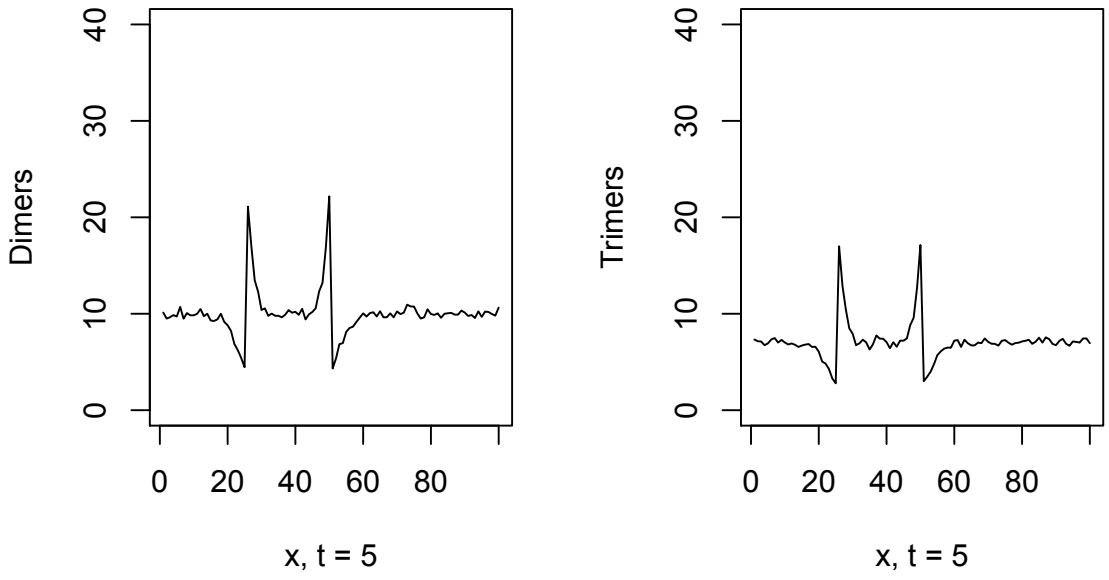

Figure 4.5: Profiles of the number of dimer and trimer complexes formed under diffusion scheme 2 at time $t = 5$.

This strange behaviour is addressed in van Milligen et al. [78], in which the authors note that, whereas in most cases it is sufficient to apply Fick's Law to diffusion systems:

$$\Gamma(x,t) = -D\frac{\partial n(x,t)}{\partial x} \tag{4.1}$$

(where $\Gamma(x,t)$ denotes the particle flux), this rule assumes that the value of D is constant for the medium in which particles diffuse. For the general case, however, it is necessary to solve the Fokker-Planck diffusivity law[64]:

$$\Gamma(x,t) = -\frac{\partial}{\partial x}[D(x)n(x,t)] \tag{4.2}$$

The authors show that analytical solutions of the Fokker-Planck diffusivity law approximate well the generalised master equation describing particle dynamics in their system of interest and reproduce the phenomenon in a series of physical experiments involving the diffusion of dye in a gelatine medium that had been set in two separate connected blocks,

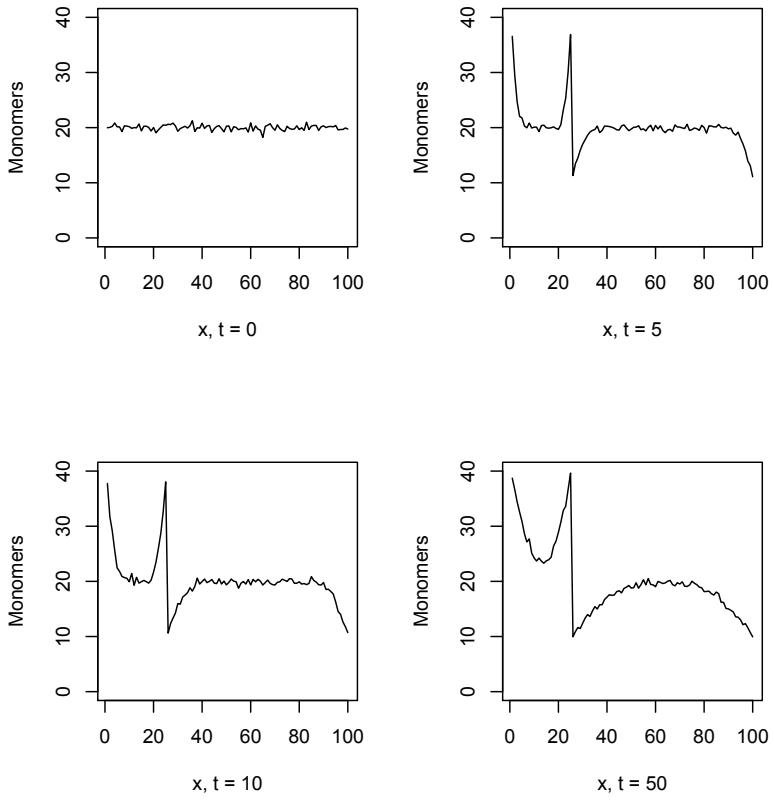

Figure 4.6: Evolution of the diffusion scheme 3 at subsequent time points. The space is initially seeded randomly with 2000 monomers over 100 grid points.

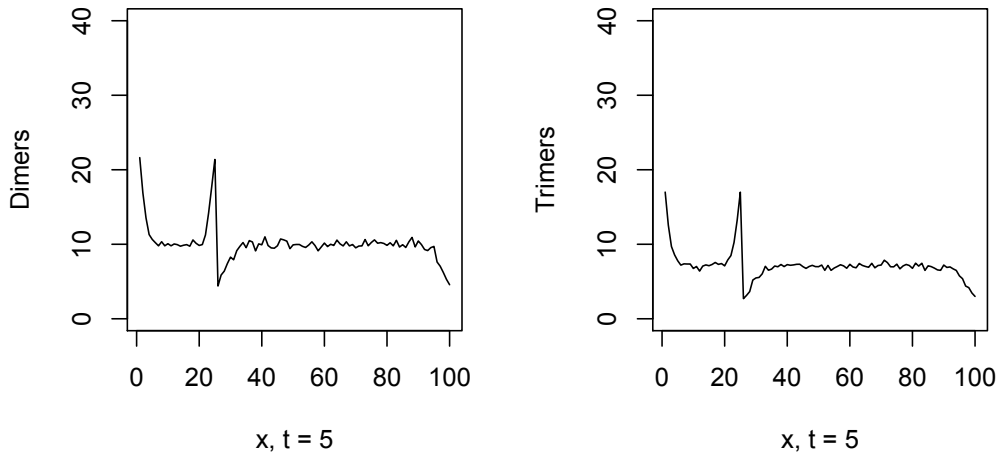

Figure 4.7: Profiles of the number of dimer and trimer complexes formed under diffusion scheme 3 at time $t = 5$.

one of which had a greater ratio of gelatine to water and hence a higher viscosity.

Just as in the numerical and analytical solutions, the authors found that a sharp boundary in colour intensity formed in time as the discontinuity in diffusion rate formed an effective flux in dye particles from the low viscosity region into the high viscosity region.

The results of the experiments are shown in Figure 4.8. Notably, the analytical solution derived in the paper has a very similar form to our numerical simulation shown in Figure 4.2.

The analytical solution to the Fokker-Planck diffusivity law listed in [78] is:

$$n_L(x,t) = n_0\frac{\sqrt{D_R}}{\sqrt{D_L}} + \left(n_0\frac{\sqrt{D_R}}{\sqrt{D_L}} - n_0\right)\cdot \operatorname{erf}\left(\frac{x}{2\sqrt{D_L t}}\right) \tag{4.3}$$

$$n_R(x,t) = n_0\frac{\sqrt{D_L}}{\sqrt{D_R}} - \left(n_0\frac{\sqrt{D_L}}{\sqrt{D_R}} - n_0\right)\cdot \operatorname{erf}\left(\frac{x}{2\sqrt{D_R t}}\right) \tag{4.4}$$

As the derivation is not listed in the paper, we re-derive the solution step by step in Appendix B. A plot of our derived solution to the system is shown in Figure 4.9 which, again, matches well with the concentration profiles simulated in diffusion scheme 1 shown in Figure 4.2. Note that there is no stationary distribution for this system. Rather,

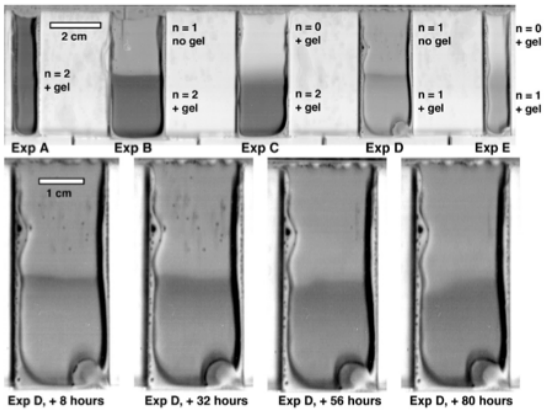

(a) Dye particles diffusing in gelatine

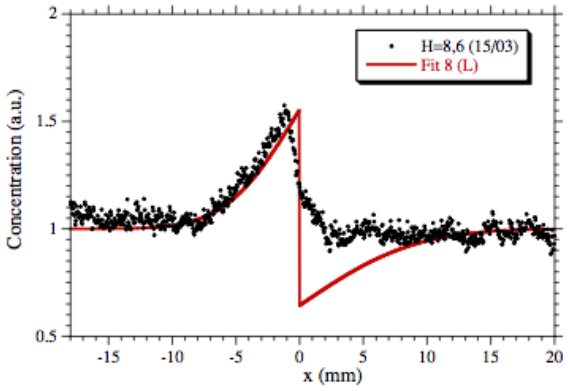

(b) Analytical solution fitted to colour intensity measurements

Figure 4.8: The formation of a boundary in colour intensity in an experiment involving dye particles diffusing in a heterogeneous gelatine medium and an analytical solution to the Fokker-Planck diffusivity law fitted to measurements of the colour intensity. Reproduced from [78] with permission of Boudewijn van Milligen.

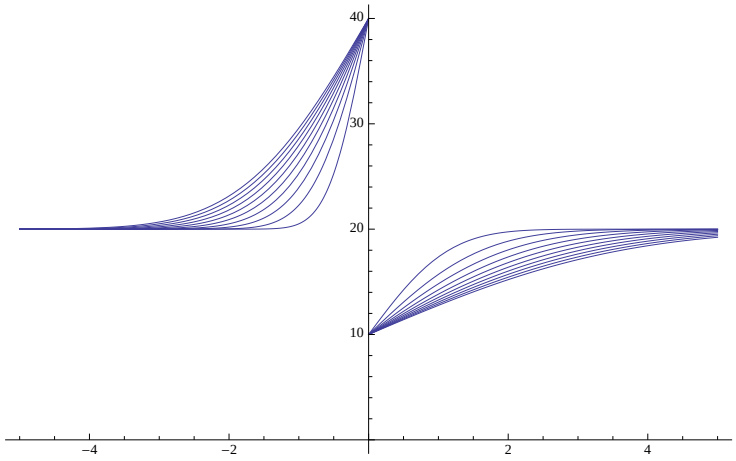

Figure 4.9: Solutions of n with respect to x for the values $n_0 = 20$, $D_L = 1$, $D_R = 4$ and $t = 0.1, 0.2, \ldots 1.0$.

particles continue to diffuse from the positive half-line into the negative half-line. In the plotted example above, all values of n tend towards 40 for $x < 0$ and towards 10 for $x > 0$.

In this section, we re-derived and calculated several individual solutions of Equation 4.7 as demonstrated in [78]. This system, however is of limited value for rafts of finite size as the space extends to $\pm\infty$. The limiting behaviour of the system in general is for the concentration to tend to:

$$n(x) = \begin{cases} \frac{n_0\sqrt{D_R}}{\sqrt{D_L}} & x < 0 \\ \frac{n_0\sqrt{D_L}}{\sqrt{D_R}} & x < 0 \end{cases} \tag{4.5}$$

To more realistically model microdomains of a finite size, we require more than a single discontinuity in the diffusion coefficient. In the next section, we derive a novel solution for diffusion of monomers on a space with a diffusion coefficient with the form of a square function in x.

4.3.1 Two-boundary system

In this section we use a similar approach to the previous in order to model diffusion in and out of a single microdomain on an infinite one-dimensional space.

We examine a system where the diffusion coefficient differs on a finite length in the range $(0, a)$ where $a > 0$. So we have:

$$D(x) = \begin{cases} D_R & x < 0 \\ D_L & 0 \leq x \leq a \\ D_R & x > a \end{cases} \tag{4.6}$$

A diagram illustrating the initial distribution of particles together with the spatial variation of the diffusion coefficient is shown in Figure 4.10. Analogously to the mathematical approach taken in appendix B, we will concern ourselves with solving the Fokker-Planck diffusivity law on the quantity $Dn(x,t)$, for the two separate systems: $D = D_L$ and $D = D_R$ and then applying constraints to ensure that a combination of the two solutions is still smooth and continuous at the point of discontinuity.

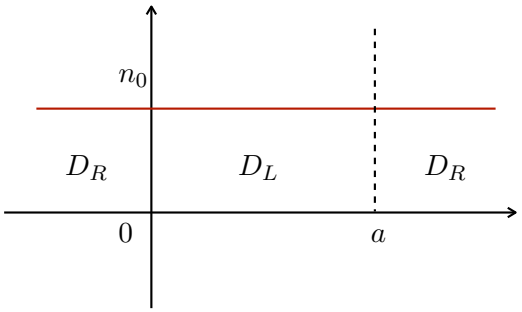

Figure 4.10: The system begins with a uniform distribution of particles at concentration n_0. The diffusion coefficient is D_R for $x < 0$, D_L for $0 < x < a$ and D_R for $x > a$.

As such, we consider now the evolution of Dn, with initial conditions:

$$Dn(x,0) = \begin{cases} D_R n_0 & x < 0 \\ D_L n_0 & 0 \leq x \leq a \\ D_R n_0 & x > a \end{cases} \tag{4.7}$$

the fundamental solution of the heat equation gives us a solution to this system of the form:

$$Dn(x,t) = B \cdot \left(\operatorname{erf}\left(\frac{x-a}{2\sqrt{Dt}} \right) - \operatorname{erf}\left(\frac{x}{2\sqrt{Dt}} \right) \right) + C \tag{4.8}$$

with $\frac{\partial B}{\partial x}$ and $\frac{\partial C}{\partial x}$ equal to zero. Here the values of B and C are different within and without the area of lower diffusion. i.e. $B = B_L$ for $0 \leq x \leq a$ and B_R otherwise. Similarly for C_L and C_R. B and C may be functions of time, but not of x.

Now, we require that $\frac{\partial Dn}{\partial x}$ is continuous. Taking derivatives and comparing values to the left and right of $x = 0$, we have:

$$\frac{B_L}{2\sqrt{D_L t}} \left\{ \operatorname{erf}'\left(\frac{-a}{2\sqrt{D_L t}} \right) - \operatorname{erf}'(0) \right\} = \frac{B_R}{2\sqrt{D_R t}} \left\{ \operatorname{erf}'\left(\frac{-a}{2\sqrt{D_R t}} \right) - \operatorname{erf}'(0) \right\} \tag{4.9}$$

and so:

$$B_R = B_L \frac{\sqrt{D_R}}{\sqrt{D_L}} \left\{ \frac{\operatorname{erf}'\left(\frac{a}{2\sqrt{D_L t}} \right) - \operatorname{erf}'(0)}{\operatorname{erf}'\left(\frac{a}{2\sqrt{D_R t}} \right) - \operatorname{erf}'(0)} \right\} \tag{4.10}$$

since the derivative of $\operatorname{erf}(x)$ with respect to x is even.

Now consider Dn for $0 < x < a$ and for $t = 0$. As $t \to 0$, we have $Dn \to D_L n_0$ and so:

$$C_L - 2B_L = D_L n_0 \text{ at } t = 0 \tag{4.11}$$

Finally consider C for $x < 0$ and $x > a$. At $t = 0$, we have $Dn = D_R n_0$ and we know that $Dn \to D_R n_0$ as $x \to \pm\infty$. Hence we have $C_R = D_R n_0$ outside the interval $[0, a]$. Then, requiring continuity at $x = 0$ we have:

$$C_L = D_R n_0 + B_L \left\{ \text{erf}\left(\frac{a}{2\sqrt{D_L t}}\right) - \frac{\sqrt{D_R}}{\sqrt{D_L}} \left\{ \frac{\text{erf}'\left(\frac{a}{2\sqrt{D_L t}}\right) - \text{erf}'(0)}{\text{erf}'\left(\frac{a}{2\sqrt{D_R t}}\right) - \text{erf}'(0)} \right\} \text{erf}\left(\frac{a}{2\sqrt{D_R t}}\right) \right\} \tag{4.12}$$

Now we simply need to determine B_L. Evaluating C_L at $t = 0$ gives:

$$C_L(0) = D_R n_0 + B_L \left(1 - \frac{\sqrt{D_R}}{\sqrt{D_L}}\right) \tag{4.13}$$

and hence

$$B_L \left(1 + \frac{\sqrt{D_R}}{\sqrt{D_L}}\right) = D_R n_0 - D_L n_0 \tag{4.14}$$

$$B_L = \frac{D_R n_0 - D_L n_0}{1 + \frac{\sqrt{D_R}}{\sqrt{D_L}}} \tag{4.15}$$

Example solutions to the system $Dn(x, t)$ are shown in Figure 4.11. Here we set a value of $a = 20$, and D_L and D_R as before at 1 and 4 units per timestep. This plot demonstrates how the solutions obtained above satisfy the conditions for smoothness and continuity between the solutions $D_L n$ and $D_R n$ at the points $x = 0$ and $x = a$. The plots show how the sharp, square-function initial condition decays into a smooth function, with the solutions of the higher diffusion system and the lower diffusion system eventually converging as $t \to \infty$. In Figure 4.12 we plot example solutions of $n(x, t)$ using the same parameters as above. This models how the spatial profile of monomers diffusing on an infinite plane with a finite region of lower diffusivity evolve over time. In a similar result to the single discontinuity case in the previous example, we see a sharp increase in concentration im-

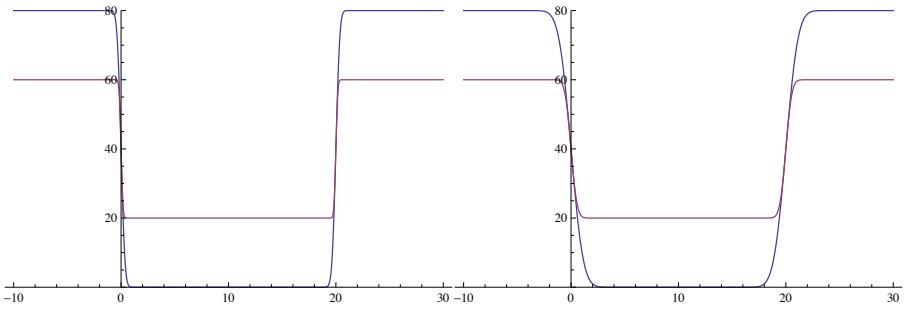

(a) $t = 0.01$

(b) $t = 0.1$

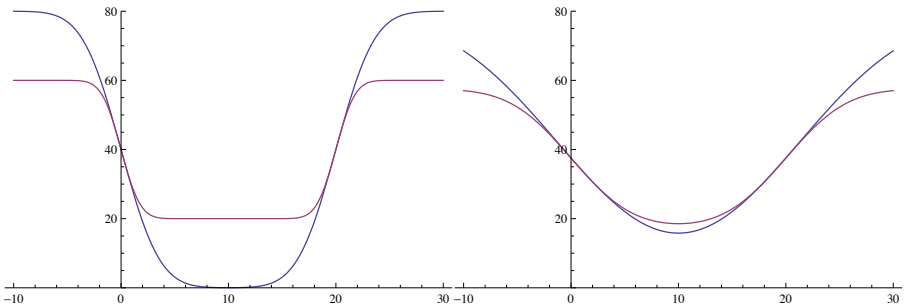

(c) $t = 1$

(d) $t = 10$

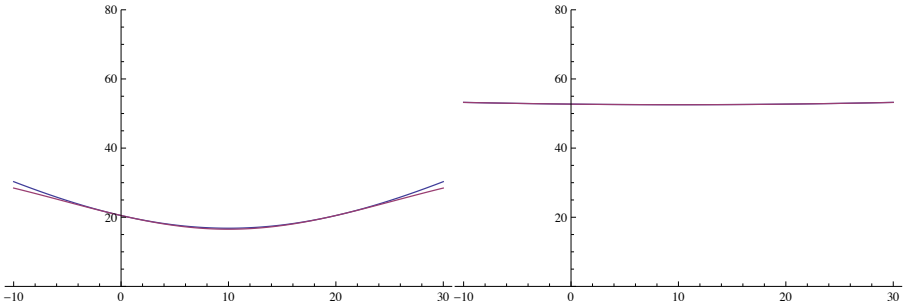

(e) $t = 100$

(f) $t = 1000$

Figure 4.11: Six snapshots of the two solutions $D_L n(x,t)$ and $D_R n(x,t)$ at logarithmically increasing values of t.

mediately inside the microdomain (lower diffusivity) region. The maxima and minima of the spike are also the same values as in the previous example.

We see different behaviour once the perturbation on both sides of the microdomain meets. Whereas, in the last example, the values of n at $0 \mp \epsilon$ remained fixed at $\frac{n_0\sqrt{D_R}}{\sqrt{D_L}}$ and $\frac{n_0\sqrt{D_L}}{\sqrt{D_R}}$ respectively, here we see that there is considerable variation in the value of n over time in the immediate neighbourhood of the discontinuities. For example, at $t = 100$ we see the within-microdomain concentration fall back to the initial concentration, before eventually climbing again as t becomes very large.

To make sense of this, we recall that the solution is derived from a solution of the heat equation where the initial condition is a uniform distribution with a finite section of lower temperature. As the uniform temperature extends to an infinite space to both sides of the discontinuity, the system will eventually tend to a uniform temperature distribution equal to the outside temperature.

In the case of our diffusion problem, the within-microdomain concentration will tend to $\frac{D_R n_0}{D_L}$ as $t \to \infty$ and the concentration in the rest of the space will tend to n_0. Although this seems to violate mass conservation when viewed in a narrow spatial window, the increased mass in the entire system is zero because there is only a finite increase spread over an infinite space. We can observe this change in the within- and without-microdomain concentration profile by plotting the local value of two points of interest over time. Taking the value of $D_L n$ in the centre of the microdomain at $x = 10$ and the value of $D_R n$ in a point some distance outside the microdomain at $x = 50$, we see the time evolution in Figure 4.13. Note that, in the centre of the microdomain (the dashed line in the figure), the value initially increases by a small amount, falls again to its initial value before steadily increasing up to the initial value of the exterior system. At the point outside the microdomain we see the solution hold its initial value for a short period of time, then a single wave passes in which it decreases in value before finally returning to its initial magnitude. The novel solution to this particular example of interest displays interesting properties, particularly the non-monotonic behaviour in time whereby concentration within microdomains increases transiently, then falls before finally increasing to a high

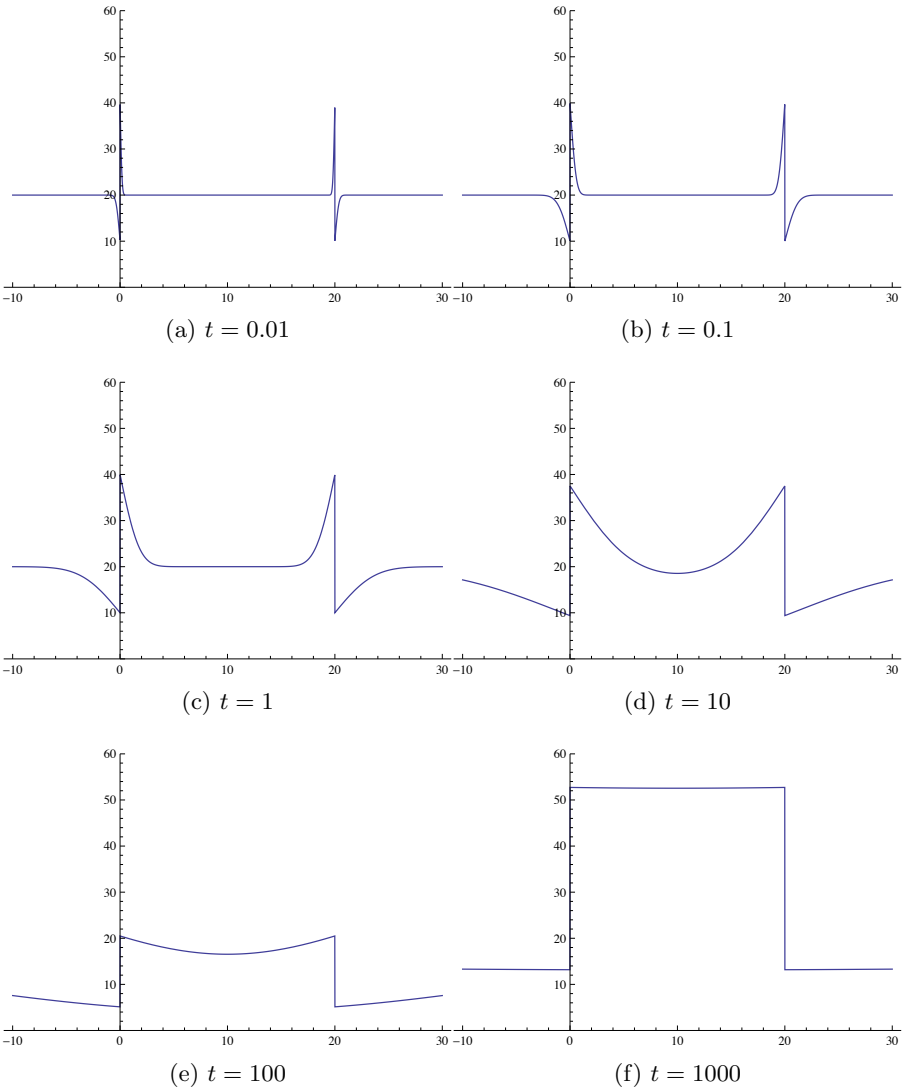

(a) $t = 0.01$ (b) $t = 0.1$

(c) $t = 1$ (d) $t = 10$

(e) $t = 100$ (f) $t = 1000$

Figure 4.12: Six snapshots of the solution $n(x, t)$ at logarithmically increasing values of t.

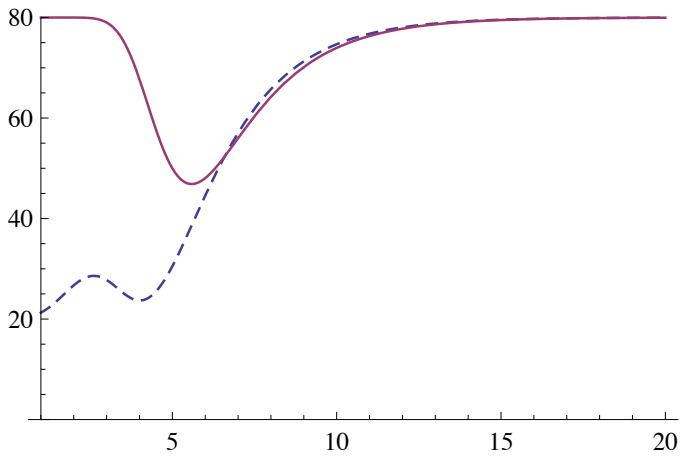

Figure 4.13: The behaviour in the limit of large time values. Here, the dashed line shows the value of $D_L n(x,t)$ at the point $x = 10$ and the solid line shows the value of $D_R n(x,t)$ at the point $x = 50$. The horizontal axis is in $\ln(t)$.

and constant level.

The example is still lacking, however, if we wish to model multiple such domains, since the behaviour of the system considered is so dependent on the infinite extension of space to both sides of the area of interest.

A more appropriate approach would be to consider a system with periodic boundary conditions, which would more accurately describe a series of such microdomains.

4.3.2 Periodic boundary conditions case

In this section, we consider a repeating pattern of regions of different diffusion coefficients such that a length $0 < x < a$ has a diffusion coefficient of D_L followed by a length $a < x < b$ with a diffusion coefficient of D_R. We consider just a finite space of length b with the conditions:

$$D_L n(0,t) = D_R n(b,t) \tag{4.16}$$

$$\frac{\partial}{\partial x}(D_L n)(0,t) = \frac{\partial}{\partial x}(D_R n)(b,t) \tag{4.17}$$

A diagram of the initial distribution of monomers and the variation in diffusion rate is depicted in Figure 4.14. Note, however, that the space does not extend to $\pm\infty$ on the x axis, but is periodic between the range $[0 - b)$. This system is analogous to the problem

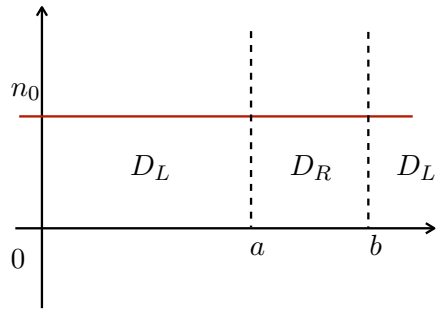

Figure 4.14: Solutions of Dn with respect to x for the values $n_0 = 20$, $D_L = 1$, $D_R = 4$, $a = 10$ and $t = 0.1, 0.2, \ldots 1.0$. The blue plots show the solution of the system for $D = D_R$, valid for $x < 0$ and $x > a$ the purple plots show the solution of the system for $D = D_R$, valid for $0 < x < a$.

of heat flow in a circular ring. For such a system, solutions have the form of the series:

$$Dn(\theta, t) = \frac{1}{2}c_0 + \sum_{i=1}^{\infty} e^{-Di^2 t}[c_i \cos(i\theta) + d_i \sin(i\theta)] \tag{4.18}$$

where the system considered is the interval $0 < \theta < 2\pi$ and the coefficients c_i and d_i are given by the integrals:

$$c_i = \frac{1}{\pi}\int_0^{2\pi} g(\theta)\cos(i\theta)d\theta \tag{4.19}$$

$$d_i = \frac{1}{\pi}\int_0^{2\pi} g(\theta)\sin(i\theta)d\theta \tag{4.20}$$

where the function $g(\theta)$ is the initial condition $Dn(\theta, 0)$.

Since our approach multiplies the system of interest by a factor of D to solve the two systems, and we are interested in conservation of mass in the solution of $n(\theta, t)$ rather than $Dn(\theta, t)$, let us assume that the function g varies in both space and time such that:

$$g_L(x,t) = \begin{cases} A_L(t)n_0, & 0 < \theta < \alpha \\ B_L(t)n_0, & \alpha < \theta < 2\pi \end{cases} \tag{4.21}$$

for the system $D_L n(\theta, t)$ and

$$g_R(x,t) = \begin{cases} A_R(t)n_0, & 0 < \theta < \alpha \\ B_R(t)n_0, & \alpha < \theta < 2\pi \end{cases} \tag{4.22}$$

having mapped the interval $(0, b)$ onto $(0, 2\pi)$ and where Δ_L and Δ_R are the rescaled diffusion coefficients in the interval $(0, 2\pi)$ and α is $\frac{2\pi a}{b}$.

This means we can derive:

$$c_{i,L} = \frac{1}{\pi}\left(\int_0^{\alpha} A_L n_0 \cos(i\theta)d\theta + \int_{\alpha}^{2\pi} B_L n_0 \cos(i\theta)d\theta\right) \tag{4.23}$$

$$= \frac{n_0}{i\pi}\sin(i\alpha)\left(A_L - B_L\right) \tag{4.24}$$

Similarly:

$$d_{i,L} = \frac{n_0}{i\pi}\left\{1 - \cos(i\alpha)\right\}\left(A_L - B_L\right) \tag{4.25}$$

In an analagous manner in the higher diffusion system, we derive:

$$c_{i,R} = \frac{n_0}{i\pi}\sin(i\alpha)\left(A_R - B_R\right) \tag{4.26}$$

$$d_{i,R} = \frac{n_0}{i\pi}\left\{1 - \cos(i\alpha)\right\}\left(A_R - B_R\right) \tag{4.27}$$

To find the coefficient c_0, we evaluate:

$$\frac{1}{\pi}\int_0^{2\pi} g(\theta)d\theta = \frac{1}{\pi}\left(\Big[\theta g(\theta)\Big]_0^{\alpha} + \Big[\theta g(\theta)\Big]_{\alpha}^{2\pi}\right) \tag{4.28}$$

which gives us:

$$c_{0,L} = 2B_L n_0 + \frac{\alpha n_0}{\pi}(A_L - B_L) \tag{4.29}$$

$$c_{0,R} = 2B_R n_0 + \frac{\alpha n_0}{\pi}(A_R - B_R) \tag{4.30}$$

Combining these expressions, we see that the solution of the system can be expressed as:

$$n_X(x,t) = \frac{1}{D_X}\Big\{B_X n0 + \frac{\alpha n0}{2\pi}(A_X - B_X) + \frac{n0}{\pi}(A_X - B_X)\sum_{i=1}^{\infty}(\frac{e^{-\Delta_X i^2 t}}{i}(\sin(i\alpha - i\theta) + sin(i\theta))\Big\} \tag{4.31}$$

where X is either L or R for the two respective systems.

We know that our initial conditions require that $A_L(0)$ is Δ_L and that $B_R(0)$ is Δ_R. Let us further assume that $A_L(t) = \Delta_L$ for all t.

This leaves us with three functions in t to determine: $A_R, B_L and B_R$. These can be determined by applying three conditions:

1. Conservation of mass: $\int_0^\alpha n_L(\theta,t)d\theta + \int_\alpha^{2\pi} n_R(\theta,t)d\theta = 2\pi n_0$ for all t
2. Smoothness: $\frac{\partial \Delta_L n_L}{\partial d\theta} = \frac{\partial \Delta_R n_R}{\partial d\theta}$ at $\theta = \alpha$ for all t
3. Continuity: $\Delta_L n(\alpha,t) = \Delta_R n(\alpha,t)$ for all t

First, addressing the smoothness condition and taking derivatives with respect to θ, we obtain the relation:

$$(A_L - B_L)\sum_{i=1}^{\infty} e^{-\Delta_L i^2 t}(\cos i\theta - 1) = (A_R - B_R)\sum_{i=1}^{\infty} e^{-\Delta_R i^2 t}(\cos i\theta - 1) \tag{4.32}$$

and so

$$B_L = \Delta_L - \frac{\sum_{i=1}^{\infty} e^{-\Delta_R i^2 t}(\cos i\alpha - 1)}{\sum_{i=1}^{\infty} e^{-\Delta_L i^2 t}(\cos i\alpha - 1)}(A_R - B_R) \tag{4.33}$$

Note, however that

$$\sum_{i=1}^{\infty} e^{-\Delta_L i^2 t}(\cos i\theta - 1) = -\sqrt{\frac{\pi}{4Dt}} \tag{4.34}$$

for all θ. And so:

$$B_L = \Delta_L - \sqrt{\frac{\Delta_L}{\Delta_R}}(A_R - B_R) \tag{4.35}$$

For the sake of brevity, let $S_{\alpha,D} = \sum_{i=1}^{\infty} \frac{e^{-Di^2 t}}{i\pi}\sin(i\alpha)$.

The continuity condition (dividing by n_0) requires:

$$B_L = B_R + \frac{\alpha}{2\pi}(A_R - B_R) + (A_R - B_R)S_{\alpha,\Delta_R} - \frac{\alpha}{2\pi}(A_R - B_R)\sqrt{\frac{\Delta_L}{\Delta_R}} - (A_R - B_R)\sqrt{\frac{\Delta_L}{\Delta_R}}S_{\alpha,\Delta_L} \tag{4.36}$$

Finally, taking the conservation of mass condition and multiplying through by $\frac{\Delta_L \Delta_R}{n0}$ we arrive at the relation:

$$\Delta_L(2\pi - \alpha)(\Delta_R - B_R) = (A_R - B_R)\Big\{\sqrt{\Delta_L\Delta_R}\frac{\alpha^2}{2\pi} + \frac{2}{\pi}\sqrt{\Delta_L\Delta_R}\sum_{i=1}^{\infty}\frac{e^{-\Delta_L i^2 t}}{i^2}(1 - \cos(i\alpha)) \tag{4.37}$$

$$+ \Delta_L\alpha - \frac{2}{\pi}\Delta_L\sum_{i=1}^{\infty}\frac{e^{-\Delta_R i^2 t}}{i^2}(1 - \cos(i\alpha)) - \frac{\alpha^2}{2\pi}\Delta_L - \sqrt{\Delta_L\Delta_R}\alpha\Big\} \tag{4.38}$$

Combining the conditions for smoothness and continuity, we derive an expression for A_R in terms of B_R:

$$A_R = \frac{\Delta_L - B_R}{\sqrt{\frac{\Delta_L}{\Delta_R}}\left(1 - \frac{\alpha}{2\pi} - S_{\alpha,\Delta_L}\right) + \frac{\alpha}{2\pi} + S_{\alpha,\Delta_R}} + B_R \tag{4.39}$$

Recombining this with the condition for mass conservation, we finally derive the function $B_R(t)$ as:

$$B_R(t) = \frac{\Delta_L F_1(t) - \Delta_L\Delta_R(2 * \pi - \alpha)F_2(t)}{F_2(t)(F_1(t) - \Delta_L(2\pi - \alpha)) + F_1(t)(1 - F_2(t))} \tag{4.40}$$

where

$$F_1(t) = \sqrt{\Delta_L\Delta_R}\frac{\alpha^2}{2\pi} + \frac{2}{\pi}\sqrt{\Delta_L\Delta_R}\sum_{i=1}^{\infty}\frac{e^{-\Delta_L i^2 t}}{i^2}(1 - \cos(i\alpha)) \tag{4.41}$$

$$+ \Delta_L\alpha - \frac{2}{\pi}\Delta_L\sum_{i=1}^{\infty}\frac{e^{-\Delta_R i^2 t}}{i^2}(1 - \cos(i\alpha)) - \frac{\alpha^2}{2\pi}\Delta_L - \sqrt{\Delta_L\Delta_R}\alpha \tag{4.42}$$

and

$$F_2(t) = \sqrt{\frac{\Delta_L}{\Delta_R}}\left(1 - \frac{\alpha}{2\pi} - S_{\alpha,\Delta_L}\right) + \frac{\alpha}{2\pi} + S_{\alpha,\Delta_R} \tag{4.43}$$

4.3.3 Results

In section 4.3.1 we saw that quantities that would be treated as constants in a homogeneous system become time dependent when we solve the system with inhomogeneous diffusion rates. In the previous subsection, we also saw that the key to fulfilling all three dynamical conditions was to determine the evolution of the functions A_L, B_L, A_R and B_R over time. These values depend on time, and also the diffusion coefficients inside and outside the microdomain, but are independent of n_0 and the spatial coordinate x (or θ in the scaled system). The evolution of these four values in the scaled system are shown in Figure 4.15. Recall that A_L is set as a constant Δ_L. We see that these parameters do indeed behave as constants for very small and very large values of t, but that there is considerable variation in the range $-2 < \ln(t) < 2$. Applying these parameters to generate solutions to

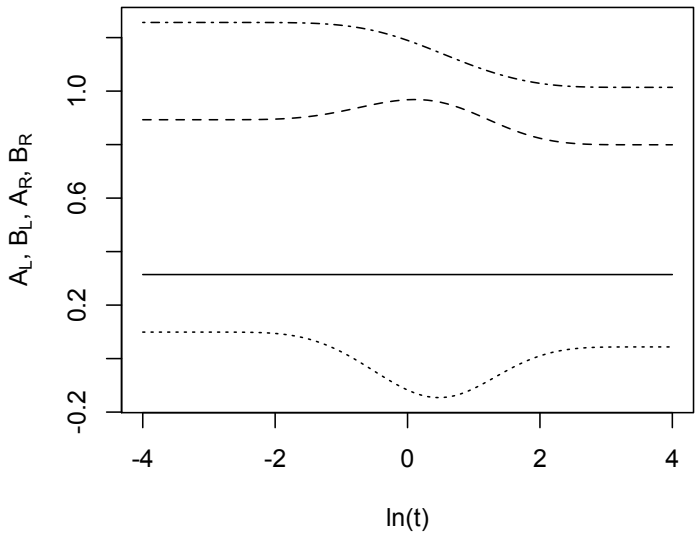

Figure 4.15: Values of the time-dependent parameters $A_{L,R}$ and $B_{L,R}$. In the above figure, A_L is shown by the solid line, B_L, by the dashed line, A_R by the dotted line, and B_R by the dashed and dotted line.

Equation 4.3.2 we may derive the evolution of the periodic system. Figure 4.16 shows one such solution for six individual timepoints. Because the solution involves infinite sums, these are numerical approximations to the analytical solution, using sums of the first 1000

terms in order to calculate $F_1(t)$ and $F_2(t)$ as well as the solutions to Equation 4.3.2. The solution profiles were generated using an R script[114]. This particular solution uses a value of $a = 5$, with 25% microdomain coverage.

Comparing these numerical results with those of the previous two examples, we see that the initial concentration increase just within the microdomain is less than in the infinite system with a single discontinuity. We also see a monotonic increase of monomer concentration within the microdomain as t increases, in contrast to the non-monotonic behaviour seen in Section 4.3.1. The within-microdomain concentration appears to be

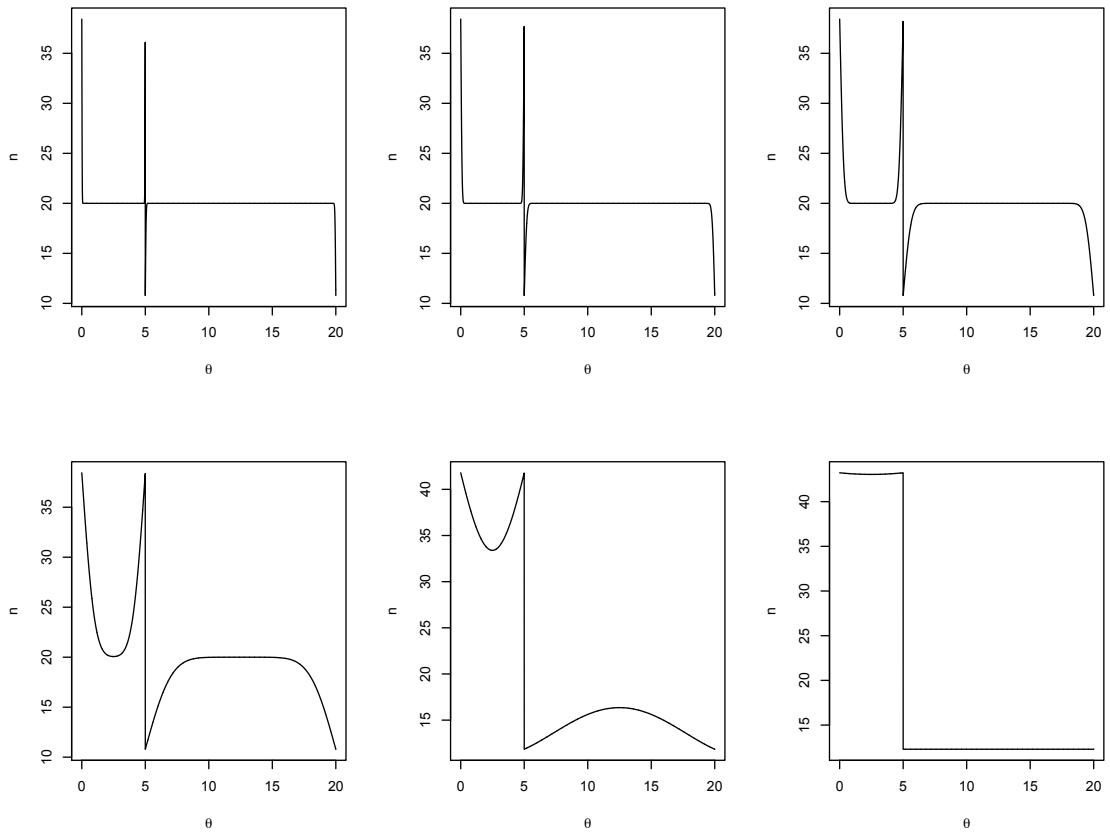

Figure 4.16: Solutions of $n(\theta, t)$ for six timepoints: $t = 0.0001, 0.001, 0.01, 0.1, 1$ and 10. Parameters are $D_L = 1$, $D_R = 4$, $a = 5$ and $b = 20$ with Δ_L and Δ_R scaled accordingly.

increasing to a level higher than seen in Appendix B, but less than that seen in Section 4.3.1. The latter observation is to be expected as the pool of monomers outside of the microdomain region cannot be depleted in the example where the microdomain exists on

an infinite space.

In Figure 4.17 we plot the concentration at two points of interest: the centre of the microdomain region and the centre of the non-microdomain region. We see that, in this case, and in contrast to Section 4.3.1, the concentration profile increases monotonically to a steady level within the microdomain and decreases monotonically to a steady level outside the microdomain.

This behaviour differs clearly from the single diffusion discontinuity on an infinite space. Although, in that system, the concentration of any particular point tended towards a steady value as $t- > \infty$, one could also find a point sufficiently far from the origin where the concentration was still at its initial value, for any given value of t. We can also examine

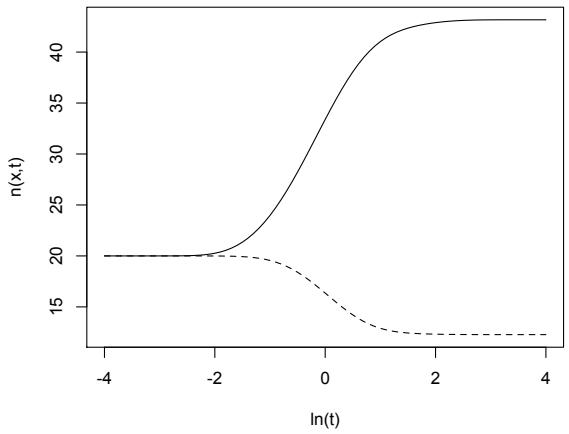

Figure 4.17: The concentration within the microdomain region at the point $x = 2.5$ (solid line) and the concentration in the non-microdomain region at the point $x = 12.5$ shown with a logarithmic time scale on the horizontal axis.

the dependence on the microdomain length, a, in the sequestering of monomers into the microdomain region. Figure 4.18 depicts the ratio of the mean monomer concentration within the microdomain region to the mean monomer concentration at $t = 0$. As can be seen, at early time points the within-microdomain concentration is increase in smaller microdomains, and the ratio decreases monotonically as microdomain length increases. Note that the ratio of the lengths of the alternating microdomain/nonmicrodomain regions is kept constant so the total fraction of the space occupied by the low-diffusion region is

constant.

The increase in monomer concentration is relatively small at early time points, but reaches over 2.5 times the original concentration in microdomains of length 30 at time $t = 10$.

At longer timescales, however, we note that the relationship between the concentration increase and microdomain length is no longer monotonic. Instead we see a clear peak at around the length $a = 30$. This suggests that the existence of 'optimal' sizes for microdomains in their ability to concentrate diffusing proteins is dependent on time; if microdomain existence is transitory then the existence of an optimal length scale may depend on their having a lifetime of a certain length also. We have seen that analytical solutions

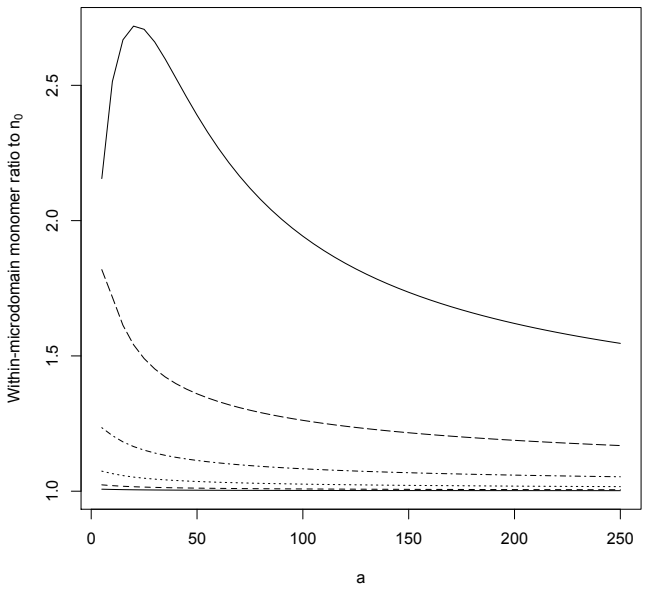

Figure 4.18: The ratio of the mean monomer concentration within the microdomain region to the initial concentration for six timepoints: $t = 0.0001, 0.001, 0.01, 0.1, 1$ and 10. Parameters are $D_L = 1$, $D_R = 4$, and $b = 4a$ with Δ_L and Δ_R scaled accordingly.

of the diffusion equation with particular constraints suggest a role for low-diffusion regions in sequestering diffusing monomers and increasing their local concentration in comparison to the surrounding space. In the following section, we introduce reaction schemes to determine whether concentrating components in a finite space can enable increased organisation

of dimeric or trimeric complexes over the whole space.

4.4 Application to reaction-diffusion

In the previous section we determined an analytical solution to the problem of a monomer diffusing in a one-dimensional space with heterogeneous diffusion coefficients, which took the form of a variety of step functions. In this section, we combine the results from the previous section with reaction dynamics in order to determine how heterogeneity in a model membrane might influence the formation of dimeric and trimeric protein complexes.

4.4.1 Dimer reaction

Consider now a system of proteins diffusing on the membrane. If protein-protein reaction is fast compared to diffusion then the system will reach equilibrium locally before components diffuse away. We consider such a case.

Considering a local neighbourhood in which proteins are close enough to interact. We will first consider a heterodimerisation reaction, which proceeds as follows:

$$A + B \rightleftharpoons AB \tag{4.44}$$

This system is governed by the system of differential equations:

$$\frac{\partial [AB]}{\partial t} = k_c[A][B] \tag{4.45}$$

$$\frac{\partial [A]}{\partial t} = k_d[AB] \tag{4.46}$$

Assuming that both $[A]$ and $[B]$ start at a concentration of n_0 and that there are no dimers initially, we see that the system reaches equilibrium when:

$$k_d(n_0 - [A]) = k_c[A]^2 \tag{4.47}$$

$$\text{i.e. } k_c[A]^2 + k_d[A] - k_d n_0 = 0 \tag{4.48}$$

this is at the point:

$$[A] = \frac{-k_d + \sqrt{k_d^2 + 4k_c k_d n_0}}{2k_c} \tag{4.49}$$

We combined this with the diffusion model in Section 4.3.2 in order to model whether the increase in concentration within the microdomain region led to an overall increase in dimer organisation, despite the decreased concentration of monomers in the larger region outside the microdomain.

Figure 4.19 shows a plot of the mean concentration of dimers over the whole space for systems with microdomain lengths in the range 1–250. The behaviour is remarkably similar to the increase in monomer concentration within the microdomain, plotted in Figure 4.18. We see that, indeed, dimer formation is increased compared to a system with no microdomains and that, for sufficient timescales, there is a clearly defined optimal length which maximises dimer organisation.

Notably, however, the increase in dimer formation is very small when compared to the increase in within-microdomain monomer concentration: only around a 2–3% increase. This would be unlikely to have any significant biological effect *in vivo*. We have demonstrated that simple analytical models for reaction and diffusion support a mechanism for an increased rate of dimer formation in the presence of small microdomains with lowered diffusion rates. Although the increases were relatively small, this mathematical result supports conclusions of the purely computational model in Chapter 3.

The previous chapter modelled trimer, rather than dimer, formation. In the next section we derive a model for determining trimer formation in the same heterogeneous system.

4.4.2 Trimer reaction

In the case of the formation of a heterotrimer, as considered in the previous chapter, we begin with the two-step reaction:

$$A + B + C \rightleftharpoons AB + C \rightleftharpoons ABC \tag{4.50}$$

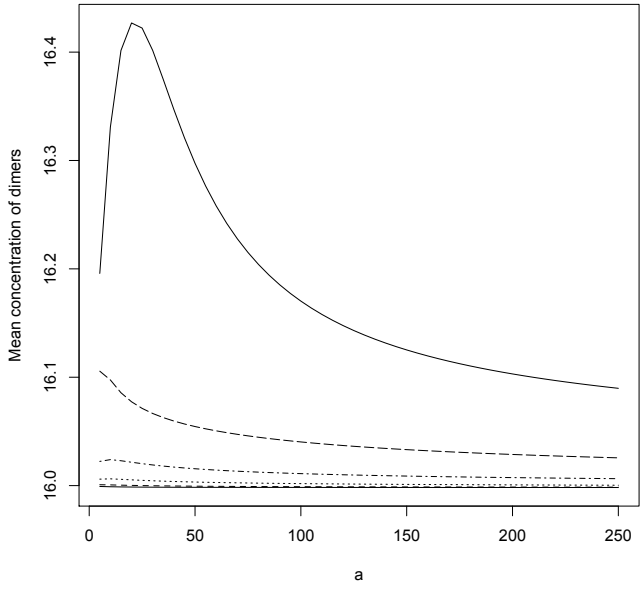

Figure 4.19: This plot shows the mean concentration of dimers with increasing microdomain size on the a axis. The various plots are taken at subsequent time points $t = 0.0001, 0.001, 0.01, 0.1, 1$ and 10 with the lowest line in the plot being the earliest time point and the highest line the latest.

For simplicity, let us assume that both forward reactions proceed at a rate k_c and the backward reactions at the rate k_d. In differential equation form, we have:

$$\frac{\partial[ABC]}{\partial t} = k_c[AB][C] - k_d[ABC] \tag{4.51}$$

$$\frac{\partial[AB]}{\partial t} = k_c[A][B] + k_d[ABC] - k_c[AB][C] - k_d[AB] \tag{4.52}$$

$$\frac{\partial[A]}{\partial t} = k_d[AB] - k_c[A][B] \tag{4.53}$$

by symmetry, $\frac{\partial[B]}{\partial t} = \frac{\partial[A]}{\partial t}$ and $\frac{\partial[C]}{\partial t} = -\frac{\partial[ABC]}{\partial t}$.

Making the further simplifying assumption that all monomers are unbound at t_0 and exist at an equal initial concentration n_0, we also see that $[C] = n_0 - [ABC]$ and that $[A] = [B] = n_0 - [ABC] - [AB]$. This means that, at equilibrium:

$$k_c[AB][C] - k_d\left(n0 - [C]\right) = 0 \tag{4.54}$$

$$k_d[AB] - k_c\left([C] - [AB]\right)^2 = 0 \tag{4.55}$$

Combining the above two relations and simplifying, we derive the following quartic equation for the equilibrium concentration of species C:

$$k_c^2[C]^4 + 2k_c k_d[C]^3 + 2(k_d^2 - k_c d_d n_0)[C]^2 - 3k_d^2 n_0[C] + k_d^2 n_0^2 = 0 \tag{4.56}$$

We solved the above equation using equation solving software [127]. Two solutions of the quartic exist in the complex plane for positive values of k_c and k_d and so can be discarded. The other two solutions return real values. By inspection of the modelled equilibrium concentrations of the species A, AB and ABC when k_d is fixed, we can see that only the first solution is appropriate, as the second returns negative concentrations of the monomer A. Two possible real solutions to this equation are shown in Figure 4.20. We model the formation of heterotrimers from equal numbers of diffusing monomers by modelling monomer diffusion for each of the constituent monomers, solving Equation 4.56 to determine the local concentration of species C (here representing the IL2-Rα component), and then applying the relation:

$$[ABC](x,t) = n(x,t) - [C](x,t) \tag{4.57}$$

at each point in space.

The results are shown in the following section.

4.4.3 Results

Optimal sizes exist for microdomains in transient time

In general, smaller microdomain lengths led to a greater increase in the monomer concentration within the raft region, dimer formation and trimer formation. Figure 4.21 shows the mean system concentration of trimers for microdomain lengths in the range 1–250. The various series shown in the plot show the mean concentration at subsequent time points and we see that there is a clear maximum in trimer organisation around the value $a = 30$ at the point $t = 10$. As in the case with the within-microdomain monomer concentration and the systemic dimer concentration, the optimal length scale only exists at

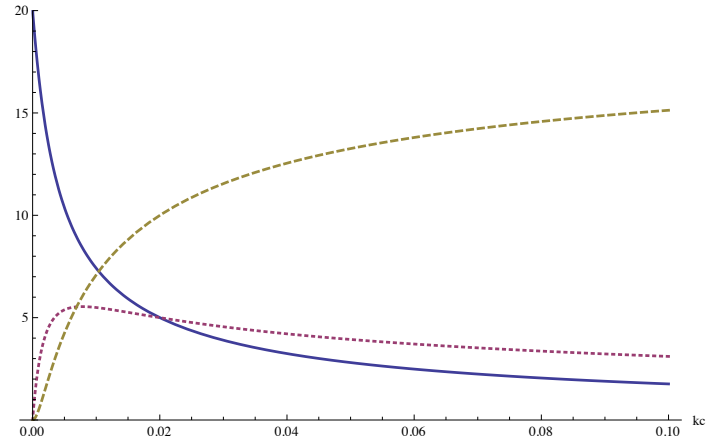

(a) Modelled equilibrium concentrations of A (solid), AB (dotted) and ABC (dashed) with k_d=0.1

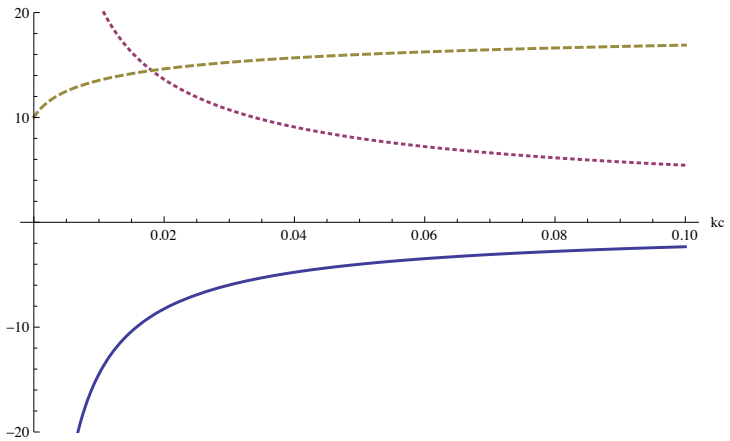

(b) A second solution of the equilibrium concentrations

Figure 4.20: Modelled concentrations of A, AB and ABC, based on two real solutions of Equation 4.56.

the later time point $t = 10$.

Again, the relative increase in trimer organisation is small, though the maximum in the figure represents an increase of around 3.5%: slightly greater than the enhancement of dimer organisation. This is heuristically plausible as the increase in local concentration affects all three of the trimer's constituent components, rather than two. Notably, though, increases on this scale do not support the argument that sequestering proteins with diffusion traps play a key role in facilitating immunological signalling.

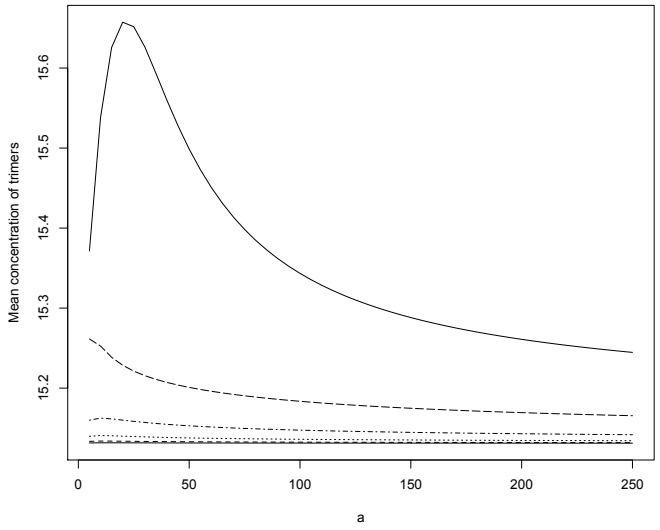

Figure 4.21: This plot shows the mean concentration of trimers with increasing microdomain size on the a axis. The various plots are taken at subsequent time points $t = 0.0001, 0.001, 0.01, 0.1, 1$ and 10 with the lowest line in the plot being the earliest time point and the highest line the latest.

Low affinity reactions are more sensitive to spatial effects

So far we have mostly examined the dependence of protein complex formation on spatiotemporal parameters: microdomain length, total membrane coverage and the time in which microdomains exist in the system. We also varied chemical parameters: the forward and backward rates of the dimerisation and trimerisation processes, in order to quantify whether microdomain-mediated effects depended on such chemical properties.

For the dimer formation and trimer formation systems described above, we varied the

backward rate of the reaction, k_d in the range 0.01–100, keeping the forward rate of the reaction constant at $k_c = 1$.

Figure 4.22 shows the results of varying k_d on the mean systemic concentration of dimer complexes at $t = 10$. Higher backward reaction rates led to a greater increase in dimer organisation, both in absolute terms and in relative terms with respect to the 'control system' with no microdomains present. This value is depicted by the faint line in the figure.

Of course, a high backwards rate means that fewer complexes are organised in the first place, so these results imply that there could be a more important role for microdomains to play in facilitating low affinity complex formation. The situation is similar in the

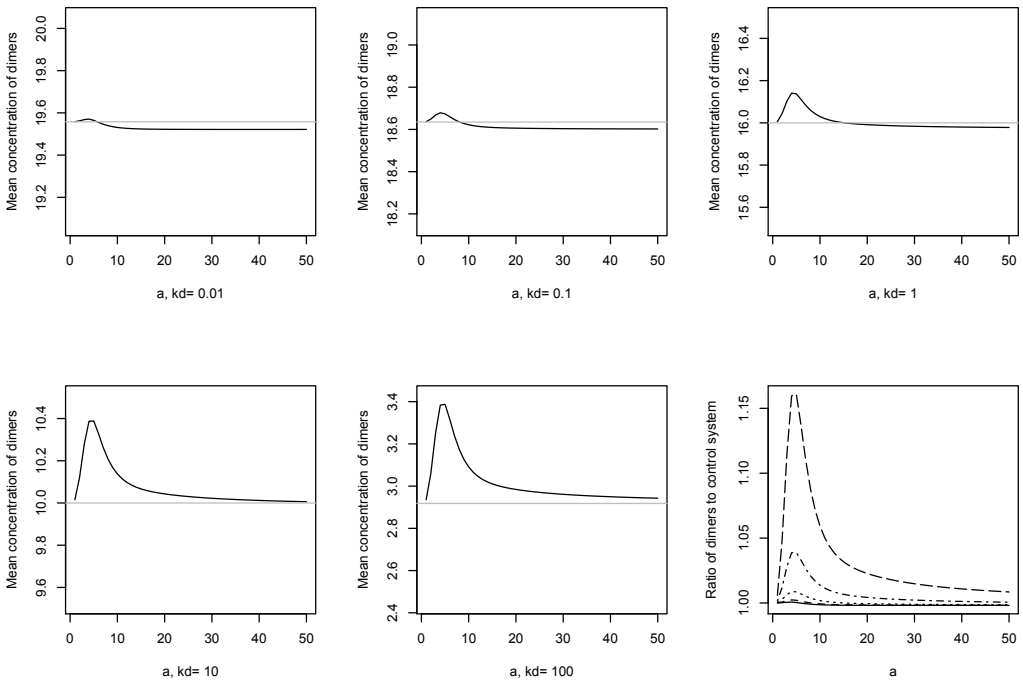

Figure 4.22: The first five plots depict the mean concentration of dimers organised at the point $t = 10$ plotted against increasing microdomain size. Each plot shows a different value for the off rate of the reaction, k_d. The faint line shows the 'control' mean dimer concentration if no microdomains were present. The final plot shows the ratio of the mean concentration in the system with microdomains to the control system. The higher values of k_d are shown by the higher lines.

case of trimer formation. Here, however, the absolute increase in trimer formation at the

optimal microdomain length is greatest at a moderate k_d value (10). The relative increase, however, is still greatest for the highest value of k_d, leading to a roughly 60% increase in trimer organisation in the entire model space.

This is a considerable increase – the respective value in the dimer system was only around 16%, and provides stronger evidence for a role for microdomains in aiding complex formation, but only for low-affinity complexes over relatively long timescales.

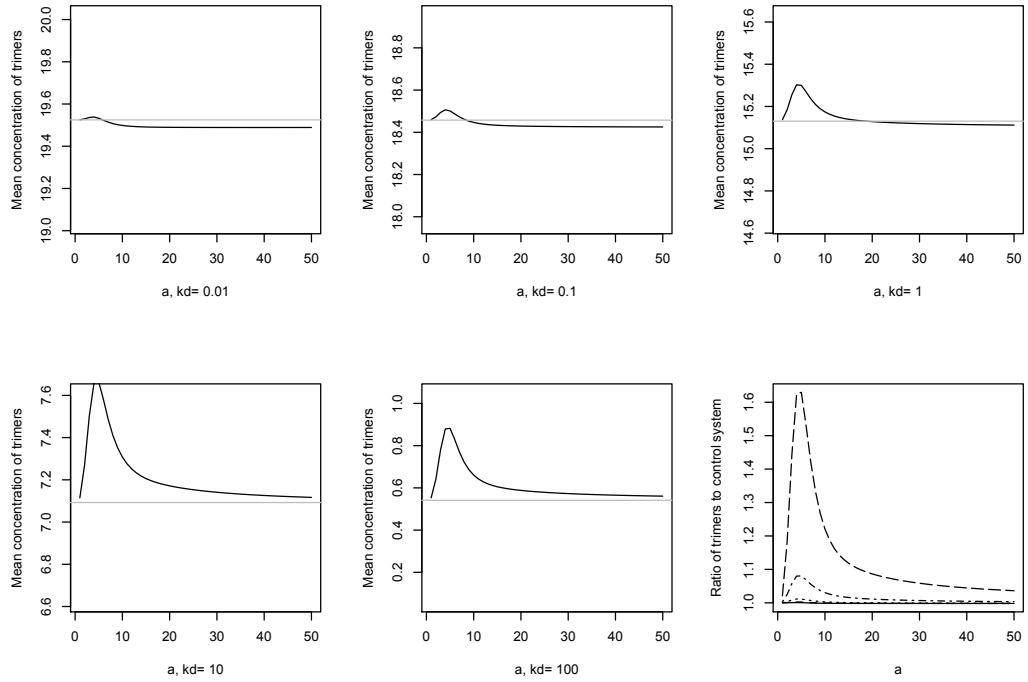

Figure 4.23: Mean concentration of trimers at $t = 10$ plotted against increasing microdomain size for five values of k_d.

Low microdomain coverage enhances complex formation for small microdomains

We also examined the effect, as in Chapter 3, of varying total membrane coverage; testing four different values of 50%, 25%, 10% and 5%.

We found that monomer concentration was maximised in microdomains at 5% membrane coverage and that increasing coverage led to a monotonic decrease in monomer concentration at $t = 10$. At 50% coverage, there was barely any increase in monomer concentration within the microdomain region. This relationship, as well as the model results

for dimer and trimer formation are depicted in Figure 4.24.

Interestingly, the relationship between microdomain length and total membrane coverage is more complex when protein-protein reaction is taken into account: in both cases, high membrane coverage leads to the fewest complexes being organised when microdomains are small. At higher microdomain lengths, however, more complexes are organised in the 50% coverage system than in systems with a lesser microdomain fraction.

In both dimer formation and trimer formation, the peak was almost indistinguishable at the optimal length between the 5% and 10% coverage cases. The results in this section are interesting in that they support the two dimensional simulation results in Chapter 3, Figure 3.5, in which the 10% and 25% coverage system lead to a greater number of receptors being formed at low microdomain radii, but the 50% microdomain fraction system organises more receptors at higher microdomain radii. The result also raises important questions about whether upregulating raft formation in cell membranes would facilitate increased signalling, if the number of complexes organised in fact occurs at a lower microdomain fraction.

Larger microdomains favour complex formation in long time scales

The results in Figure 4.21 suggest that complex formation is optimised for a particular microdomain length at a particular timescale. Specifically, at longer timescales, eventual complex organisation is maximised in systems with microdomains of greater length. The behaviour of the system on extreme timescales is shown in Figure 4.25. Here we see, despite the clear advantage of small microdomains at short timescales, as $t \to \infty$, the equilibrium number of trimers formed in the system is maximised in models with larger microdomains. This result suggests that our, and other authors' previous modelling work may not have fully explored the evolution of the system on long enough timescales to determine the equilibrium outcome, since our results in Chapter 3 as well as results from Nicolau et al. [81] and other papers suggest that small microdomains maximise protein-protein interactions.

Of course, the plot also shows that small microdomains organise trimers at a faster

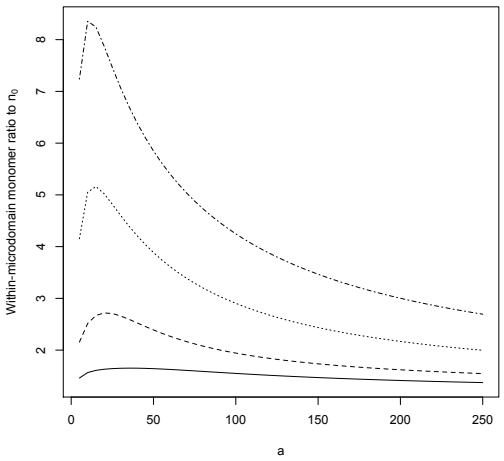

(a) Ratio of mean monomer concentration within microdomain to initial level

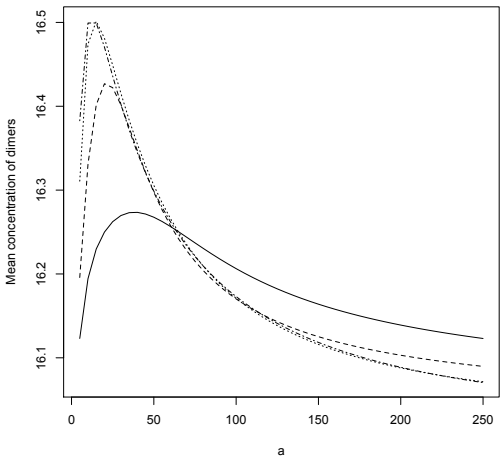

(b) Mean dimer concentration over whole space

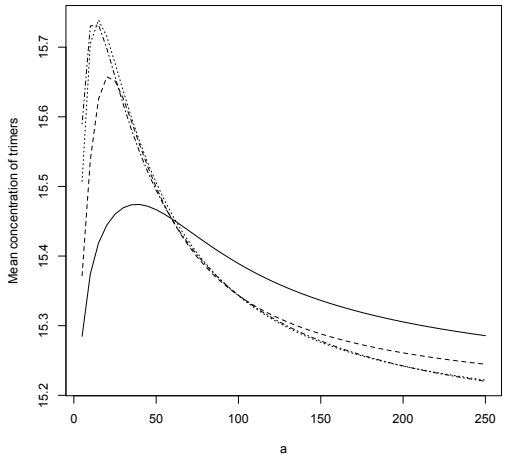

(c) Mean trimer concentration over whole space

Figure 4.24: This plot shows the dependence of monomer, dimer and trimer concentration on microdomain size. Monomer concentration is measured within the microdomain area and normalised by the initial level. Dimer and trimer concentrations are the mean over the whole space. The various plots show total microdomain coverage of 50% (solid line), 25% (dashed line), 10% (dotted line), and 5% (dashed and dotted line).

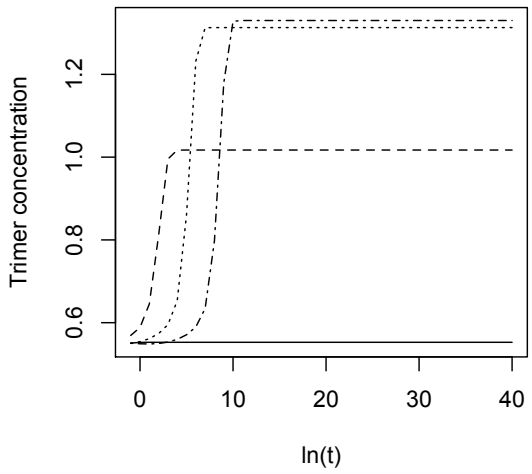

Figure 4.25: The limiting behaviour in large values of t for microdomain sizes of 1 (solid), 5 (dashed), 25 (dotted) and 125 (dashed and dotted).

rate initially, despite reaching a plateau relatively early. And if microdomains are only transient, rather than stable, structures then the ability to facilitate receptor complexes quickly before they dissipate may be a greater advantage than reaching a higher equilibrium concentration over a great period of time.

We have seen some agreement in the results of the analytical modelling in this chapter with the simulation results of Chapter 3; in the next section we test our analytical model by comparing it with the numerical simulations generated at the beginning of this chapter.

4.5 Model verification

We may use the numerical simulation generated at the beginning of this chapter in order to verify the analytical model just derived. Plotting both sets of data on the same axis we see that the analytical solution provides a good model of the related stochastic system. Figure 4.26 shows the two systems plotted over one another at four subsequent time points. The fit is particularly good for small values of t, though there appears to be a slight discrepancy within the microdomain region at $t = 50$. Figures 4.27 and 4.28 compare the analytical model with the scheme 3 reaction-diffusion systems in which dimers and trimers form from

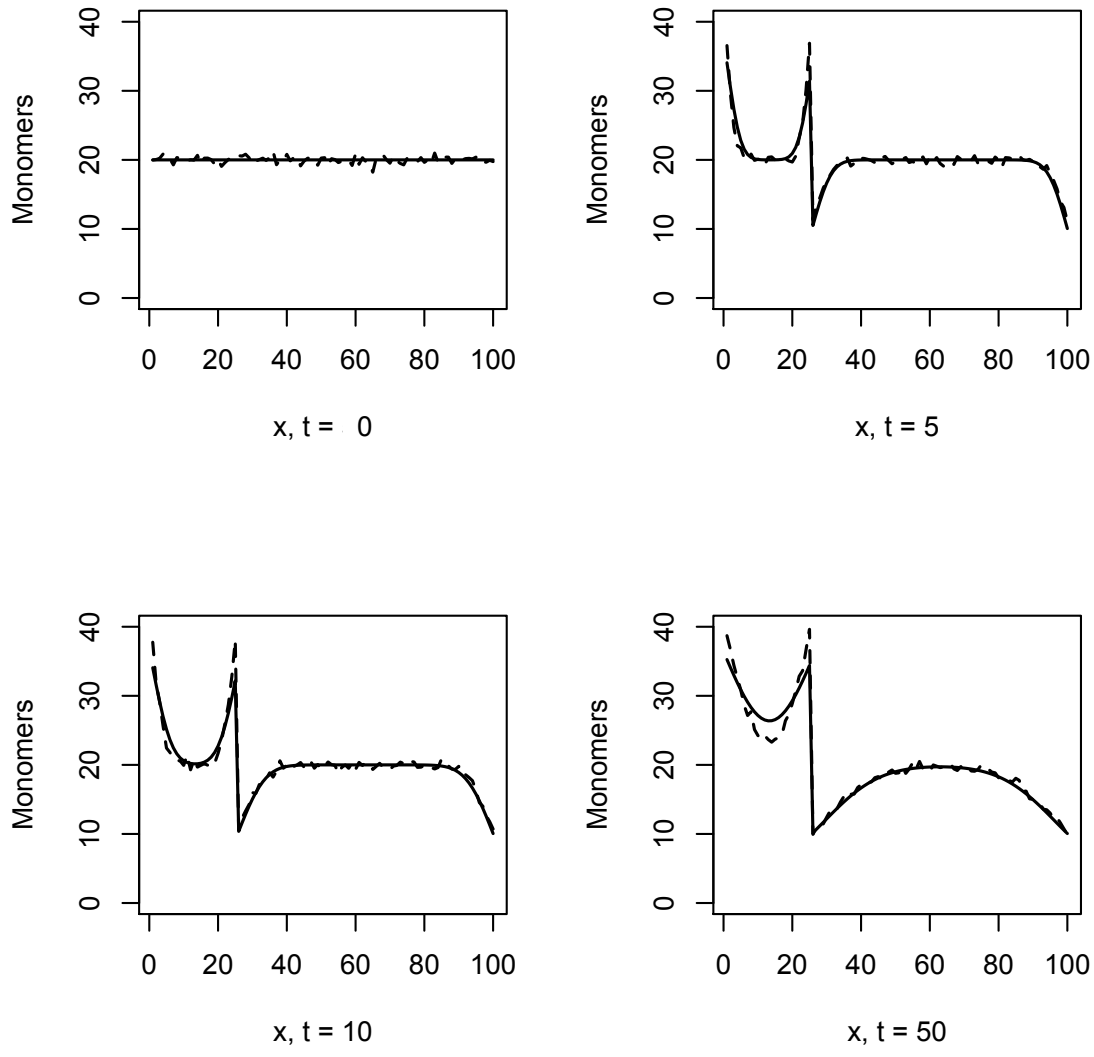

Figure 4.26: A numerical approximation to the analytical solution for monomer diffusion in the periodic case, plotted over the numerical simulations generated at the start of this chapter. The analytical model solution is plotted as a solid line and the numerical solutions are plotted as a dashed line.

the pool of diffusing monomers. In addition to verifying the diffusion behaviour of the analytical model, the good fit of these two systems supports the simplifying assumptions that we made regarding the formation of the multimeric complexes: that the system would be treated as though it had reached an equilibrium at each individual point in the one dimensional space.

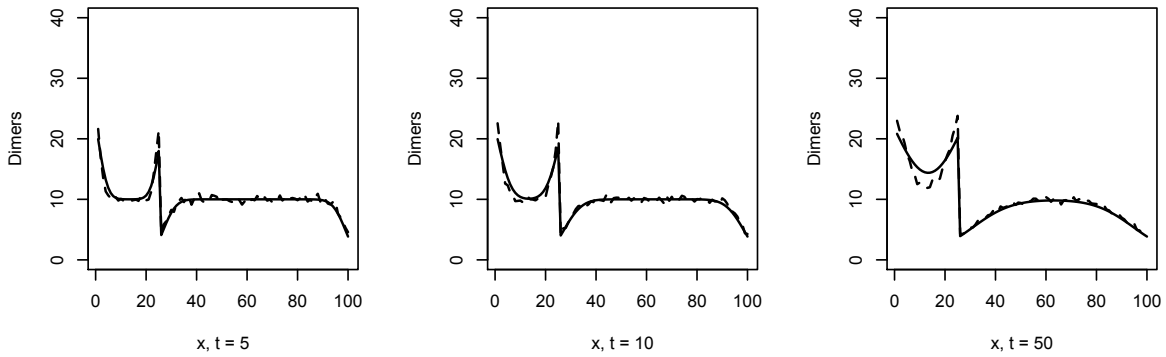

Figure 4.27: A numerical approximation to the analytical solution for dimer formation in the periodic system, plotted over the numerical simulation. The analytical model solution is plotted as a solid line and the numerical solutions are plotted as a dashed line.

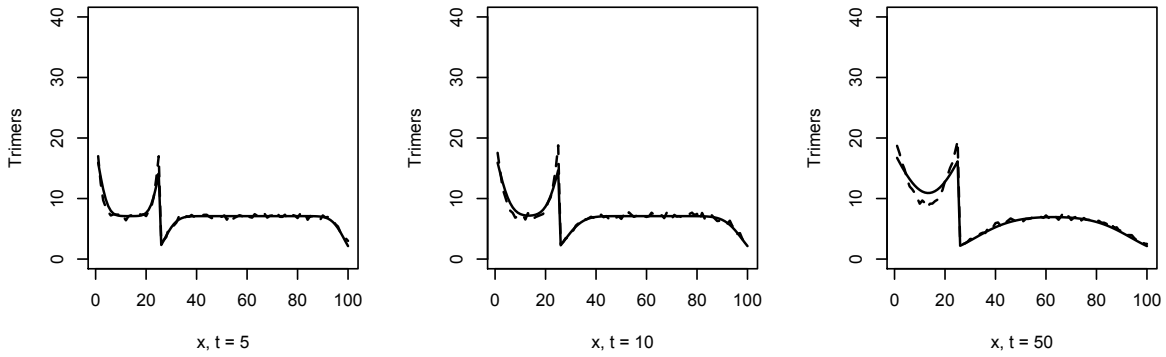

Figure 4.28: A numerical approximation to the analytical solution for trimer formation in the periodic, plotted over the numerical simulations. The analytical model solution is plotted as a solid line and the numerical solutions are plotted as a dashed line.

4.6 Further work

We have further clarified the nature of protein sorting found in the simulations in Chapter 3; first by focusing in greater spatial detail on numerical simulations in a slice across the two dimensional space and then by building increasingly complex analytical reaction-diffusion models to mimic the systems of interest.

A limitation of the work in this chapter is, of course, that we have confined ourselves to a single dimension. While this makes solution of the analytical system more amenable, it makes the results harder to compare to the results of the previous chapter and also to a biological system. Because a space comprising circular microdomains embedded in a plane has distinct topological properties from finite lengths embedded in a straight line, there could yet be non-trivial qualitative differences in the behaviour of the system. For example, migrating proteins can traverse the plane without ever entering an embedded microdomain, whereas proteins in the 'membrane' region are confined between the surrounding microdomain regions. In further work, we would look to extend the analytical approach to two dimensions and determine what, if any, qualitative differences in the system were.

A more generalised approach to particle diffusion in inhomogeneous media is taken in Bringuier [15], in which the author derives diffusion behaviours as particles diffuse in a three dimensional volume with diffusivity varying either geometrically, defined by specific structures as in our case, or depending on the local temperature of the medium (thermal inhomogeneity). Further development of microdomain-mediated diffusion models could build on the results in the above paper.

A second simplifying assumption in this chapter was that all monomer species were seeded at the same initial concentration and that all complexation and degradation events took place at the same rate. It would not be difficult to explore more realistic complexation rates, which differ for the dimerisation step and the trimer formation; or to seed the space with different numbers of constituent monomers. Expression of the IL2-α subunit, especially, varies considerably in relation to the β and γ subunits [36]. In future work, we would explore how one variation in the initial expression of one subunit affected the

evolution of the system in time.

4.7 Appendix B

In the paper by van Milligen et al. [78] the authors present an analytic solution to the problem of particles diffusing on an infinite one-dimensional space with a discontinuity in the diffusion coefficient at $x = 0$. As the method is not included in the paper, we re-derive the solution below.

Particles diffuse on an infinite 1 dimensional space such that the diffusion rate for $x < 0$ is D_L and the diffusion rate for $x > 0$ is D_R.

Diffusion governed by the equation:

$$\frac{\partial n}{\partial t} = \frac{\partial^2}{\partial x^2}(Dn) \tag{4.58}$$

Where $n(x,t)$ is the concentration of particles. Also assume that $\frac{\partial n}{\partial x} = 0$ at $\pm\infty$.

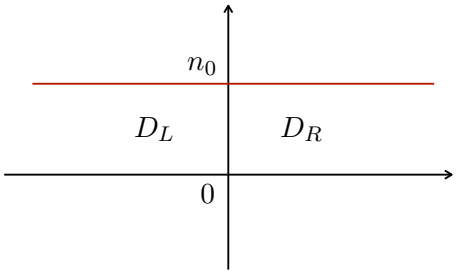

Figure 4.29: The system begins with a uniform distribution of particles at concentration n_0. The diffusion coefficient is D_L for $x < 0$ and D_R for $x > 0$.

This system has a smooth, uniform initial distribution of particles, but simulations show that the distribution immediately becomes discontinuous at $x = 0$.

Consider the derivative of Dn with respect to t:

$$\frac{\partial(Dn)}{\partial t} = D\frac{\partial n}{\partial t} + n\frac{\partial D}{\partial t} \tag{4.59}$$

Since D is constant in time, we have:

$$\frac{\partial(Dn)}{\partial t} = D\frac{\partial n}{\partial t} = D\frac{\partial^2}{\partial x^2}(Dn) \tag{4.60}$$

The initial conditions for this system are: $Dn = D_L n_0$ for $x < 0$ and $Dn = D_R n_0$ for $x > 0$.

Now, from the fundamental solution of the heat equation, solutions to systems of this type have the form:

$$Dn(x,t) = B \cdot \text{erf}\left(\frac{x}{2\sqrt{Dt}}\right) + C \tag{4.61}$$

where

$$\text{erf(x)} = \frac{2}{\sqrt{\pi}} \int_0^x e^{-s^2} ds \tag{4.62}$$

Note that erf($-\infty$) = -1; erf($-\infty$) = -1 and erf(0) = 0.

Now, allowing D to be discontinuous in x, we seek values of B and C such that both Dn and $\frac{\partial(Dn)}{\partial x}$ are continuous.

At $x = -\infty$, for all $t > 0$ we have:

$$D_L n_0 = C - B \tag{4.63}$$

and so $B = C - D_L n_0$.

Then, taking the derivative of Dn:

$$\frac{\partial D_L n_L}{\partial x} = \frac{C - D_L n_0}{2\sqrt{D_L t}} \cdot \text{erf}'\left(\frac{x}{2\sqrt{D_L t}}\right) \tag{4.64}$$

$$\frac{\partial D_R n_R}{\partial x} = \frac{C - D_R n_0}{2\sqrt{D_R t}} \cdot \text{erf}'\left(\frac{x}{2\sqrt{D_R t}}\right) \tag{4.65}$$

since the derivative is continuous, we have:

$$\frac{C - D_L n_0}{\sqrt{D_L}} \cdot \text{erf}'\left(\frac{x}{2\sqrt{D_L t}}\right) = \frac{C - D_R n_0}{\sqrt{D_R}} \cdot \text{erf}'\left(\frac{x}{2\sqrt{D_R t}}\right) \tag{4.66}$$

at $x = 0$. i.e.

$$C(\sqrt{D_R} - \sqrt{D_L}) = n_0(D_L\sqrt{D_R} - D_R\sqrt{D_L}) \tag{4.67}$$

$$C = n_0\sqrt{D_R D_L} \tag{4.68}$$

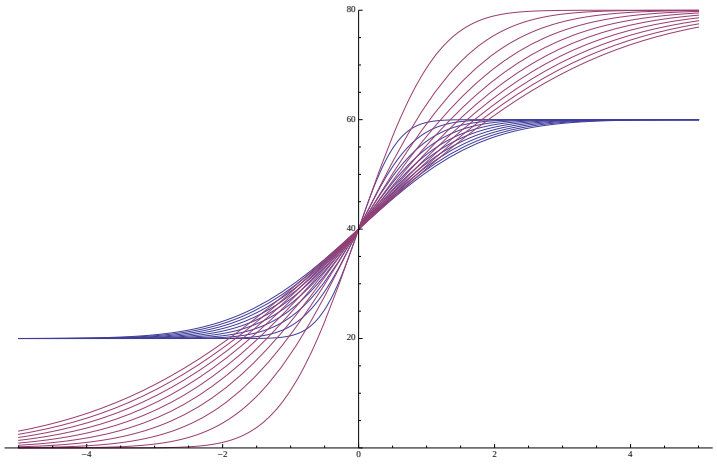

Figure 4.30: Solutions of Dn with respect to x for the values $n_0 = 20$, $D_L = 1$, $D_R = 4$ and $t = 0.1, 0.2, \ldots 1.0$. The blue plots show the solution of the system for $D = D_L$, valid for $x < 0$ and the purple plots show the solution of the system for $D = D_R$, valid for $x > 0$.

Hence, dividing these solutions by D on each side of the boundary, we derive:

$$n_L(x,t) = n_0\frac{\sqrt{D_R}}{\sqrt{D_L}} + \left(n_0\frac{\sqrt{D_R}}{\sqrt{D_L}} - n_0\right)\cdot \operatorname{erf}\left(\frac{x}{2\sqrt{D_L t}}\right) \tag{4.69}$$

$$n_R(x,t) = n_0\frac{\sqrt{D_L}}{\sqrt{D_R}} - \left(n_0\frac{\sqrt{D_L}}{\sqrt{D_R}} - n_0\right)\cdot \operatorname{erf}\left(\frac{x}{2\sqrt{D_R t}}\right) \tag{4.70}$$

as in van Milligen et al. [78].

Chapter 5

T cell proliferation responses to microdomain-mediated signalling

5.1 Introduction

In the preceding chapters, we have investigated the formation of a simplified trimeric IL-2 receptor, depending on the structure and properties of the membrane in which its constituent monomers are diffusing. The formation of such a receptor, however, is only a single piece in an immune response of considerable complexity.

As discussed in Chapter 2, IL-2 is a potent autocrine signalling molecule for T cell proliferation in lymph nodes and in the periphery. Signalling is in response to a threshold level of signalling via the TCR. In this chapter, we combine the model of the previous chapter with existing, tested models of T cell proliferation in order to quantify the degree to which receptor organisation can determine cell population expansion, and how membrane microdomains could influence this mechanism.

The threshold-mediated response to stimulatory signals is a common feature of immunological signalling networks. As we discussed in the Literature Review, T cell stimulation by the TCR is determined by threshold numbers of pMHC bound in the TCR clusters in the immunological synapse[72]. Likewise, Smith et al. postulated a threshold-mediated proliferative response in T cells to IL-2 signalling [21, 108], whereby cell population growth

is negligible below a certain number of bound receptors per cell, and increases sharply to a constant growth rate above that threshold. This behaviour is also seen in studies of epidermal growth factor stimulation [92] and IL-7 signalling [86, 85] and fits well with the observed proliferative response of T cell populations in *in vitro* studies[37].

Busse et al. combined mathematical modelling with experimental work to confirm that T_H cells also react to stimulation by IL-2 with a threshold-type behaviour and suggest that the secretion of IL-2 receptors above a certain level of exposure to extracellular ligand controls this phenomenon [19]. They also note that the presence of T_{reg} cells shifts the value of the threshold at which T_H cells are activated.

Threshold activation behaviour may also occur at the cell population level. Feinerman et al. [38] modelled how the density of T_H cells affected the ability to produce the sustained levels of STAT5 needed for immune response and also found that a threshold density of cells controlled whether or not immunostimulatory signalling was sustained in the population.

The ligation of the IL-2 receptor is the first step in the T cell proliferative response. Depending on the concentration of extracellular IL-2 the subsequent size of the T cell population can vary greatly. As well as the rate of cell division, IL-2 signalling strength can affect the rate of cell death after the first division[31].

5.2 Cell proliferation models

There exist several models of T cell proliferation in response to extracellular IL-2. One such is that by Fallon & Lauffenburger [36], which uses a system of coupled ODEs, combined with an empirically derived function relating the proliferation rate to the number of bound membrane complexes.

The model describes the time evolution of unbound IL-2 receptors, bound receptors and free IL-2 in a two-compartment system: both on the cell surface (or the extracellular space in the case of IL-2 ligand) and in the endosome. The components and parameters making up the model are described in Table 5.1, where internalised quantities are denoted with the subscript i. The model dynamics are described visually in Figure 5.1, which

Notation	Definition	Value	unit
R_s	Unbound surface receptors	1500	receptors per cell
R_i	Unbound internalised receptors	300	receptors per cell
C_s	Bound surface receptors	0	receptors per cell
C_i	Bound internalised receptors	0	receptors per cell
L	System concentration of IL-2	10	pM
L_i	Endosomal concentration of IL-2	0	pM
Y	Number of cells	2.5×10^8	cells
k_r	Surface dissociation rate constant	0.0138	min^{-1}
k_f	Surface association rate constant	$k_r/11.1$	$\text{pM}^{-1}\ \text{min}^{-1}$
k_{re}	Endosomal dissociation rate constant	$8k_r$	min^{-1}
k_{fe}	Endosomal association rate constant	$k_{re}/1000$	$\text{pM}^{-1}\ \text{min}^{-1}$
k_t	Receptor internalisation rate	0.007	min^{-1}
k_{syn}	Induced receptor synthesis rate	0.0011	min^{-1}
k_e	Bound receptor internalisation rate	0.04	min^{-1}
k_x	Recycling rate constant	0.15	min^{-1}
k_h	Degradation rate constant	0.035	min^{-1}
V_s	Constitutive receptor synthesis rate	11	min^{-1}
V_e	Total endosomal volume	10^{-14}	L/cell
N_A	One picomole	6.022×10^{11}	-

Table 5.1: Model variables and parameters in the Fallon model

represents the following system of coupled equations:

$$\frac{\partial R_s}{\partial t} = -k_t L R_s + (k_r + k_{syn})C_s - k_t R_s + V_s \tag{5.1}$$

$$\frac{\partial C_s}{\partial t} = k_f L R_s - (k_r + k_e)C_s \tag{5.2}$$

$$\frac{\partial R_i}{\partial t} = -k_{fe} L_i R_i + k_{re} C_i + k_t R_s - k_h R_i \tag{5.3}$$

$$\frac{\partial C_i}{\partial t} = k_{fe} L_i R_i - (k_{re} + k_h)C_i + k_e C_s \tag{5.4}$$

$$\frac{\partial L}{\partial t} = \left(\frac{-k_f L R_s + k_r C_s + k_x L_i V_e N_A}{N_A} \right) Y \tag{5.5}$$

$$\frac{\partial L_i}{\partial t} = \frac{k_{re} C_i - k_{fe} L_i R_i}{V_e N_A} - k_x L_i \tag{5.6}$$

$$\frac{\partial Y}{\partial t} = \max\left(\frac{600 C_s}{250 + C_s} - 200, 0 \right) \times 10^3 \tag{5.7}$$

The model describes the eventual population expansion of T cells, in response to the binding and internalisation of IL-2 ligand to pre-formed IL-2 receptors. The cell population growth rate is described by the final equation and is based on a phenomenological fitting of a growth curve to experimental data generated by the authors in an earlier paper [37].

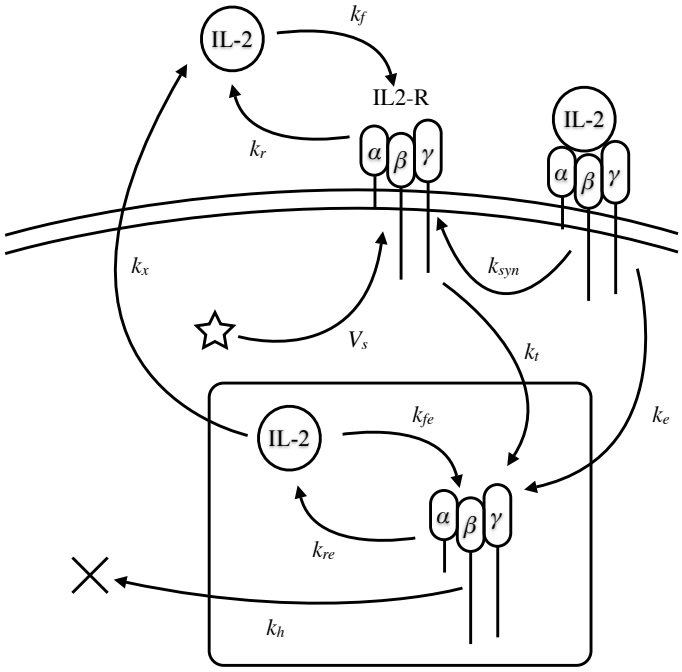

Figure 5.1: A cartoon of the dynamics described by the Fallon model.

The equation results in a threshold behaviour where cell growth is zero when the number of bound surface receptors (C_s) is below 125, and rapidly plateaus as the number of bound surface receptors increases.

The change in concentration of the extracellular ligand, L, is determined by the balance between ligand binding to cell surface receptors (R_s), the disassociation of ligand from bound receptor complexes (C_s) and the recycling of internalised ligand from the endosome (L_i). This is modelled as the net change in concentration (measured in picomoles) per cell, multiplied by the total number of cells in the population Y.

We re-implemented the ODE model above as a numerical system solved using an R script (listed in Appendix C), employing the Euler method to calculate the updated values of all the variables involved. We solved the system using a fixed timestep of 0.2 minutes; larger timesteps led to numerically unstable solutions.

Running the simulation with the initial values listed in Table 5.1 we see the profile over time of the cell receptor states, the systemic concentration of IL2, and the proliferation of T cells in response to the IL2 signal. This output is shown in Figure 5.2. Starting from an extracellular concentration of 10pM free IL-2 ligand, the extracellular signalling molecule

is consumed in around 8000 minutes as it is taken up by surface receptors, internalised and lysed. Note that a small fraction of the IL-2 is recycled into the extracellular space at a rate determined by the parameter k_x. The model is initiated with 1500 free receptors expressed on the cell surface and 300 in the endosome. The number of free receptors per cell rapidly drops in the first few hundred minutes as they bind the IL-2 ligand, and then returns slowly to its initial level as the signalling molecule is depleted. Cell density also rises steeply in the first 2000 minutes, but only to around 15% higher than its starting value. These numerical solutions to the ODEs above match well with the figures published

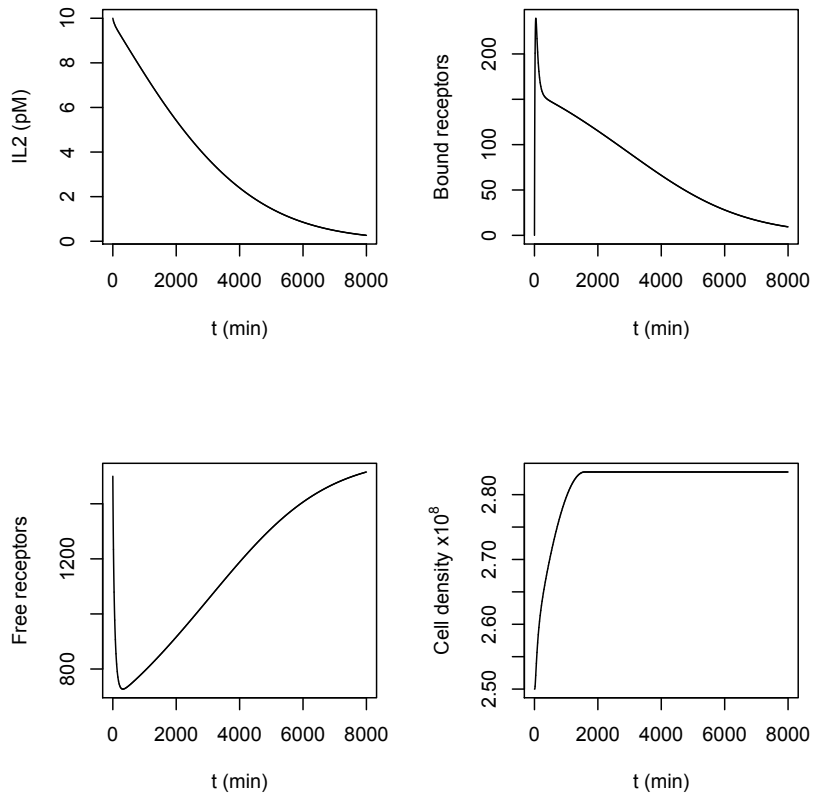

Figure 5.2: The first 8000 minutes of the T cell proliferation model, with an initial cell count of 2.5×10^8 and an initial IL2 concentration of 10pM.

by Fallon & Lauffenburger.

Several other theoretical approaches to T cell proliferation signalling are also worthy of note.

Deenick et al. [31] created an event-based stochastic model of T cell proliferation and measured T cell numbers in timed harvests for a range of IL-2 concentrations in order to determine the dependence of the time-evolution of T cell population size on ligand concentration. They found that increased IL-2 signalling strength did not affect the time to the first cell division, but that it decreased the time between subsequent divisions and also increased the survival probability of T cells from one generation to the next.

Bidot et al. [13] adapted the model of Fallon & Lauffenburger to include earlier upstream events, including the ligation, activation and internalisation of the TCR; the spatial effects dependent on the organisation of the immunological synapse; the cellular expression of CD69 and IL-2 in response to TCR activation; and feedback loops between IL-2, IL-2 receptor, and CD69 expression. This model however considered only a single cell embedded in a small extracellular space and did not model increases in cell population density.

In the following section, we take the model of Fallon & Lauffenburger and perturb key parameters in order to quantify the significance of surface receptor expression on system behaviour.

5.3 Sensitivity to surface receptor number

The earlier modelling chapters monitored the increased propensity of a reaction-diffusion system to organise trimers on the cell surface. In the Fallon model, trimeric IL-2 surface receptors are represented by the quantity R_s. These are constitutively expressed at a rate V_s and internalised at a rate k_t.

For the purpose of this chapter, we will interpret the surface expression of new receptors as a two step process in which the components of the receptor are first expressed as monomers and then the receptor subsequently organises on a timescale significantly less than the length of the simulation. We will take the maximum time period for a receptor to organise to be 1 minute.

In this way, any increased level of trimer formation can be expressed within the model as a coefficient of the constitutive receptor synthesis rate. We will name this quantity the

perturbation coefficient and represent it with the symbol C_p.

In this section, the equation modelling the change in surface receptor numbers is now:

$$\frac{\partial R_s}{\partial t} = -k_t L R_s + (k_r + k_{syn})C_s - k_t R_s + C_p V_s \tag{5.8}$$

We tested the sensitivity of the system to variations in C_p over 5 values: 0.25, 0.5, 1, 2 and 4. We also ran the simulation at a high initial IL-2 concentration of 100pM as in the original paper[36].

The results of these experiments are shown in Figures 5.3 and 5.4.

In the low initial concentration simulation, lowering the rate of constitutive receptor expression lowered the consumption rate of ligand and decreased the degree of proliferation to almost nothing. The balance between receptor internalisation and expression was disturbed so both bound and unbound surface receptors fell to very low levels, where they remained for the duration of the simulation.

Increasing V_s had the opposite effect: IL-2 ligand was depleted rapidly – within 2000 minutes when expression was increased fourfold – and the increase in cell density was much higher for both twofold and fourfold increases in receptor expression rate. The cell population increased by roughly another 70% of its starting density.

With a fourfold increase in surface receptor expression, the number of unbound surface receptors climbed to over 4 times the original level and, after peaking early, the number of bound receptors fell to zero at around 2000 minutes as the extracellular ligand was fully depleted. The behaviour of the system responding a high initial concentration of IL-2 was slightly different. Again, the cell population with the highest rate of constitutive receptor expression consumed the extracellular ligand in the shortest time. Even though the initial concentration of ligand was increased tenfold from the previous set of simulations, it was all depleted in less than twice the time for the highest rate ($C_p = 4$) of receptor expression.

Notably, in this set of experiments the cell density increased to the highest value for intermediate receptor expression rates. Whereas, in the low initial concentration simulations, increasing C_p above 1 led to a higher eventual cell density; in this set of simulations, the faster rate of receptor expression meant that the cell density increased more quickly,

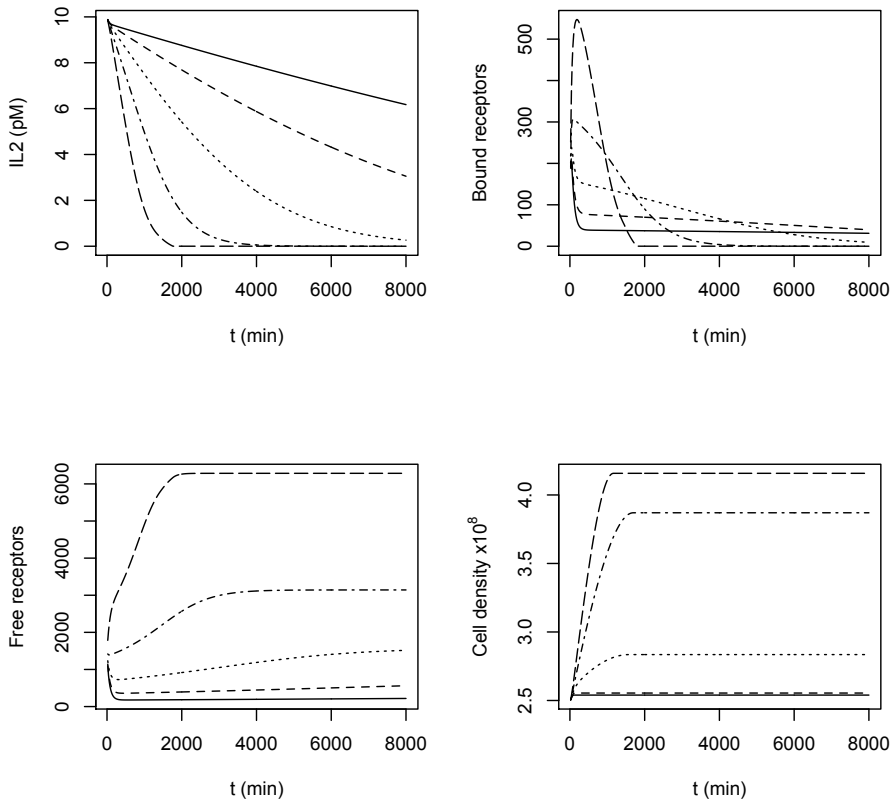

Figure 5.3: T cell proliferation in response to IL2 with the receptor synthesis rate multiplied by a factor of 0.25 (solid line), 0.5 (dashed line), 1 (dotted line), 2 (dashed and dotted line) and 4 (long dashed line). The initial IL2 concentration was 10 pM.

but then plateaued at an earlier point. The control system ($C_p = 1$) was still increasing in cell density at the end of the simulation and had already surpassed the highest expression rate ($C_p = 4$) at that point. These initial results show the scope for optimising membrane

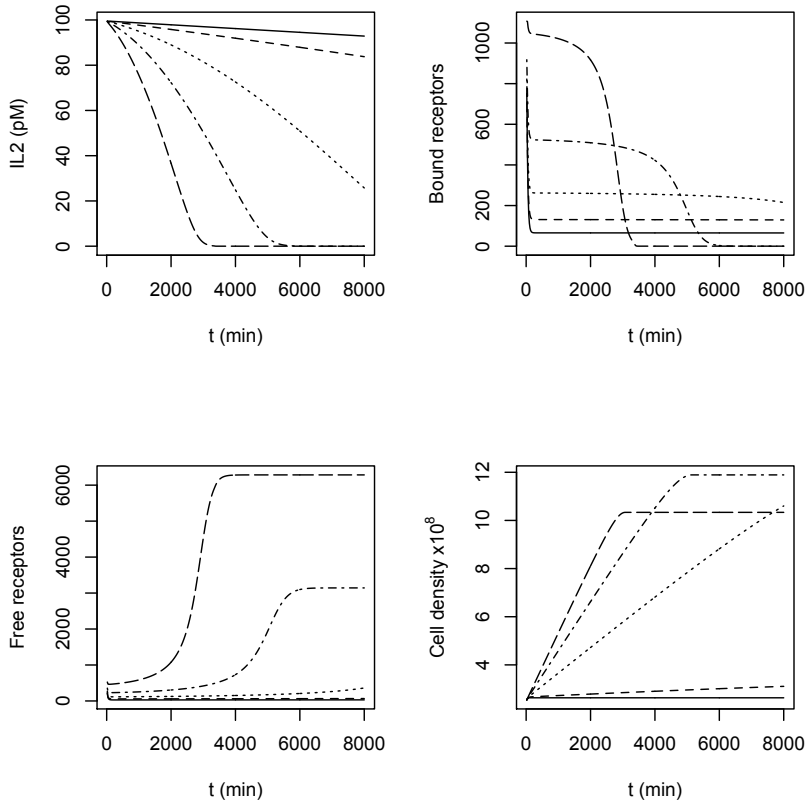

Figure 5.4: T cell proliferation in response to a raised initial IL2 concentration of 100 pM. The receptor synthesis rate was multiplied by a factor of 0.25 (solid line), 0.5 (dashed line), 1 (dotted line), 2 (dashed and dotted line) and 4 (long dashed line).

receptor complex organisation in influencing the degree of cell proliferation. Importantly, there appears to be a non-monotonic relationship: when initial ligand concentrations are high then there exists an optimal rate of receptor expression to maximise eventual cell population density. For lower initial concentrations, increasing receptor expression rates appears always to increase the eventual population density, though more exhaustive parameter testing would be needed to verify this.

5.4 Parameter exploration

5.4.1 Method

In the previous section, we saw that perturbations to the constitutive expression of IL-2 receptor in the Fallon model led to wide variation in the rate of cell proliferation and eventual population size. In this section, we explore which range of biologically plausible parameters may lead to a sufficiently large perturbation in IL-2 receptor expression.

We return to the analytical model in Chapter 4 in order to calculate how the surface microdomain structure might affect IL-2 receptor formation. Recall, however, that the model generated a complex relationship between microdomain size and trimer formation over time in that larger microdomains tended to form trimers more slowly, but eventually reached a higher equilibrium value.

In order to take this behaviour into account within the dynamics of the second model, we will make the further assumption that microdomains have a fixed lifetime, τ, and that they decay after that timepoint. In this way, we can calculate the number of trimers organised within a single microdomain lifetime and return this as the value for the constitutive receptor expression at each timestep of the model.

Using Fallon's model as a control system, we require an extra calculation step to determine the effect of membrane heterogeneity on system behaviour. If we interpret V_s as the number of trimers organised under control conditions, then we must calculate the number of monomer species necessary to form that number of trimers under control conditions. We determine this relationship by solving Equation 4.56 for n_0 instead of $[C]$.

We re-ran the R script to solve the analytical model of the previous chapter, varying six model parameters: a (the microdomain length), τ (the microdomain lifetime), ϕ (the membrane coverage), k_d (the complex dissociation rate), ρ (the ratio of the high-speed diffusion constant to the low-speed diffusion constant), and V_s (the number of trimers organised in the control system). The complex association rate, k_c was fixed at 1 and the high-speed diffusion rate was fixed at $0.05\mu\text{m}^2\text{s}^{-1}$ (see Section 5.4.2).

With each run of the model, we inferred the necessary number of monomers $n_{mono}(v_s)$ at time t_0 to organise the specified number of trimers given by V_s. We then recalculated

the modelled number of trimers formed in the presence of microdomain regions in the same time frame. From this we calculated the perturbation constant:

$$C_p = \frac{\bar{T}(a, \tau, \phi, k_d, \rho, n_{mono}(v_s))}{v_s} \tag{5.9}$$

where $\bar{T}$ denotes a function returning the mean number of trimers organised by unit length.

5.4.2 Choice of parameter range

The choice of parameters tested in this section is informed by the values taken from the various studies reviewed in Chapter 2.

- Length, a: Nicolau et al. [81] modelled microdomains in the range 6–50nm; Pralle et al. estimated microdomain size as 26±13nm using single particle tracking; Veatch et al. detected l_o domains in multilamellar vesicles of diameter 80nm; microdomains in a ternary lipid model by de Almeida et al. [27] existed in two forms: 20–75nm in binary lipid mixtures and 75–100nm in ternary mixtures.

- Lifetime, τ: Kusumi et al. [62] review several studies estimating raft lifetimes including Subczynski et al. [110], which posits the existence of multiple types of microdomain with lifetimes varying from 100ns to several minutes.

- Microdomain coverage, ϕ: the fractions tested follow the values used in Nicolau et al. [81]; studies by Hao et al. indicate that in some cases, 'raft' fractions could make up 30–50% of the total membrane area; Prior et al. found that raft fractions covered around 35% of the cell membrane in a BHK model.

- Difference in diffusion rate, ρ: Pralle et al. determined that local viscous drag was between one twice and five times as great inside lipid rafts as in the membrane.

- Baseline receptor expression, V_s: Fallon et al. use a value of 11 receptors per minute.

The above ranges form the basis of the parameter ranges investigated in the following section. The exact values tested are shown in Table 5.2.

Notation	Definition	Unit	Range of values
a	Microdomain length	μm	$0.001, 0.005, 0.025, \ldots, 3.125$
τ	Microdomain lifetime	min	$10^{-5}, 10^{-4} \ldots, 10^{-1}, 1$
ϕ	Microdomain coverage	-	$50\%, 25\%, 10\%, 5\%$
k_d	Dissociation rate	min^{-1}	$10^{-3}, 10^{-2}, \ldots, 10^{3}$
ρ	Retardation constant ($\frac{D_R}{D_L}$)	-	$2, 4, 8, 16$
V_s	Baseline trimer concentration	pM	$1.25, 2.5, 5, 10, 20, 40, 80$

Table 5.2: Parameters varied from Chapter 4 model. D_R is fixed at $0.05\mu\text{m s}^{-1}$.

5.4.3 Coarse-grained parametric analysis

We calculated multiple solutions to the analytical model in Chapter 4, based on the parameter sets specified in Table 5.2. For each instance of the model, we calculated the perturbation coefficient C_p. This generated an array of 28224 values for C_p. The maximum of the array was $C_p = 7.873$ and the minimum was $C_p = 0.995$. This shows that in the parameter range explored, the presence of microdomains does not significantly impede the formation of trimers, and that certain parameter sets see an almost eightfold increase in receptor expression compared to a system with no microdomains.

The set of parameters which lead to a large increase in receptor organisation, however, is relatively narrow. Figure 5.5 shows a logarithmic plot of the number of parameter sets of all those tested that result in perturbation constants in the range 1.0–8.0. From the figure, one can see that the vast majority of parameter sets tested result in only a negligible increase in trimer formation, which implies that microdomain mediated complex formation may be highly dependent on the interplay between the parameters of the system. Of the entire set of parameters tested, 43 sets led to a greater than twofold increase in trimer formation and 9 sets led to a greater than fourfold increase.

Of the 9 parameter sets which resulted in a greater than fourfold increase in trimer organisation, the length of the microdomains in each case was 0.125μm and the lifetime of the microdomains was at the upper end of the scale at 1 minute. They also all had a high dissociation rate of 1000 min^{-1}. The remainder of the parameter values in this subset are shown in Table 5.3. Figure 5.6 shows contour plots of the dependence of C_p on both microdomain length and baseline receptor expression rate. The three subfigures

ϕ	ρ	V_s	C_p
10%	16	1.25	5.849
10%	16	2.5	4.995
10%	16	5.0	4.195
5%	8	1.25	5.321
5%	8	2.5	4.450
5%	16	1.25	7.873
5%	16	2.5	6.365
5%	16	5.0	5.079
5%	16	10.0	4.023

Table 5.3: Parameter sets resulting in over fourfold increase in trimer formation.

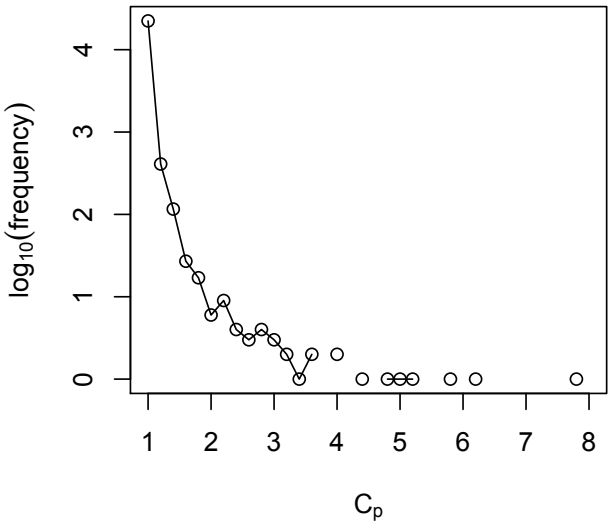

Figure 5.5: The base 10 logarithm of the number of parameter sets explored in Section 5.4.3 resulting in a perturbation constant of magnitude C_p.

depict solutions to the model for three different values of ρ. As can be seen in the figure, the receptor organisation is optimised around the approximate 0.125μm range, which is invariant for all values of ρ. The value of C_p is maximised for high ρ values and low V_s values, i.e. protein diffusion is greatly slowed within microdomains and receptors are expressed sparsely in the control system. The contour plot for the case $\rho = 2$ is not shown as all C_p values were in the range 1–2. The membrane coverage, ϕ was held constant at 5% for the plots in this figure. Figure 5.7 shows a similar plot where ρ is held constant at 16 and the membrane coverage, ϕ, is increased over four values. Here, again, we see that low microdomain coverage increases the amplifying effect of microdomain-mediated complex organisation. For the two lowest coverage values (5–10%) we see that the optimal length scale again appears to be around 0.125μm. When coverage increases to the 25–50% range, however, it appears that the optimal length scale also increases. This suggests that the existence of optimal length scales in enhancing complex formation is dependent on total membrane coverage as well as the lifetime of the microdomains. In Figure 5.8, we see a similar plot with a more detailed depiction of the change in C_p with respect to microdomain length. Again, this is at a relatively long timescale (τ = 1 min) and the values of ϕ and ρ are 5% and 16 respectively. The previous figures all depict the state of the model at the longest timescale of 1 minute. It was only at this timescale that C_p values greater than 4 were observed. Figure 5.9 shows the evolution of the system up to that point at the two prior timescales tested: 0.01 min and 0.1 min. Note that the first two subfigures are plotted on an axis with a range of 1.0–1.8 and the third subfigure is plotted on an axis with a range of 1.0–8.0.

Notably, there is little increase in C_p at short timescales, even up to six seconds; all of the enhancement of trimer formation depends on microdomains existing for between 6 and 60 seconds, or possibly longer.

5.5 Finer-grained parameter exploration

In the previous section we identified sets of parameters that maximised the amplifying effect of microdomain presence on trimer formation, within a predetermined range of

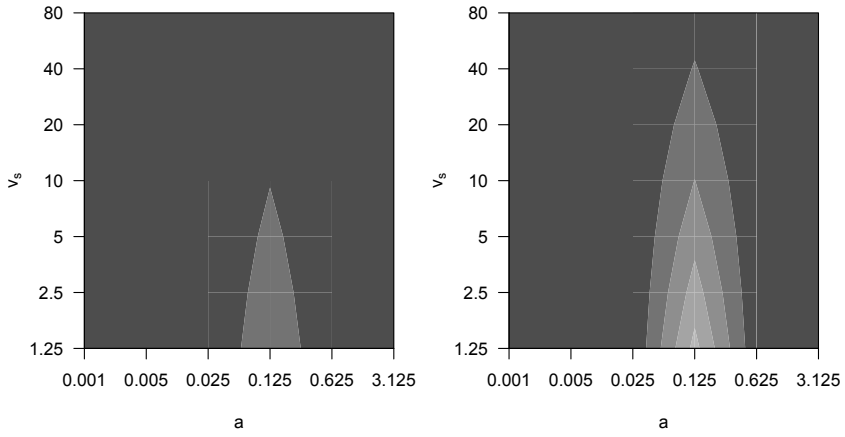

(a) $\rho = 4$ (b) $\rho = 8$

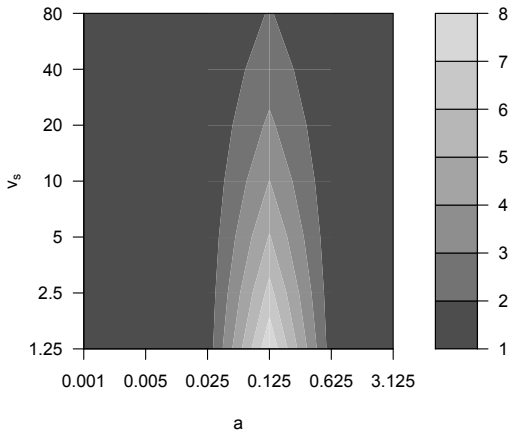

(c) $\rho = 16$

Figure 5.6: Increased trimer formation for increased values of ρ with other parameter values set at: τ=1min, $\phi = 5\%$ and k_d=1000. Microdomain length is shown on the horizontal axis on a $\log_5$ scale and V_s is on the vertical axis on a $\log_2$ scale. The increase in trimer formation for $\rho = 2$ is less than twofold for all values of a and V_s.

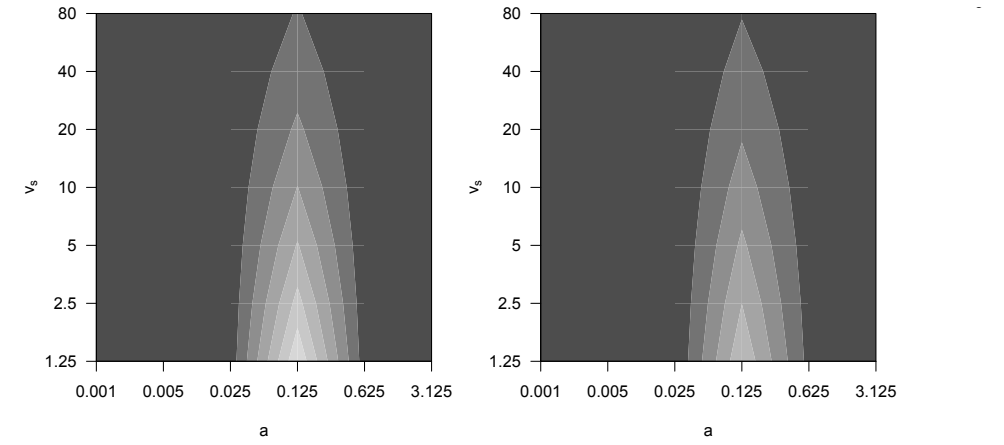

(a) $\phi = 5\%$ (b) $\phi = 10\%$

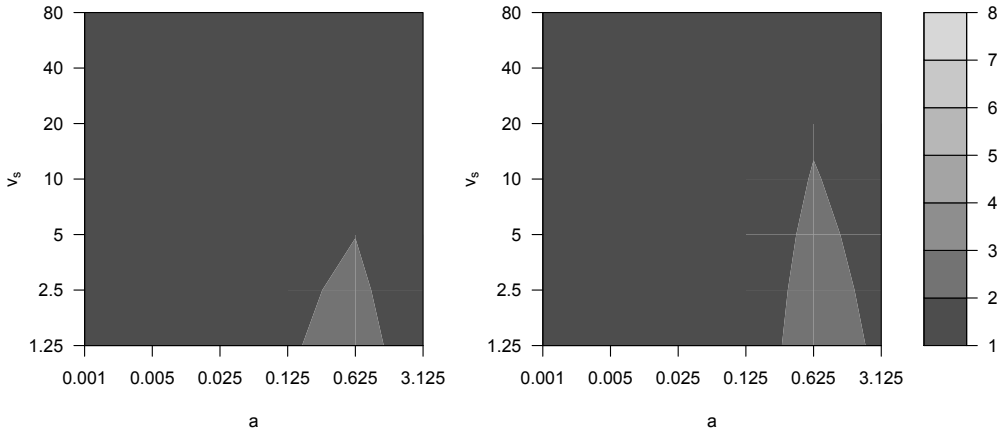

(c) $\phi = 25\%$ (d) $\phi = 50\%$

Figure 5.7: Increased trimer formation for increasing values of ϕ with other parameter values set at: τ=1min, $\rho = 16$ and k_d=1000. Microdomain length is shown on the horizontal axis on a $\log_5$ scale and V_s is on the vertical axis on a $\log_2$ scale.

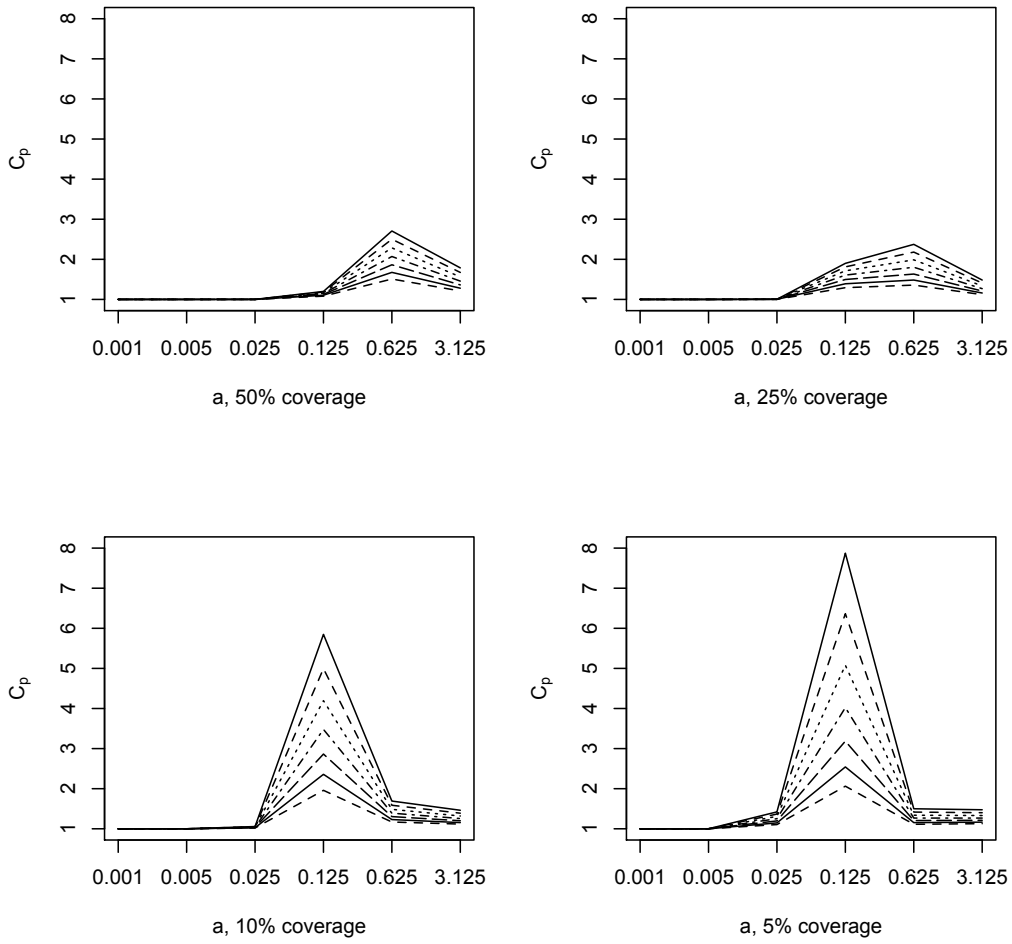

Figure 5.8: Increased rate of trimer formation (C_p) plotted against a ($\log_5$ scale) for four different values of microdomain coverage. The various series show different values of V_s where the uppermost solid line shows a V_s value of 1.25pM μm^{-2} and the lower series show higher values of V_s.

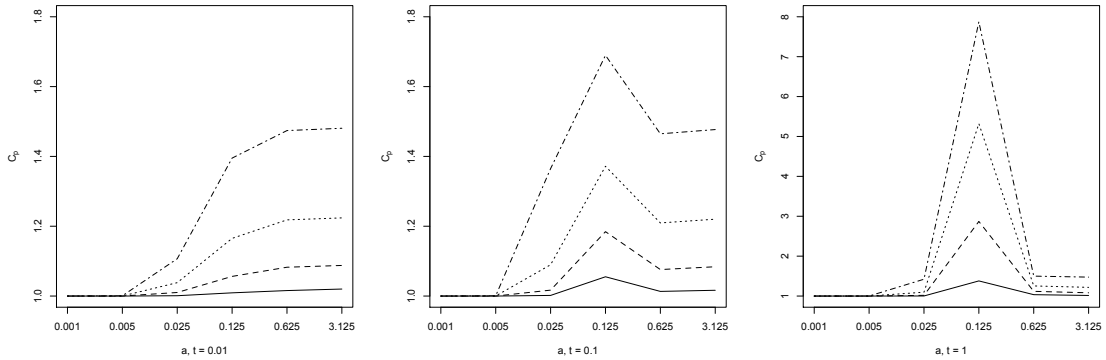

Figure 5.9: Increased rate of trimer formation (C_p) plotted against a ($\log_5$ scale) at three subsequent time points. The various series show different values of ρ where the lowest, solid line depicts $\rho = 2$ and the higher series show higher values of ρ.

Notation	Definition	Unit	Range of values
a	Microdomain length	μm	$0.05, 0.075, 0.1, 0.125, 0.0.15, 0.175, 0.2$
ϕ	Microdomain coverage	-	$1\%, 2\%, \ldots, 10\%$
V_s	Baseline trimer concentration	pM	$1, 2, \ldots, 10$

Table 5.4: Parameter variation for Section 5.5 results. Other parameter values are held fixed at $\tau = 1$ min, $k_d = 1000$ s^{-1} and $\rho = 16$.

biologically plausible values. In this section, we examine the model output in greater detail around the parameter space previously identified, fixing parameter values that were highly invariant and varying others linearly rather than exponentially.

Although the microdomain length was a highly invariant parameter in terms of producing an optimised increase in trimer formation, we will still explore length dependence in this section, but at a finer resolution than in Section 5.4.3. The parameter sets tested in this section are listed in Table 5.4. This range of parameters returned the model output as a 700 element array. Of these, 658 parameter sets generated an increase in trimer formation of greater than twofold; 325 generated an increase in trimer formation of greater than fourfold; and 27 generated an increase of greater than eightfold. The maximum C_p value was 15.057 and the minimum was 1.435, indicating that trimer formation was enhanced in all of the experimental setups tested in this section.

A logarithmic plot of the number of parameter sets resulting in an increase of the value of C_p is shown in Figure 5.10. As can be seen, the mode of the distribution is

around a fourfold increase in receptor formation, and many sets result in increases up to 8 or 9 times the baseline expression rate. The interplay between microdomain length and

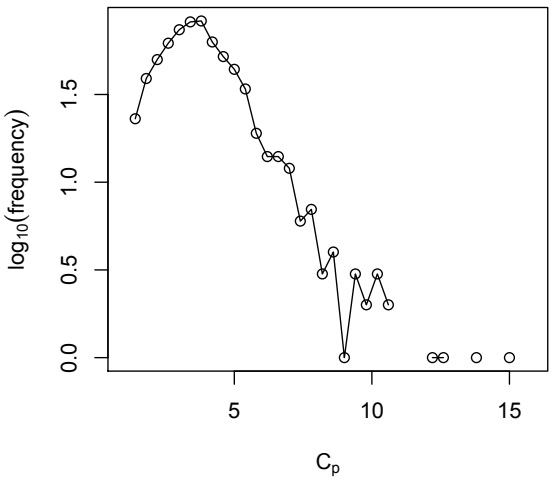

Figure 5.10: The base 10 logarithm of the number of parameter sets explored in Section 5.5 resulting in a perturbation constant of magnitude C_p.

baseline expression rate is depicted in the contour plots in Figure 5.11. As shown in the figure, when total membrane coverage is very low (1%), only very small microdomains and very low baseline receptor expression result in an increase in complex formation. The 'optimal length scale' seems to exist at higher membrane coverage values: at around 0.1 μm for 5% coverage and around 0.14 μm at 10% coverage.

5.6 Discussion and further work

The results in this chapter give the strongest evidence yet for a significant role for microdomains to play in facilitating receptor organisation, although the wide distribution in values for the quantity C_p suggests that mechanisms depending on spontaneous protein sorting into low-diffusion regions are highly dependent on the lifetime of those regions, the chemical kinetics of the proteins involved and the relative diffusion rates in and out of the microdomains.

In this chapter we have modelled how the presence and geometric properties of mi-

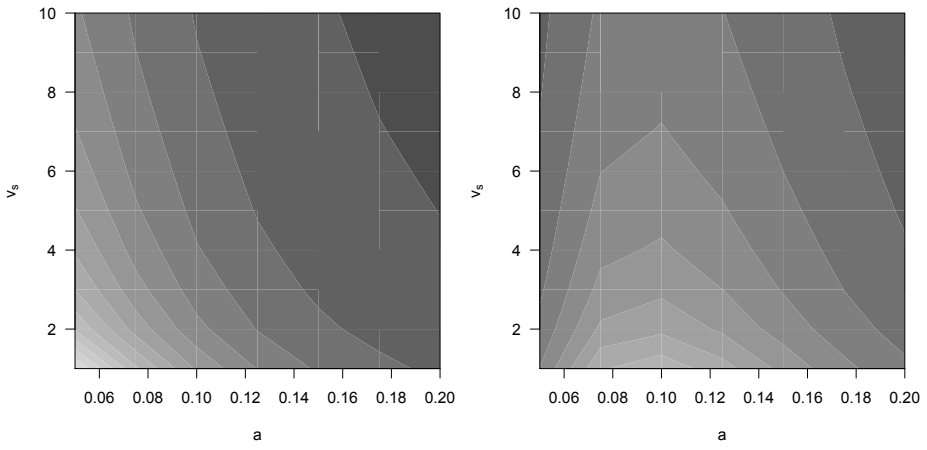

(a) $\phi = 1\%$

(b) $\phi = 5\%$

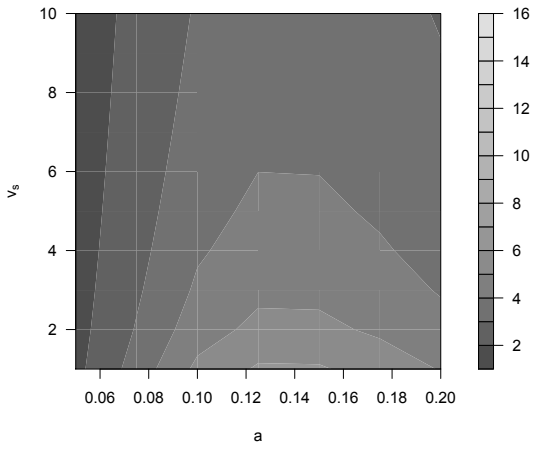

(c) $\phi = 10\%$

Figure 5.11: Increased trimer formation for increasing values of ϕ with other parameter values set at: τ=1min, $\rho = 16$ and k_d=1000. Microdomain length is shown on the horizontal axis on a $\log_5$ scale and V_s is on the vertical axis on a $\log_2$ scale.

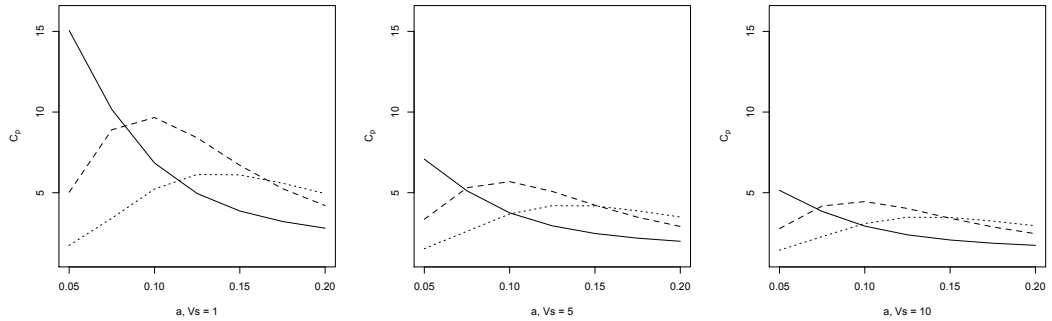

Figure 5.12: Increased rate of trimer formation (C_p) plotted against a (linear scale) for three increasing values of V_s. The various series show different values of ϕ with the solid series depicting $\phi = 1\%$, the dashed series depicting $\phi = 5\%$ and the dotted series depicting $\phi = 10\%$.

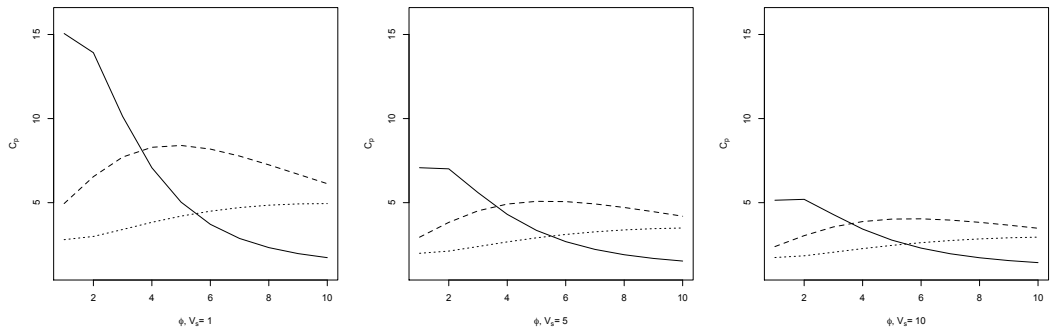

Figure 5.13: Increased rate of trimer formation (C_p) plotted against ϕ (linear scale) for three increasing values of V_s. The various series show different values of a with the solid series depicting $a = 0.05\%$, the dashed series depicting $a = 0.125\%$ and the dotted series depicting $a = 0.2$.

crodomains might influence the proliferative behaviour of a population of T cells. This was based on the assumption that proliferation is determined by a threshold number of high-affinity (trimeric) receptors being bound at the cell surface.

As our model for cell proliferation, we adapted an earlier model by Fallon & Lauffenburger [36], and investigated the influence of the rate of high-affinity receptor expression, V_s, on subsequent cell density and extracellular IL-2 consumption.

We defined a factor, C_p, which acted as a coefficient modulating the magnitude of V_s, which was dependent on our model from the previous chapter. In the absence of membrane microdomains C_p is equal to 1.

By solving a system of mass-action reaction equations, we determined the appropriate initial conditions for our earlier reaction-diffusion model, in order to calculate values of C_p for a wide range of parameter values and then examined the results to determine which combinations of parameter values resulted in sufficiently large increases in trimer formation to have a significant effect on the system behaviour, when coupled with the proliferation model by Fallon et al.

Although we have tried where possibly to use biologically plausible parameter ranges as input into the model, the simplifications made in order to solve the analytical formulation of the reaction-diffusion processes considered mean that the model output is not necessarily as plausible. For example: by a process of identifying regions of parameter space that maximised complex formation we identified parameter sets which engendered increases of trimer formation fifteen fold. This effect was dependent on selecting spatial and chemical parameters which led to a great increase in the within-microdomain monomer concentration. In our system, the only constraint preventing large increases in within-microdomain concentration is the concomitant concentration-dependent increase in flux out of the microdomain. In a real system, however, spatial crowding effects would constrain the total concentration of any protein species within the microdomain to a fixed upper limit. This would likely rule out dramatic increases in trimer organisation rate to fifteen times the control case.

In future work, we would seek to clarify the constraints on spatial crowding in cell

membranes. These constraints could readily be added to the probabilistic model described in Chapter 3, but we would also seek to integrate this consideration into our analytical model to generate a more realistic range of outcomes.

We would also seek to validate the model against *in vitro* experiments: our modelling results from the simple perturbation of the rate of surface receptor expression suggests a means of further verifying the Fallon model against an experimental system. We would also seek to better understand the dependence of receptor formation on an individual monomer level, rather than treating the receptor as a pre-formed unit as in [36].

We would expand the scope of the model to include broader cell population dynamics including cell death processes. This approach would be informed by the results of Deenick et al. [31].

It is not clear to what extent the membrane composition changes over successive generations of daughter cells. In a first approximation we would assume that the microdomain fraction of the membrane and microdomain characteristics are unchanged over successive generations. We plan to search the experimental literature to investigate whether, for example, cholesterol content in the membrane is decreased after cell division and whether this might affect the formation of membrane microdomains of daughter cells. If there is evidence that microdomain structure evolves over successive generations of T cells then we would also incorporate this change into the proliferation model.

Finally, we would also seek to incorporate the microdomain model on populations of multiple cell types. This would be informed by the work on the crossregulation model of immunity developed by Carneiro, León et al. [22] and further developed by García Martínez and León [41]. The model describes the balance between tolerance and immunity determined by the relative cell population growth of T_{reg} and T_H cells as the cells compete for extracellular IL-2. Incorporating a dependence on the level of IL-2 membrane receptors into the model would help in understanding additional variables in designing effective IL-2 modulation therapies.

5.7 Appendix C

This appendix lists the code for the implementation of the model by Fallon & Lauffenburger

```
tPoints=seq(1:80000)
#Kinetic constants (from Lauffenburger)
kf = 0.0138/11.1 #on rate for ligand binding
kr = 0.0138 #off rate for ligand binding
kre = 8*kr #off rate in endosome
kfe = kre/1000 #on rate in endsome
kt = 0.007 #constitutive internalisation const
vs = 11 #Constitutive receptor synthesis
ksyn = 0.0011 #induced receptor synthesis
ke = 0.04 #internalisation const
kx = 0.15 #recycling rate constant
kh = 0.035 #degradation rate const
ve = 10^(-14) #volume of cell in litres

#Other constants
area = 4*pi*(3.5*10^(-6))^2 #Sphere with radius 3.5micrometres
picomolar = 10^(-11)
avo = 6.022*10^23 #Avogadro's constant
na = avo/(10^12)

#Parameter
vsvals = c(0.125,0.25,0.5,1,2,4,8)

#Quantities
IL2=array(10,c(length(tPoints),length(vsvals)))
receptor=array(1500,c(length(tPoints),length(vsvals)))
bound=array(0,c(length(tPoints),length(vsvals)))
```

```
intIL2=array(0,c(length(tPoints),length(vsvals)))
intreceptor=array(300,c(length(tPoints),length(vsvals)))
intbound=array(0,c(length(tPoints),length(vsvals)))
numcells=array(2.5*10^8,c(length(tPoints),length(vsvals)))

#This is assuming that timepoints are equal to 1 minute
timeshift=0.1

for(val in 1:length(vsvals)) {
  for(t in 2:length(tPoints)) {
    delIL2 = (kr*bound[t-1, val] - kf*IL2[t-1, val]*receptor[t-1, val]
      +kx*intIL2[t-1, val]*ve*na)*numcells[t-1, val]/na
    delreceptor = (kr+ksyn)*bound[t-1, val] - kf*IL2[t-1, val]*receptor[t-1, val]
      - kt*receptor[t-1, val] + vsvals[val]*vs
    delbound = kf*IL2[t-1, val]*receptor[t-1, val] - (kr+ke)*bound[t-1, val]
    delintIL2 = (kre*intbound[t-1, val]
      - kfe*intIL2[t-1, val]*intreceptor[t-1, val])/(na*ve)
      - kx*intIL2[t-1, val]
    delintreceptor = kre*bound[t-1, val]
      - kfe*intIL2[t-1, val]*intreceptor[t-1, val] + kt*receptor[t-1, val]
      - kh*intreceptor[t-1, val]
    delintbound = kfe*intIL2[t-1, val]*intreceptor[t-1, val]
      - (kre+kh)*intbound[t-1, val] + ke*bound[t-1, val]

    delnumcells = max((600*bound[t-1, val])/(250+bound[t-1, val])-200, 0)*1000

    IL2[t, val]=max(IL2[t-1, val]+delIL2*timeshift,0)
    receptor[t, val]=max(receptor[t-1, val]+delreceptor*timeshift)
    bound[t, val]=max(bound[t-1, val]+delbound*timeshift)
```

```
    intIL2[t, val]=max(intIL2[t-1, val]+delintIL2*timeshift)

    intreceptor[t, val]=max(intreceptor[t-1, val]+delintreceptor*timeshift)

    intbound[t, val]=max(intbound[t-1, val]+delintbound*timeshift)


    numcells[t, val]=numcells[t-1, val]+delnumcells*timeshift
  }
}
```

Chapter 6

Discussion and evaluation

6.1 Thesis summary

We summarised the biological context for the studies undertaken in this thesis in Chapter 2. This provided an overview of the current state of research in microdomain-mediated signalling, protein sorting, membrane imaging and analysis of the composition of distinct membrane fractions. We examined the evidence in favour and against the significance of transient microdomains in organising signalling complexes and saw how studies suggest the existence of multiple types of microdomain as well as 'picket fence' structures influencing the long-range diffusion of membrane-bound proteins.

Because of this diversity of evidence, we decided to focus mainly on the reduction in diffusion rate as a mechanism for concentrating proteins in a confined area. In Chapter 3 we created a probabilistic model describing reaction-diffusion processes in a two-dimensional space and tested how varying spatial parameters – the radius and total microdomain coverage of the membrane – influenced formation of a heterotrimer. We also tested alternative schemes involving an affinity term for one or all of the monomers comprising the complex. These alternative schemes influenced entry and exit probabilities for the diffusing proteins and were based on specific mechanistic hypotheses from the literature.

The model in Chapter 3 supported the existence of a mechanism by which microdomain formation assisted the organisation of trimeric signalling receptors, although not by a great

degree. The parameter sets tested suggested the existence of optimal length scales for the microdomains, although these length scales were in turn dependent on the total microdomain area fraction covering the membrane surface. In order to support the results of the simulation, we returned to the fundamental reaction and diffusion equations governing trimer organisation in a space filled with diffusing monomers. For the sake of simplicity, we solved these equations for a one-dimensional space in Chapter 4 and again found that the solution to the equations supported a microdomain-mediated mechanism for receptor organisation. To verify the relationship between the analytical solution and the approach taken in Chapter 3, we re-ran a one-dimensional analogue of the probabilistic model to generate concentration profiles in a small neighbour hood of an individual microdomain and found a good fit between the analytical and simulated solutions both for the diffusion and the reaction-diffusion systems.

In Chapter 5, we reimplemented an existing model of T cell proliferation as a numerical simulation and adapted the model in order to determine the significance of the rate of surface receptor organisation on T cell-ligand interactions and cell population growth. We found that, according to the model, an increased rate of receptor expression led to greater population growth when the cells were exposed to a low concentration stimulus. When the stimulus was at a greater concentration, we found that a higher rate of receptor expression led to a faster initial population growth, but that intermediate expression rates led to a greater overall population density.

In the same chapter, we ran a more thorough exploration of the parameter space in the model from Chapter 4, informed by plausible parameter ranges taken from data encountered in the literature. This exploration identified approximate combinations of parameter values that resulted in a significant increase in the rate of receptor organisation and, subsequently, cell population growth. Using the approximate parameter values as a guide, we ran a second, finer-grained exploration of parameter space to determine sensitivity of the solution to microdomain length, coverage, and initial monomer levels. This exploration identified parameter combinations leading to much greater increases in trimer organisation than seen in Chapter 4 – up to 15 times – although the lack of accounting for crowding

effects means that increases of this level would be unlikely in a physical system.

6.2 Context, criticism and further work

In this work we have sought to find a compromise between creating simple models from which fundamental relations can be inferred and relevance to a real biological system. The 'raft debate' rages on [101] and much of the recent work suggests that any microdomain organisation is driven by clustered proteins rather than by spontaneous lipid organisation. For this reason, we sought to sidestep the question of how microdomains are formed and which molecular interactions drive their organisation and instead to focus on hypothesised physical properties of microdomains, namely the retardation of freely diffusing membrane proteins.

The most similar study in the literature is that by Nicolau et al. [81, 82]. In addition to the decreased diffusion in small membrane patches, the authors study the influence of modelled picket-fence structures on protein-protein interaction. We find agreement with their results in many cases: the appearance of small optimal length scales and the preference for low total membrane coverage. Nicolau et al. also consider mobile microdomains, finding that protein concentrating effects are increased in this case. We chose not to investigate mobile microdomains and instead have considered static domains. Despite this, we have found clear evidence for a protein sequestering mechanism. The analytical work in Chapter 4 would also have been extremely difficult to derive in the case of a moving boundary.

We have laid the mechanism contributing to microdomain-mediated protein sorting on a stronger foundation than in [81] by deriving analytical solutions to the fundamental diffusion equations and demonstrating the correspondence between these solutions and the simulated system.

There are a several features of this study that deserve criticism and should be addressed in future work.

Firstly, the results of Chapter 4 are based on solving a one-dimensional system. These are then integrated into a model based on a two-dimensional surface interaction in Chapter

5. This is clearly an oversimplification and so the results should be treated as illustrative of the mechanism, rather than as concrete predictions.

Other simplifications to make the system amenable to analysis include using fixed diffusion rates across all the constituent protein species and fixed association and dissociation constants for all of the steps involved in the formation and degradation of dimeric and trimeric complexes. Although we have concerned ourselves with the context of IL-2 receptor signalling, much of the work in this thesis applies to the formation of a generic heterotrimeric membrane complex and more work is necessary to source realistic forward and backward reaction rates for the formation of the IL-2 receptor in the membrane in order to increase the relevance of our results to the target system.

As discussed in Chapter 4 we would also aim to take into account steric hindrance between diffusing proteins in any future modelling work, ruling out unrealistic increases in concentration over very small areas. This addition to the model would improve our ability to test the plausibility of simple entropic traps being able to facilitate protein-protein interactions in the absence of any other contributing factor.

We would also like to further investigate microdomain lifetime effects on systemic receptor formation. Although we approached this in Chapter 5 by setting a fixed time in which complex formation was allowed to take place, we think that this feature would be well suited to testing with a stochastic model with a distribution of microdomain lifetimes in order to examine how more dynamic microdomain recycling affects the equilibrium behaviour of the system. Computational modelling approaches have examined similar systems to this in examining the function of Ras nanoclusters under rapid organisation and degradation [116], finding that this system provides a higher-fidelity transduction of extracellular signalling than more static membrane structures.

An important aspect to successful studies employing biological modelling is validation against experimental data. Although we have here aimed to test hypotheses about model systems (i.e. hypotheses in the literature) rather than microdomains *in vivo*, we would seek to more closely test predictions made by our model against real behaviours. In any future work we would be interested in collaborating with groups undertaking high-

frequency single-particle tracking experiments of the protein subunits of interest in order to better parameterise the model. The computational model could be easily adapted to output single particle trajectories rather than local concentrations and in that way we could directly compare reaction-diffusion behaviours with experimental results.

Although this research is relatively theoretical, the medical implications of better understanding interleukin signalling should not be ignored. Various therapies targeting IL-2 and IL-15 receptors in order to treat autoimmune disorders among other diseases[124]. Monoclonal antibody therapy directed towards the α subunit of the IL-2 receptor has been approved by the FDA to treat allograft rejection and has also been demonstrated to be partially effective in treating multiple sclerosis [125]. Understanding proliferative signals is also important in treating T cell leukaemias: the IL-2Rα subunit is overexpressed on malignant cells in patients with T cell leukaemia, cutaneous T cell lymphoma, hairy cell B-cell leukaemia, Hodgkin's disease and granulocytic leukaemia [122]. Thomas Waldmann, the lead researcher in this field, writes:

> [T]ranslation of basic insights concerning the IL-2/IL-2 receptor system obtained using the monoclonal antibody daclizumab provided a useful strategy for the prevention of organ allograft rejection and the treatment of patients with select autoimmune diseases or T-cell leukemia/lymphoma [125].

This success motivates the further study of the detailed spatiotemporal organisation of cell membrane receptors and receptor components as an important developmental step in designing novel therapies for life threatening conditions.

Chapter 7

Summary and conclusions

We have developed a range of novel modelling approaches to answer fundamental questions about the subtle diffusional dynamics associated with membrane microdomains. This diversity of approach has allowed us to attempt to address specific biological hypotheses while also probing the general behaviour of the model system and inferring more general dynamical principles. Although we made improvements to our understanding of the underlying diffusion mechanism in Chapter 4, the example model output did not appear to generate behaviour that would be highly significant in a biological system. Through a systematic exploration of the model parameters, combined with a focus on ranges more relevant to experimental data, we identified small parameter spaces that produces much larger amplifying effects on complex organisation. These results were then discussed in the context of other modelling and experimental work in Chapter 6 and ways in which it could be improved and extended were suggested.

In this chapter, we appraise the contributions made by this thesis in the context of its original objectives and state our conclusions.

7.1 Summary

The objectives of this thesis (Section 1.1) have all been fulfilled as follows:

1. Satisfied in Chapters 3–4. The diffusion Scheme 1 of Chapter 3 explored variation in diffusion rate in two dimensions and the numerical simulations in Chapter 4 repeated

this in a one dimensional space.

2. Satisfied in Chapter 3. Schemes 2 and 3 introduced affinity effects by controlling the entry and exit of microdomain areas for particular protein species.

3. Satisfied in Chapter 4. The novel analytical solution to monomer species undergoing reaction-diffusion on a periodic space with heterogeneous diffusion rates matched well with numerical solutions.

4. Satisfied in Chapters 3–5. Numerical and analytical results all indicate the existance of optimal length scales, although these are dependent on time scales among other parameters.

5. Satisfied in Chapters 4–5. Chapter 4 explored the model space in the ranges tested in numerical simulations and Chapter 5 explored the model space in ranges with biologically relevant magnitudes.

6. Satisfied in Chapter 5. The trimer formation model was combined with an existing T cell signalling and proliferation model.

7. Satisfied in Chapter 5. In addition to the dependence on length scale, parameter testing identified diffusion rates, total microdomain coverage, surface concentrations and dissociation constants that optimised microdomain effects.

7.1.1 Specific contributions

The primary contribution of this thesis is in further clarifying the plausibility of the mechanisms proposed for the formation of functional signalling platforms in the lipid raft hypothesis. Through simple reaction-diffusion models we have explored hypotheses in the literature on the role of microdomains in facilitating immunological receptor formation, specifically the trimeric IL-2 receptor.

A list of specific contributions follows:

- Reviewed the literature relating to microdomain-mediated immunological signalling, including both experimental and modelling approaches

- Created a novel model simulating protein diffusion in the cell membrane and the formation of trimeric receptor complexes
- Simulated specific reaction-diffusion schema in order to test existing hypotheses on possible roles for membrane microdomains
- Predicted the lateral concentration profile of diffusing proteins in the vicinity of microdomains based on one-dimensional numerical simulations
- Derived novel analytical solutions to Fokker-Planck diffusion law subject to specific distributions of diffusion coefficient and spatial periodicity
- Combined analytical solutions with reaction equations to predict spatial distribution of dimeric and trimeric complexes
- Validated analytical model and numerical model against each other
- Embedded receptor formation model in existing T cell proliferation model to generate new hypotheses on cell population responses to IL-2 signalling
- Demonstrated that fundamental reaction-diffusion equations support a role for static microdomains in facilitating multimeric receptor organisation
- Supported the hypothesis that optimal length scales exist for such microdomains
- Demonstrated that such length scales are highly dependent on microdomain lifetime as well as other physical and chemical parameters
- Identified parameter spaces which maximise the enhancing effect of microdomain presence

7.2 Conclusions

Researchers engaging in biological modelling are faced with a perennial choice: whether to draw inspiration from biology only as a starting point to a beautiful problem or to employ the rigour of mathematical and computational frameworks to bring added precision or

comprehensiveness to the dialogue among experimental biologists. If modelling is to make greater inroads into high-profile biological research then more of the latter approach than the former is necessary, despite mathematicians often aspiring to G.H. Hardy's pride in uselessness, and the difficulty of researchers communicating across disciplines unused to working together.

In this thesis we have travelled a little of the way down both paths: aiming to apply our simplified models as closely as possible to real biological systems in Chapters 3 and 5 and indulging in the purer mathematical formulation of the problem in Chapter 4. This combined approach helped us to maintain a more rigorous dynamical, rather than purely phenomenological, design to the models while always keeping the complexity of the real biological system in mind.

We conclude that, in the model formalisms developed in this thesis, microdomain presence has an amplifying effect on modelled receptor complex formation. This is supported both by probabilistic models of particle diffusion as well as deterministic models governing the spatial distribution of particle ensembles over time, developed from particular solutions of the heat equation. We note the simplifications made in order to make this modelling approach feasible and have highlighted the parameter values and model output that seems biologically implausible. We suggest that adding steric hindrance effects, adapting the analytical work to a two-dimensional space and refining parameters such as relative monomer numbers and kinetic constants to those of our target system, while adding a layer of complexity to the model formulation, would allow us to make experimentally testable predictions, rather than to infer more general features of the model system described.

Although we attempted to take as agnostic an attitude as possible to the existence question of microdomains, the results of the modelling offer evidence both in favour and against the role of microdomains in the original formulation by Simons & Ikonen [104]. We did find deterministic mechanisms supporting lipid microdomains playing a role in protein sorting and complex organisation. The parameter space in which this enhancement of receptor organisation took place, however, was so narrow that it seems unlikely to be

a general rule. Further study to validate the model against experimental results and identify the exact dynamic and kinetic parameters governing receptor formation is needed in order to further clarify the answer to this question. If signalling platforms based on lipid heterogeneity are significant in biological signalling processes, it seems likely, as stressed in [62] that further stabilisation of the structures is needed on medium to long-term timescales in order to have a discernible effect on downstream mechanisms.

We are, however, further convinced that spatiotemporal organisation in the cell in general needs further attention among the modelling and experimental community and that the improved understanding of the spatial and temporal organisation of cellular signalling processes will provide new insight into the function of combinatorial modules in the complex cell signalling landscape.

Bibliography

[1] S. M. Alam, G. M. Davies, C. M. Lin, T. Zal, W. Nasholds, S. C. Jameson, K. A. Hogquist, N. R. Gascoigne, and P. J. Travers. Qualitative and quantitative differences in T cell receptor binding of agonist and antagonist ligands. *Immunity*, 10(2):227–237, Feb. 1999.

[2] M. Aleksic, O. Dushek, H. Zhang, E. Shenderov, J.-L. Chen, V. Cerundolo, D. Coombs, and P. A. van der Merwe. Dependence of T cell antigen recognition on T cell receptor-peptide MHC confinement time. *Immunity*, 32(2):163–174, Feb. 2010.

[3] P. F. F. Almeida, A. Pokorny, and A. Hinderliter. Thermodynamics of membrane domains. *Biochimica et biophysica acta*, 1720(1-2):1–13, Dec. 2005.

[4] P. S. Andersen, C. Menné, R. A. Mariuzza, C. Geisler, and K. Karjalainen. A response calculus for immobilized T cell receptor ligands. *The Journal of biological chemistry*, 276(52):49125–49132, Dec. 2001.

[5] A. Asano, V. Selvaraj, D. E. Buttke, J. L. Nelson, K. M. Green, J. E. Evans, and A. J. Travis. Biochemical characterization of membrane fractions in murine sperm: identification of three distinct sub-types of membrane rafts. *Journal of cellular physiology*, 218(3):537–548, Mar. 2009.

[6] R. Azuma, T. Kitagawa, H. Kobayashi, and A. Konagaya. Particle simulation approach for subcellular dynamics and interactions of biological molecules. *BMC Bioinformatics*, 7(Suppl 4):S20, Jan. 2006.

[7] M. Bagnat and K. Simons. Cell surface polarization during yeast mating. *Proceedings of the National Academy of Sciences of the United States of America*, 99(22):14183–14188, Oct. 2002.

[8] M. Bagnat and K. Simons. Lipid rafts in protein sorting and cell polarity in budding yeast Saccharomyces cerevisiae. *Biological chemistry*, 383(10):1475–1480, Oct. 2002.

[9] T. Baumgart, S. Hess, and W. Webb. Imaging coexisting fluid domains in biomembrane models coupling curvature and line tension. *Nature*, 425(6960):821–824, 2003.

[10] L. Bene, J. Szöllösi, G. Szentesi, L. Damjanovich, R. Gáspár, T. A. Waldmann, and S. Damjanovich. Detection of receptor trimers on the cell surface by flow cytometric fluorescence energy homotransfer measurements. *Biochimica et biophysica acta*, 1744(2):176–198, June 2005.

[11] M. Berkowitz. On the Nature of Lipid Rafts: Insights from Molecularly Detailed Simulations of Model Biological Membranes Containing Mixtures of Cholesterol and Phospholipids. In *Current Topics in Membranes*, pages 257–279. Elsevier, 2008.

[12] T. Beyer, M. Busse, K. Hristov, S. Gurbiel, M. Smida, U.-U. Haus, K. Ballerstein, F. Pfeuffer, R. Weismantel, B. Schraven, and J. A. Lindquist. Integrating signals from the T-cell receptor and the interleukin-2 receptor. *PLoS Computational Biology*, 7(8):e1002121, Aug. 2011.

[13] C. Bidot, F. Gruy, C. S. Haudin, F. E. Hentati, B. Guy, and C. Lambert. Mathematical Modeling of T-Cell Activation Kinetic. *Journal of Computational Biology*, 15, Jan. 2008.

[14] A. Bodnár, E. Nizsalóczki, G. Mocsár, N. Szalóki, T. A. Waldmann, S. Damjanovich, and G. Vámosi. A biophysical approach to IL-2 and IL-15 receptor function: localization, conformation and interactions. *Immunology Letters*, 116(2):117–125, Mar. 2008.

[15] E. Bringuier. Kinetic theory of inhomogeneous diffusion. *Physica A-Statistical Mechanics And Its Applications*, 388(13):2588–2599, Jan. 2009.

[16] D. Brown. Structure and function of membrane rafts. *International journal of medical microbiology : IJMM*, 291(6-7):433–437, Feb. 2002.

[17] D. A. Brown and J. K. Rose. Sorting of GPI-anchored proteins to glycolipid-enriched membrane subdomains during transport to the apical cell surface. *Cell*, 68(3):533–544, Feb. 1992.

[18] M. A. Burchill, J. Yang, K. B. Vang, and M. A. Farrar. Interleukin-2 receptor signaling in regulatory T cell development and homeostasis. *Immunology Letters*, 114(1):1–8, Nov. 2007.

[19] D. Busse, M. de la Rosa, K. Hobiger, K. Thurley, M. Flossdorf, A. Scheffold, and T. Höfer. Competing feedback loops shape IL-2 signaling between helper and regulatory T lymphocytes in cellular microenvironments. *Proceedings of the National Academy of Sciences*, 107(7):3058–3063, Feb. 2010.

[20] R. E. Callard and A. J. Yates. Immunology and mathematics: crossing the divide. *Immunology*, 115(1):21–33, May 2005.

[21] D. A. Cantrell and K. A. Smith. The interleukin-2 T-cell system: a new cell growth model. *Science*, 224(4655):1312–1316, June 1984.

[22] J. Carneiro, K. León, I. Caramalho, C. van den Dool, R. Gardner, V. Oliveira, M.-L. Bergman, N. Sepúlveda, T. Paixão, J. Faro, and J. Demengeot. When three is not a crowd: a Crossregulation model of the dynamics and repertoire selection of regulatory CD4+ T cells. *Immunological reviews*, 216:48–68, Apr. 2007.

[23] R. M. Chicz, R. G. Urban, W. S. Lane, J. C. Gorga, L. J. Stern, D. A. A. Vignali, and J. L. Strominger. Predominant naturally processed peptides bound to HLA-DR1 are derived from MHC-related molecules and are heterogeneous in size. *Nature*, 358(6389):764–768, Aug. 1992.

[24] J.-H. Cho, H.-O. Kim, C. D. Surh, and J. Sprent. T cell receptor-dependent regulation of lipid rafts controls naive CD8+ T cell homeostasis. *Immunity*, 32(2):214–226, Feb. 2010.

[25] J. Cordy, N. Hooper, and A. Turner. The involvement of lipid rafts in Alzheimer's disease (Review). *Molecular Membrane Biology*, 23(1):111–122, Jan. 2006.

[26] S. Damjanovich, L. Bene, J. Matkó, A. Alileche, C. K. Goldman, S. Sharrow, and T. A. Waldmann. Preassembly of interleukin 2 (IL-2) receptor subunits on resting Kit 225 K6 T cells and their modulation by IL-2, IL-7, and IL-15: a fluorescence resonance energy transfer study. *Proceedings of the National Academy of Sciences of the United States of America*, 94(24):13134–13139, Nov. 1997.

[27] R. F. M. de Almeida, L. M. S. Loura, A. Fedorov, and M. Prieto. Lipid rafts have different sizes depending on membrane composition: a time-resolved fluorescence resonance energy transfer study. *Journal of molecular biology*, 346(4):1109–1120, Mar. 2005.

[28] B. I. de Bakker, A. Bodnár, E. M. H. P. van Dijk, G. Vámosi, S. Damjanovich, T. A. Waldmann, N. F. van Hulst, A. Jenei, and M. F. Garcia-Parajo. Nanometer-scale organization of the alpha subunits of the receptors for IL2 and IL15 in human T lymphoma cells. *Journal of Cell Science*, 121(Pt 5):627–633, Mar. 2008.

[29] R. J. De Boer, V. V. Ganusov, D. Milutinovic, P. D. Hodgkin, and A. S. Perelson. Estimating lymphocyte division and death rates from CFSE data. *Bulletin of mathematical biology*, 68(5):1011–1031, July 2006.

[30] V. de Mello Coelho, D. Nguyen, B. Giri, A. Bunbury, E. Schaffer, and D. D. Taub. Quantitative differences in lipid raft components between murine CD4+ and CD8+ T cells. *BMC immunology*, 5:2, Jan. 2004.

[31] E. Deenick, A. Gett, and P. Hodgkin. Stochastic Model of T Cell Proliferation: A Calculus Revealing IL-2 Regulation of Precursor Frequencies, Cell Cycle Time, and Survival. *The Journal of Immunology*, 170(10):4963, May 2003.

[32] C. Dietrich, B. Yang, T. Fujiwara, A. Kusumi, and K. Jacobson. Relationship of lipid rafts to transient confinement zones detected by single particle tracking. *Biophysical Journal*, 82(1 Pt 1):274–284, Jan. 2002.

[33] M. L. Dustin and D. Depoil. New insights into the T cell synapse from single molecule techniques. *Nature Reviews Immunology*, 11(10):672–684, Oct. 2011.

[34] J. M. Ellery and P. J. Nicholls. Possible mechanism for the alpha subunit of the interleukin-2 receptor (CD25) to influence interleukin-2 receptor signal transduction. *Immunology and Cell Biology*, 80(4):351–357, Aug. 2002.

[35] J. Ellis, B. Chain, and D. H. Davies. Antigen presentation by dendritic cells provides optimal stimulation for the production of interleukin (IL) 2, IL 4 and interferon by allogeneic T cells. *European journal of Immunology*, 1991.

[36] E. M. Fallon and D. A. Lauffenburger. Computational model for effects of ligand/receptor binding properties on interleukin-2 trafficking dynamics and T cell proliferation response. *Biotechnology progress*, 16(5):905–916, Jan. 2000.

[37] E. M. Fallon, S. F. Liparoto, K. J. Lee, T. L. Ciardelli, and D. A. Lauffenburger. Increased endosomal sorting of ligand to recycling enhances potency of an interleukin-2 analog. *The Journal of biological chemistry*, 275(10):6790–6797, Mar. 2000.

[38] O. Feinerman, G. Jentsch, K. E. Tkach, J. W. Coward, M. M. Hathorn, M. W. Sneddon, T. Emonet, K. A. Smith, and G. Altan-Bonnet. Single-cell quantification of IL-2 response by effector and regulatory T cells reveals critical plasticity in immune response. *Molecular systems biology*, 6:437, Nov. 2010.

[39] M. L. Frazier, J. R. Wright, A. Pokorny, and P. F. F. Almeida. Investigation of domain formation in sphingomyelin/cholesterol/POPC mixtures by fluorescence resonance energy transfer and Monte Carlo simulations. *Biophysical Journal*, 92(7):2422–2433, Apr. 2007.

[40] Y. Gambin, R. Lopez-Esparza, M. Reffay, E. Sierecki, N. S. Gov, M. Genest, R. S. Hodges, and W. Urbach. Lateral mobility of proteins in liquid membranes revisited. *Proceedings of the National Academy of Sciences of the United States of America*, 103(7):2098–2102, Feb. 2006.

[41] K. García-Martínez and K. León. Modeling the role of IL-2 in the interplay between CD4+ helper and regulatory T cells: assessing general dynamical properties. *Journal of Theoretical Biology*, 262(4):720–732, Feb. 2010.

[42] M. Gibson and J. Bruck. Efficient exact stochastic simulation of chemical systems with many species and many channels. *Journal of Physical Chemistry A*, Jan. 2000.

[43] J. Goebel, K. Forrest, L. Morford, and T. L. Roszman. Differential localization of IL-2- and -15 receptor chains in membrane rafts of human T cells. *Journal of leukocyte biology*, 72(1):199–206, July 2002.

[44] F. M. Goñi, A. Alonso, L. A. Bagatolli, R. E. Brown, D. Marsh, M. Prieto, and J. L. Thewalt. Phase diagrams of lipid mixtures relevant to the study of membrane rafts. *Biochimica et biophysica acta*, 1781(11-12):665–684, Jan. 2008.

[45] J. A. Gosse, A. Wagenknecht-Wiesner, D. Holowka, and B. Baird. Transmembrane sequences are determinants of immunoreceptor signaling. *Journal of immunology (Baltimore, Md : 1950)*, 175(4):2123–2131, Aug. 2005.

[46] A. Grakoui, S. Bromley, C. Sumen, M. Davis, A. Shaw, P. Allen, and M. Dustin. The immunological synapse: a molecular machine controlling T cell activation. *Science*, 285(5425):221, 1999.

[47] M. Hao, S. Mukherjee, and F. R. Maxfield. Cholesterol depletion induces large scale domain segregation in living cell membranes. *Proceedings of the National Academy of Sciences of the United States of America*, 98(23):13072–13077, Nov. 2001.

[48] T. Harder. Lipid raft domains and protein networks in T-cell receptor signal transduction. *Current Opinion in Immunology*, 16(3):353–359, June 2004.

[49] H.-T. He, A. Lellouch, and D. Marguet. Lipid rafts and the initiation of T cell receptor signaling. *Seminars in immunology*, 17(1):23–33, Feb. 2005.

[50] H. Heerklotz. Triton promotes domain formation in lipid raft mixtures. *Biophysical Journal*, 83(5):2693–2701, Nov. 2002.

[51] D. Holowka, J. A. Gosse, A. T. Hammond, X. Han, P. Sengupta, N. L. Smith, A. Wagenknecht-Wiesner, M. Wu, R. M. Young, and B. Baird. Lipid segregation and IgE receptor signaling: a decade of progress. *Biochimica et biophysica acta*, 1746(3):252–259, Dec. 2005.

[52] F. Hullin-Matsuda and T. Kobayashi. Monitoring the distribution and dynamics of signaling microdomains in living cells with lipid-specific probes. *Cellular and molecular life sciences : CMLS*, 64(19-20):2492–2504, Oct. 2007.

[53] D. J. Irvine, M. A. Purbhoo, M. Krogsgaard, and M. M. Davis. Direct observation of ligand recognition by T cells. *Nature*, 419(6909):845–849, Oct. 2002.

[54] B. A. Irving, F. W. Alt, and N. Killeen. Thymocyte development in the absence of pre-T cell receptor extracellular immunoglobulin domains. *Science*, 280(5365):905–908, May 1998.

[55] C. Janeway. *Immunobiology: The Immune System in Health and Disease*. Taylor & Francis Group; Garland Science, 6th edition, 2005.

[56] M. K. Kennedy, M. Glaccum, S. N. Brown, E. A. Butz, J. L. Viney, M. Embers, N. Matsuki, K. Charrier, L. Sedger, C. R. Willis, K. Brasel, P. J. Morrissey, K. Stocking, J. C. Schuh, S. Joyce, and J. J. Peschon. Reversible defects in natural killer and memory CD8 T cell lineages in interleukin 15-deficient mice. *The Journal of experimental medicine*, 191(5):771–780, Mar. 2000.

[57] A. K. Kenworthy. Have we become overly reliant on lipid rafts? Talking Point on the involvement of lipid rafts in T-cell activation. *EMBO reports*, 9(6):531–535, June 2008.

[58] B. N. Kholodenko, J. F. Hancock, and W. Kolch. Signalling ballet in space and time. *Nature reviews Molecular cell biology*, 11(6):414–426, June 2010.

[59] H. P. Kim, J. Imbert, and W. J. Leonard. Both integrated and differential regulation of components of the IL-2/IL-2 receptor system. *Cytokine & growth factor reviews*, 17(5):349–366, Oct. 2006.

[60] S. H. Kleinstein. Getting started in computational immunology. *PLoS Computational Biology*, 4(8):e1000128, 2008.

[61] R. Kumar, M. Ferez, M. Swamy, I. Arechaga, M. T. Rejas, J. M. Valpuesta, W. W. A. Schamel, B. Alarcon, and H. M. van Santen. Increased sensitivity of antigen-experienced T cells through the enrichment of oligomeric T cell receptor complexes. *Immunity*, 35(3):375–387, Sept. 2011.

[62] A. Kusumi, I. Koyama-Honda, and K. Suzuki. Molecular Dynamics and Interactions for Creation of Stimulation-Induced Stabilized Rafts from Small .... *Traffic*, Jan. 2004.

[63] B. C. Lagerholm, G. E. Weinreb, K. Jacobson, and N. L. Thompson. Detecting microdomains in intact cell membranes. *Annual review of physical chemistry*, 56:309–336, Jan. 2005.

[64] P. T. Landsberg. D Grad v or Grad(Dv). *Journal of Applied Physics*, 56(4):1119–1122, 1984.

[65] C. C. Lee, M. Revington, S. D. Dunn, and N. O. Petersen. The lateral diffusion of selectively aggregated peptides in giant unilamellar vesicles. *Biophysical Journal*, 84(3):1756–1764, Mar. 2003.

[66] D. Lichtenberg, F. M. Goñi, and H. Heerklotz. Detergent-resistant membranes should not be identified with membrane rafts. *Trends in biochemical sciences*, 30(8):430–436, Aug. 2005.

[67] E. Long, B. Henderson, and A. Zaikin. In silico analysis of microdomain-mediated trimer formation in the T cell membrane. *The European Physical Journal - Special Topics*, 187(1):21–30, 2010.

[68] A. Ma, R. Koka, and P. Burkett. Diverse functions of IL-2, IL-15, and IL-7 in lymphoid homeostasis. *Annual review of immunology*, 24:657–679, 2006.

[69] J. L. Macdonald and L. J. Pike. A simplified method for the preparation of detergent-free lipid rafts. *The Journal of Lipid Research*, 46(5):1061–1067, May 2005.

[70] T. R. Malek and A. L. Bayer. Tolerance, not immunity, crucially depends on IL-2. *Nature Reviews Immunology*, 4(9):665–674, Sept. 2004.

[71] T. R. Malek and I. Castro. Interleukin-2 Receptor Signaling: At the Interface between Tolerance and Immunity. *Immunity*, 33(2):153–165, Aug. 2010.

[72] B. N. Manz, B. L. Jackson, R. S. Petit, M. L. Dustin, and J. Groves. T-cell triggering thresholds are modulated by the number of antigen within individual T-cell receptor clusters. *Proceedings of the National Academy of Sciences*, 108(22):9089–9094, May 2011.

[73] M. Marmor and M. Julius. Role for lipid rafts in regulating interleukin-2 receptor signaling. *Blood*, Jan. 2001.

[74] J. Matko, A. Bodnar, G. Vereb, L. Bene, and G. Vamosi. GPI-microdomains (membrane rafts) and signaling of the multi-chain interleukin-2 receptor in human lymphoma/leukemia T cell lines. *European Journal of Biochemistry*, Jan. 2002.

[75] F. R. Maxfield and I. Tabas. Role of cholesterol and lipid organization in disease. *Nature*, 438(7068):612–621, Dec. 2005.

[76] R. Medzhitov. Recognition of microorganisms and activation of the immune response. *Nature*, 449(7164):819–826, 2007.

[77] M. J. Miller, O. Safrina, I. Parker, and M. D. Cahalan. Imaging the single cell dynamics of CD4+ T cell activation by dendritic cells in lymph nodes. *The Journal of experimental medicine*, 200(7):847–856, Oct. 2004.

[78] B. P. v. Milligen, P. D. Bons, B. A. Carreras, and R. Sánchez. On the applicability of Fick's law to diffusion in inhomogeneous systems. *European Journal of Physics*, 26(5):913–925, July 2005.

[79] S. Mukherjee and F. R. Maxfield. Role of membrane organization and membrane domains in endocytic lipid trafficking. *Traffic*, 1(3):203–211, Mar. 2000.

[80] B. H. Nelson and D. M. Willerford. Biology of the interleukin-2 receptor. *Advances in immunology*, 70:1–81, 1998.

[81] D. V. Nicolau, K. Burrage, R. G. Parton, and J. F. Hancock. Identifying optimal lipid raft characteristics required to promote nanoscale protein-protein interactions on the plasma membrane. *Molecular and cellular biology*, 26(1):313–323, Jan. 2006.

[82] D. V. Nicolau, J. F. Hancock, and K. Burrage. Sources of anomalous diffusion on cell membranes: a Monte Carlo study. *Biophysical Journal*, 92(6):1975–1987, Mar. 2007.

[83] G. Nudelman, M. Weigert, and Y. Louzoun. In-silico cell surface modeling reveals mechanism for initial steps of B-cell receptor signal transduction. *Molecular immunology*, 46(15):3141–3150, Sept. 2009.

[84] G. Orr, D. Hu, S. Ozçelik, L. K. Opresko, H. S. Wiley, and S. D. Colson. Cholesterol dictates the freedom of EGF receptors and HER2 in the plane of the membrane. *Biophysical Journal*, 89(2):1362–1373, Aug. 2005.

[85] M. J. Palmer, V. S. Mahajan, J. Chen, D. J. Irvine, and D. A. Lauffenburger. Signaling thresholds govern heterogeneity in IL-7-receptor-mediated responses of naïve CD8(+) T cells. *Immunology and Cell Biology*, 89(5):581–594, July 2011.

[86] M. J. Palmer, V. S. Mahajan, L. C. Trajman, D. J. Irvine, D. A. Lauffenburger, and J. Chen. Interleukin-7 receptor signaling network: an integrated systems perspective. *Cellular & molecular immunology*, 5(2):79–89, Apr. 2008.

[87] S. A. Pandit. Simulation of the Early Stages of Nano-Domain Formation in Mixed Bilayers of Sphingomyelin, Cholesterol, and Dioleylphosphatidylcholine. *Biophysical Journal*, 87(5):3312–3322, Aug. 2004.

[88] M. Papiernik, do Carmo Leite-de MoraesM, C. Pontoux, A. M. Joret, B. Rocha, C. Penit, and M. Dy. T cell deletion induced by chronic infection with mouse mammary tumor virus spares a CD25-positive, IL-10-producing T cell population with infectious capacity. *Journal of immunology (Baltimore, Md : 1950)*, 158(10):4642–4653, May 1997.

[89] L. J. Pike. Lipid rafts: heterogeneity on the high seas. *The Biochemical journal*, 378(Pt 2):281–292, Mar. 2004.

[90] A.-H. Pillet, V. Lavergne, V. Pasquier, F. Gesbert, J. Thèze, and T. Rose. IL-2 induces conformational changes in its preassembled receptor core, which then migrates in lipid raft and binds to the cytoskeleton meshwork. *Journal of molecular biology*, 403(5):671–692, Nov. 2010.

[91] A. Pralle, P. Keller, E. L. Florin, K. Simons, and J. K. Hörber. Sphingolipid-cholesterol rafts diffuse as small entities in the plasma membrane of mammalian cells. *The Journal of cell biology*, 148(5):997–1008, Mar. 2000.

[92] C. C. Reddy, A. Wells, and D. A. Lauffenburger. Receptor-mediated effects on ligand availability influence relative mitogenic potencies of epidermal growth factor and transforming growth factor alpha. *Journal of cellular physiology*, 166(3):512–522, Mar. 1996.

[93] D. Ribatti, E. Crivellato, and A. Vacca. The contribution of Bruce Glick to the definition of the role played by the bursa of Fabricius in the development of the B cell lineage. *Clinical and Experimental Immunology*, 145(1):1–4, July 2006.

[94] G. Richardson, L. J. Cummings, H. J. Harris, and P. O'Shea. Toward a mathematical model of the assembly and disassembly of membrane microdomains: comparison with experimental models. *Biophysical Journal*, 92(12):4145–4156, June 2007.

[95] H. J. Risselada and S. J. Marrink. The molecular face of lipid rafts in model membranes. *Proceedings of the National Academy of Sciences of the United States of America*, 105(45):17367–17372, Nov. 2008.

[96] T. Rose, A.-H. Pillet, V. Lavergne, B. Tamarit, P. Lenormand, J.-C. Rousselle, A. Namane, and J. Thèze. Interleukin-7 compartmentalizes its receptor signaling complex to initiate CD4 T lymphocyte response. *Journal of Biological Chemistry*, 285(20):14898–14908, May 2010.

[97] P. G. Saffman and M. Delbrück. Brownian motion in biological membranes. *Proceedings of the National Academy of Sciences of the United States of America*, 72(8):3111–3113, Aug. 1975.

[98] S. Sakaguchi, N. Sakaguchi, M. Asano, M. Itoh, and M. Toda. Immunologic self-tolerance maintained by activated T cells expressing IL-2 receptor alpha-chains (CD25). Breakdown of a single mechanism of self-tolerance causes various autoimmune diseases. *Journal of immunology (Baltimore, Md : 1950)*, 155(3):1151–1164, Aug. 1995.

[99] M. Salzmann and M. F. Bachmann. Estimation of maximal affinities between T-cell receptors and MHC/peptide complexes. *Molecular immunology*, 35(2):65–71, Feb. 1998.

[100] H. Schorle, T. Holtschke, T. Hünig, A. Schimpl, and I. Horak. Development and function of T cells in mice rendered interleukin-2 deficient by gene targeting. *Nature*, 352(6336):621–624, Aug. 1991.

[101] A. S. Shaw. Lipid rafts: now you see them, now you don't. *Nature immunology*, 7(11):1139–1142, Nov. 2006.

[102] E. D. Sheets, G. M. Lee, R. Simson, and K. Jacobson. Transient confinement of a glycosylphosphatidylinositol-anchored protein in the plasma membrane. *Biochemistry*, 36(41):12449–12458, Oct. 1997.

[103] K. Simons and R. Ehehalt. Cholesterol, lipid rafts, and disease. *The Journal of clinical investigation*, 110(5):597–603, Sept. 2002.

[104] K. Simons and E. Ikonen. Functional rafts in cell membranes. *Nature*, 387(6633):569–572, June 1997.

[105] S. Singer and G. Nicolson. The fluid mosaic model of the structure of cell membranes. *Science*, 175(4023):720–731, 1972.

[106] S. J. Singer and G. L. Nicolson. The fluid mosaic model of the structure of cell membranes. *Science*, 175(23):720–731, Feb. 1972.

[107] K. A. Smith. Interleukin-2: inception, impact, and implications. *Science*, 240(4856):1169–1176, May 1988.

[108] K. A. Smith. Cell growth signal transduction is quantal. *Annals of the New York Academy of Sciences*, 766:263–271, Sept. 1995.

[109] D. J. Stauber, E. W. Debler, P. A. Horton, K. A. Smith, and I. A. Wilson. Crystal structure of the IL-2 signaling complex: paradigm for a heterotrimeric cytokine receptor. *Proceedings of the National Academy of Sciences of the United States of America*, 103(8):2788–2793, Feb. 2006.

[110] W. K. Subczynski and A. Kusumi. Dynamics of raft molecules in the cell and artificial membranes: approaches by pulse EPR spin labeling and single molecule optical microscopy. *Biochimica et biophysica acta*, 1610(2):231–243, Mar. 2003.

[111] K. Suzuki, K. Ritchie, E. Kajikawa, T. Fujiwara, and A. Kusumi. Rapid Hop Diffusion of a G-Protein-Coupled Receptor in the Plasma Membrane as Revealed by Single-Molecule Techniques. *Biophysical Journal*, 88(5):3659–3680, May 2005.

[112] Y. Takahama. Journey through the thymus: stromal guides for T-cell development and selection. *Nature Reviews Immunology*, 6(2):127–135, Feb. 2006.

[113] T. Taniguchi. Cytokine signaling through nonreceptor protein tyrosine kinases. *Science*, Jan. 1995.

[114] R. D. C. Team. *R: A Language and Environment for Statistical Computing* . R Foundation for Statistical Computing, Jan. 2011.

[115] A. M. Thornton, E. E. Donovan, C. A. Piccirillo, and E. M. Shevach. Cutting edge: IL-2 is critically required for the in vitro activation of CD4+CD25+ T cell suppressor

function. *Journal of immunology (Baltimore, Md : 1950)*, 172(11):6519–6523, June 2004.

[116] T. Tian, A. Harding, K. Inder, S. Plowman, R. G. Parton, and J. F. Hancock. Plasma membrane nanoswitches generate high-fidelity Ras signal transduction. *Nature cell biology*, 9(8):905–914, Aug. 2007.

[117] M. Triantafilou, K. Miyake, D. T. Golenbock, and K. Triantafilou. Mediators of innate immune recognition of bacteria concentrate in lipid rafts and facilitate lipopolysaccharide-induced cell activation. *Journal of Cell Science*, 115(Pt 12):2603–2611, June 2002.

[118] S. Turner. Intercellular Adhesion and Cancer Invasion: A Discrete Simulation Using the Extended Potts Model. *Journal of Theoretical Biology*, 216(1):85–100, May 2002.

[119] G. Vámosi, A. Bodnár, G. Vereb, A. Jenei, C. K. Goldman, J. Langowski, K. Tóth, L. Mátyus, J. Szöllösi, T. A. Waldmann, and S. Damjanovich. IL-2 and IL-15 receptor alpha-subunits are coexpressed in a supramolecular receptor cluster in lipid rafts of T cells. *Proceedings of the National Academy of Sciences of the United States of America*, 101(30):11082–11087, July 2004.

[120] G. Vereb, J. Matkó, G. Vámosi, S. M. Ibrahim, E. Magyar, S. Varga, J. Szöllosi, A. Jenei, R. Gáspár, T. A. Waldmann, and S. Damjanovich. Cholesterol-dependent clustering of IL-2Ralpha and its colocalization with HLA and CD48 on T lymphoma cells suggest their functional association with lipid rafts. *Proceedings of the National Academy of Sciences of the United States of America*, 97(11):6013–6018, May 2000.

[121] U. von Freeden-Jeffry, P. Vieira, L. A. Lucian, T. McNeil, S. E. Burdach, and R. Murray. Lymphopenia in interleukin (IL)-7 gene-deleted mice identifies IL-7 as a nonredundant cytokine. *The Journal of experimental medicine*, 181(4):1519–1526, Apr. 1995.

[122] T. Waldmann. The structure, function, and expression of interleukin-2 receptors on normal and malignant lymphocytes. *Science*, 232(4751):727–732, May 1986.

[123] T. A. Waldmann. The multi-subunit interleukin-2 receptor. *Annual review of biochemistry*, 58:875–911, Jan. 1989.

[124] T. A. Waldmann. The IL-2/IL-15 receptor systems: targets for immunotherapy. *Journal of clinical immunology*, 22(2):51–56, Mar. 2002.

[125] T. A. Waldmann. Anti-Tac (daclizumab, Zenapax) in the treatment of leukemia, autoimmune diseases, and in the prevention of allograft rejection: a 25-year personal odyssey. *Journal of clinical immunology*, 27(1):1–18, Jan. 2007.

[126] X. Wang, M. Rickert, and K. C. Garcia. Structure of the quaternary complex of interleukin-2 with its alpha, beta, and gammac receptors. *Science*, 310(5751):1159–1163, Nov. 2005.

[127] Wolfram Research, Inc. *Mathematica Edition: Version 8.0*, Jan. 2010.

[128] S. C. Wuest, J. H. Edwan, J. F. Martin, S. Han, J. S. A. Perry, C. M. Cartagena, E. Matsuura, D. Maric, T. A. Waldmann, and B. Bielekova. A role for interleukin-2 trans-presentation in dendritic cell-mediated T cell activation in humans, as revealed by daclizumab therapy. *Nature medicine*, 17(5):604–609, May 2011.

[129] R. Xavier, T. Brennan, Q. Li, C. McCormack, and B. Seed. Membrane compartmentation is required for efficient T cell activation. *Immunity*, 8(6):723–732, June 1998.

[130] S. Yarkoni, A. Kaminitz, Y. Sagiv, I. Yaniv, and N. Askenasy. Involvement of IL-2 in homeostasis of regulatory T cells: the IL-2 cycle. *BioEssays*, 30(9):875–888, Sept. 2008.

[131] Y. Yashiro-Ohtani, T. Ohtani, and W. S. Pear. Notch regulation of early thymocyte development. *Seminars in immunology*, 22(5):261–269, Oct. 2010.

[132] A. Yethiraj and J. C. Weisshaar. Why are lipid rafts not observed in vivo? *Biophysical Journal*, 93(9):3113–3119, Nov. 2007.

[133] T. Zech, C. S. Ejsing, K. Gaus, B. de Wet, A. Shevchenko, K. Simons, and T. Harder. Accumulation of raft lipids in T-cell plasma membrane domains engaged in TCR signalling. *The EMBO journal*, 28(5):466–476, Mar. 2009.